

Brain-wide mapping of transgene expression in mouse models of neurodegenerative disease

By

Sveinung Lillehaug

A thesis submitted
to the University of Oslo
for the degree of

Philosophiae Doctor (Ph.D.)

2020



Principal supervisor: Trygve B. Leergaard

Co-supervisor: Jan G. Bjaalie

Division of Anatomy
Department of Molecular Medicine
Institute of Basic Medical Sciences
University of Oslo

© Sveinung Lillehaug, 2020

*Series of dissertations submitted to the
Faculty of Medicine, University of Oslo*

ISBN 978-82-8377-567-9

All rights reserved. No part of this publication may be reproduced or transmitted, in any form or by any means, without permission.

Cover: Hanne Baadsgaard Utigard.
Fotograf portrettfoto: Sheena Herida Lillehaug
Print production: Representralen, University of Oslo.

TABLE OF CONTENTS

Acknowledgements	III
Publications	V
Abstract	VI
Synopsis	
Introduction	1
Challenges addressed in this thesis	10
Aims and approach	13
Methods	15
Ethical considerations	17
Workflow	17
Disease models and tTA driver lines evaluated in this thesis	19
Gene constructs, tissue processing and histochemistry	21
Tg-ArcSwe	21
tTA-lines	21
Image acquisition, organization and online sharing	23
Whole slide imaging	23
The Navigator3 platform	23
Spatial registration (anchoring)	24
Data and custom code availability	24
Distribution and density analyses	25
Quantitative image analysis and statistics	25
Semi-quantitative assessment	27
Results	29
Paper I	31
Paper II	33
Paper III	35

Discussion	37
Validity of methods	37
Quantitative image analysis	37
Atlas integration and semi-quantitative analysis	38
Workflow	40
Evaluation of main findings and scientific impact	42
β -amyloid in tg-ArcSwe mice	42
Transgene expression in Nop-tTA mice	43
Online tTA resource	45
Scientific impact	46
Conclusions	49
References	53
Papers	67

ACKNOWLEDGEMENTS

The studies included in the present thesis were conducted between 2013 and 2018 at the Neural Systems Laboratory, Institute of Basic Medical Sciences, University of Oslo. The Faculty provided a personal scholarship, laboratory and computational facilities, and comprehensive training in scientific theory, relevant methods and research publication. Additional sources of funding are stated in the individual articles.

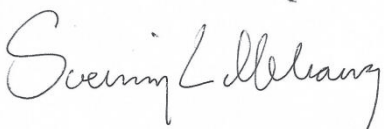
First and foremost, I would like to express my sincere gratitude to my supervisors, professors Trygve B Leergaard and Jan G Bjålie, for their continuous support of my PhD study and related research. Trygve, as my principal supervisor, has been an invaluable provider of scientific knowledge, patience, motivation, attention to detail, and, sometimes slightly heated, discussions. Jan and Trygve, together with professor emeritus Per A Brodal, are also responsible for sparking my interest in computational neuroscience back in 2001, when I was introduced to the Neural Systems Laboratory as a research assistant during summer break from medical school. Already during my student years, they gave me the freedom and responsibility to participate fully in all phases of research projects, thought me the methods and mindset of experimental neuroscience, and encouraged me to present our work in posters, abstracts, oral presentations and peer-reviewed articles. I am also truly grateful that they welcomed me back to NeSys after some years in clinical exile and took the chance to initiate the project culminating in this thesis.

During my time at the Neural Systems Laboratory, I have been introduced to a wide range of exceptional individuals, that each in their own way have left their footprints on this dissertation. Close colleagues, like Dmitri Darine, Hong Qu, Grazyna Babinska, Eszter Papp, and Gergely Csúcs, have contributed with specific expertise, day-to-day discussions, and a positive and creative work environment. Two of the articles came as a result of a long term, fruitful collaboration with Michael Yetman and prof. Joanna Jankowsky, physically located on the other side of the Atlantic. There have

been too many great colleagues, collaborators, and acquaintances to mention all by name, but each contribution, both formal and informal, are greatly appreciated.

My gratitude also goes out to a number of people not directly connected to the world of neuroscience. The path to a PhD is not always a straight one, and the aid of extraordinary individuals like Torunn and Vigdis have helped me to push forward despite some bends and bumps. I could not have completed this thesis without the support of my patient wife, best friend, and life companion, Sheena. I also thank my parents, who have always been there for support and guidance. Special thanks go to my dear niece and nephew, Maja and Morten, for being who they are. My family are the most important people in my world, and I dedicate this thesis to them.

Oslo, April 2019



Sveinung Lillehaug, MD

PUBLICATIONS

- I. Brainwide distribution and variance of amyloid-beta deposits in tg-ArcSwe mice.**
Lillehaug S*, Syverstad GH*, Nilsson LN, Bjaalie JG, Leergaard TB, Torp R.
Neurobiology of Aging 35:556-64, 2014.
DOI: [10.1016/j.neurobiolaging.2013.09.013](https://doi.org/10.1016/j.neurobiolaging.2013.09.013)
PMID: 24126157
*These authors contributed equally to this work

- II. Transgene expression in the Nop-tTA driver line is not inherently restricted to the entorhinal cortex.**
Yetman MJ*, Lillehaug S*, Bjaalie JG, Leergaard TB, Jankowsky JL.
Brain Structure and Function 221:2231-49, 2016.
DOI: [10.1007/s00429-015-1040-9](https://doi.org/10.1007/s00429-015-1040-9)
PMID: 25869275
*These authors contributed equally to this work

- III. Brain-wide distribution of reporter expression in five transgenic tetracycline-transactivator mouse lines.**
Lillehaug S, Yetman MJ, Puchades MA, Checinska MM, Kleven H, Jankowsky JL, Bjaalie JG, Leergaard TB.
Scientific Data 6:190028, 2019.
DOI: [10.1038/sdata.2019.28](https://doi.org/10.1038/sdata.2019.28)
PMID: 30806643

ABSTRACT

Neurodegenerative diseases are a major cause of progressive disability and impaired quality of life, with consequences not only for patients, but also their caregivers and the society. Genetically modified mouse models have become important tools in the effort to understand and eventually find cures for these conditions. A wide range of murine transgenic models have been developed to mimic neurodegenerative diseases, but since each model only replicates certain aspects of the human conditions, it is essential to choose one or more models that are appropriate for the questions being addressed in a particular study. Finding the most suitable model requires careful assessment of phenotype data, including empirical descriptions of the level and anatomical location of transgene expression. The quantity, quality and reproducibility of available morphological data is, however, often limited as a result of technological limitations, lack of standardization, narrow scope of analyses, insufficient documentation provided in publications, or reluctance to share data.

The aim of the present thesis was to develop, optimize and test workflows for comprehensive characterization and documentation of morphological features in transgenic mouse models of neurodegenerative disease. We utilized tools and infrastructure developed in context of the EU Human Brain Project to establish workflows for brain-wide analysis and sharing of serial microscopic images and applied these in three studies of transgenic mouse models relevant in preclinical neurodegenerative research. We demonstrated how the anatomical location and variance of transgene expression can be quantitatively assessed and how the anatomical location of cellular labeling in mouse brains can be compared across several studies by spatially relating microscopic images to a common, three-dimensional, mouse brain reference atlas. We finally showed how large collections of histological image data could be publicly shared in accordance with the F.A.I.R. principles (Wilkinson et al. 2016), ensuring that data are Findable, Accessible, Interoperable, and Reusable.

SYNOPSIS

INTRODUCTION

Neurodegenerative conditions, with Alzheimer's disease as the most common, represent a huge challenge, both in terms of human suffering and economic cost. For dementias alone, The World Alzheimer Report 2015 estimated that 46.8 million people worldwide are affected, and the total cost of US\$ 818 billion equals 1.09% of the global GDP (www.worldalzreport2015.org). As more people live to a greater age, the prevalence of age-related neurodegenerative diseases will continue to rise, and the socio-economic burden will grow proportionally. When also considering the emotional burden for patients and their relatives, friends, and caregivers, the motivation for research aimed at understanding and eventually curing neurodegenerative diseases is enormous.

Neurodegenerative diseases are a range of incurable and disabling conditions characterized by progressive loss of neurons and the accumulation of abnormal or aggregated proteins (Heemels, 2016). Depending on the affected brain regions and systems, they lead to specific symptoms of impaired mental functioning and/ or movement. Examples of neurodegenerative diseases include Alzheimer's disease, which is associated with declining cognitive function and memory loss, and Parkinson's disease, spinocerebellar ataxias and Huntington's disease, which primarily affect motor functions. Although early diagnosis of these conditions has greatly improved with advances in medical imaging (Shimizu et al. 2018) and the discovery of novel biomarkers (Beach, 2017), our ability to prevent, treat, or even slowing down the degenerative processes is still very limited (Gitler et al. 2017).

In the following section, we outline the role of genetically altered mouse models in experimental neurodegenerative research and review some of the challenges currently limiting the quantity and quality of available neuroanatomical data from such models. Second, we describe how the field of neuroinformatics has opened new avenues to address these issues and summarize the challenges addressed in the present thesis.

Over the last four decades, a wealth of information on the genetic and molecular components involved in the pathogenesis of neurodegeneration has been discovered. Genetic research has uncovered that only a few neurodegenerative diseases are monogenic (e.g. Huntington's disease; Ferrante, 2009), and that most other conditions, with the exception of some rare familial forms, are sporadic and linked to complex inheritance patterns that are yet to be fully understood (Shulman et al. 2011; Karch et al. 2014; Pihlstrøm et al. 2018;). Many of the intricate genetic mechanisms and pathological processes underlying neurodegenerative disease can only be studied in a living organism, and research animals therefore play a central role in experimental neurodegenerative science (Dawson et al. 2018).

The use of research animals increased significantly through the 19th Century, partially due to the development of better anesthetics, and by the twentieth century, animal modeling had become the method of choice for demonstrating biological significance (Ericsson et al. 2013). At that time, only outbred research animals were available, and scientists soon discovered that genetic variability was a confining factor in their research. This problem was addressed in the 1930s, by inbreeding rodents to a point that genetically identical individuals became available for experimental use, providing a consistent source of research subjects with little variation over time and from litter to litter. Animal models of neurodegenerative disease have existed since the 1950s, but for several decades, such models consisted primarily of strains of animals carrying spontaneous mutations and animals in which specific brain lesions were induced with ionizing radiation or toxins to mimic neurological conditions (Carlsson et al. 1957; Angelis et al. 2007). These models played an important role in understanding basic functional neuroanatomy but were unable to uncover underlying disease mechanisms. Today, the mouse has become the most prominent animal model in life sciences, including preclinical neuroscience (Ellenbroek & Youn, 2016). Several factors have contributed to the increasing use of mice in experimental neuroscience, such as high efficiency and low cost of breeding, the short life span facilitating aging studies, miniaturization of surgical instruments, improved small animal imaging techniques, increasingly sophisticated behavioral assays, and, perhaps most

importantly, the rapidly expanding repertoire of tools for genetic manipulation (Abbott, 2010; Pankevich et al. 2012).

In 1981, Frank Ruddle and colleagues created the first transgenic mouse in which inserted genetic material was successfully transmitted to subsequent generations (Gordon & Ruddle, 1981). Since Ruddle's initial discovery, identification of disease genes has allowed the creation of a wide range of new models, such as transgenic animals expressing human mutant genes and models with mutations in endogenous disease-related genes. In neuroscience, the new methods for manipulating the mouse genome were first applied in studies of Alzheimer's disease (AD). Clinically, AD is characterized by progressive loss of memory and other cognitive functions. Neuropathologically, one can observe amyloid plaques and neurofibrillary tangles, as well as synaptic and neuronal loss and astrocytic gliosis (Querfurth & LaFerla 2010). The first genetic lesion discovered in a family with AD was the London mutation (Goate et al. 1991) and shortly thereafter the Indiana mutation was found in an American family (Murrell et al. 1991). Both mutations are located in the gene encoding amyloid precursor protein (APP). In 1995, Games and colleagues described the neuropathology of the first transgenic AD model, where human APP cDNA with the Indiana mutation was successfully incorporated into the mouse genome (Games et al. 1995). Since then, a number of mouse models have been created with various mutations in APP causing increased β -amyloid deposition in the brain. These mice, to varying degree, replicate many important neuropathological features of human AD, such as cerebral angiopathy, amyloid neuropathology, synaptic loss, loss of synaptic plasticity and impaired learning and memory, while other typical features (e.g. neurofibrillary tangles) are absent. Further research led to the development of AD models carrying mutations in other genes, such as tau (Lee et al. 2001), presenilin, or combinations of mutations in different disease modifying genes (Elder et al. 2010; Roberson, 2012). Although studies conducted in these experimental models have provided invaluable information on the pathogenesis and molecular mechanisms underlying AD, none of the more than 160 currently available genetically altered mouse models (Alzforum; Retrieved March 30, 2019, from <http://www.alzforum>).

[org/research-models/](#)) fully replicate the spectrum of neuropathological and behavioral changes seen in humans (reviewed by Esquerda-Canals et al. 2017; Jankowsky & Zheng, 2017).

A common feature for the earlier, conventional, genetically altered disease models is that inactivation or overexpression of genes occurs continuous from embryogenesis to death. This “all or nothing” approach is not very flexible and often fails to answer more subtle questions about gene function. The conventional models do not mimic the “on-again and off-again” pattern of gene expression associated with many diseases (Doyle et al. 2012), persistent genetic change often has severe developmental consequences (in worst-case embryonic lethality) complicating studies on adult animals, and adult phenotypes may be influenced by gene expression during embryogenesis (Ray et al. 1997).

Since the 1990s, techniques for manipulating the mouse genome has become more advanced, with improved time- and tissue-specific methods for turning gene expression on or off *in vivo*, such as the Cre-Lox system (Orban et al. 1992) and the tetracycline regulatory system (Gossen & Bujard, 1992). The tetracycline regulatory system comprises of the “tetracycline on” (Tet-On/rtTA) and the “tetracycline off” (Tet-Off/tTA) systems. The key element in the Tet-Off system (fig. 1) is the *tetracycline transactivator* (tTA) that can bind to DNA at certain operator sequences (TetO). A specific promoter, also referred to as a driver, controls the spatial distribution of tTA expression. Different promoter genes can drive the expression of tTA in distinct brain regions or in specific cell types. Binding of tTA to the TetO sequence will induce transgene expression, while administration of tetracycline or one of its derivatives prevents this binding and thereby represses expression of tTA dependent genes.

More than thirty unique promoters with expression within the central nervous system have been utilized to generate Tet-Off mouse lines (Schonig et al. 2013). These lines have successfully been used in studies of a wide range of neurodegenerative conditions, such as Alzheimer’s disease (Harris et al. 2010; de Calignon et al. 2012), prion diseases (Tremblay et al. 1998),

Huntington's disease (Yamamoto et al. 2000) and spinocerebellar ataxias (Zu et al. 2004).

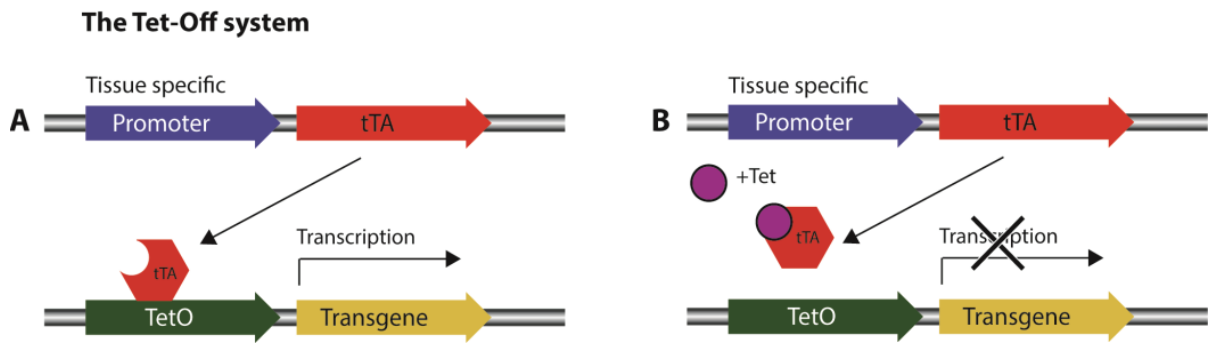


Figure 1 | *How tetracycline prevents transgene expression in the Tet-Off system. A:* A tissue specific promoter controls the expression of the tetracycline transactivator (tTA) protein, which induces transgene expression by binding to a DNA operator sequence (TetO) upstream of the transgene. **B:** Administration of tetracycline (Tet) prevents the binding of tTA to TetO and thereby represses transgene expression. (This simplified scheme is modified after an illustration by BD Biosciences Clontech, BDTM Tet-On and Tet-Off Systems brochure; www.bdbiosciences.com). Tet-On and Tet-Off are registered trademarks of Clontech Laboratories, Inc. in the United States. In the present work, we have used Tet-Off mouse lines.

Since age-related neurodegenerative diseases occur predominantly in humans and rarely occur spontaneously in animals, genetically manipulated mouse models mimicking aspects of the corresponding human diseases are essential in preclinical neuroscience (Jucker, 2010). The genetically altered mouse models serve three major purposes in experimental neurodegenerative research; 1) understanding the physiological function of a gene product (i.e. knock-out mice or transgenic mice overexpressing endogenous protein) 2) providing insight into how genetic mutations relate to neurodegeneration and associated clinical and pathological phenotypes (i.e. knock-out mice, knock-in mice, or transgenic mice overexpressing mutant protein), and 3) preclinical testing of therapeutics (Trancikova et al. 2011). Investigations of genetically altered mouse models of neurodegenerative diseases have been invaluable in

revealing common pathological and molecular features, such as their age dependent and progressive course, the selective degeneration of particular neuronal populations, and mechanisms through which genetic mutations lead to accumulation of misfolded and/ or aggregated proteins (Drechsler et al. 2016).

An ideal disease model accurately replicates the human condition, genetically, physiologically and experimentally (Justice & Dhillon, 2016; Götz et al. 2018). It is important to note, however, that today's models of neurodegenerative disease primarily recapitulate the disease-defining lesions and associated pathologies, and not the human condition as a whole. Despite increasingly sophisticated models, they do not presently display the full range of neuropathological features seen in humans. Numerous models have been created for Alzheimer's disease (Onos et al. 2016), idiopathic amyotrophic lateral sclerosis (Alrafiah, 2018), Parkinson's disease (Moore & Dawson, 2008), spinocerebellar ataxias (Alves-Cruzeiro et al. 2016) and prion disease (Brandner & Jaunmuktane, 2017), each featuring only certain aspects of the human conditions. Even for disorders caused by monogenic mutations, such as Huntington's disease, several models have been created with varying disease progression and pathophysiological changes (Menalled & Chesselet, 2002),

The fact that the genetically engineered models are incomplete (Mullane & Williams, 2019) and the wide range of available models for each disease, means that great care must be taken to select a model appropriate for the questions being addressed in a certain study (Jankowsky & Zheng, 2017). There are examples of how inappropriate models have been used in preclinical trials, leading to subsequently failed clinical trials in humans (e.g. in treatment of amyotrophic lateral sclerosis; Perrin, 2014). Finding the most suitable model requires careful assessment of empirical data on the models phenotypes, for example precise maps of where in the brain the transgenes are expressed, where the neuropathological changes occur, and empirical data on inter-individual endpoint variance for interventional studies. Obtaining, analyzing, organizing and sharing cellular level morphological data from the entire mouse brain is demanding, and

although efforts has been made to compile data based on post-hoc meta-analysis of results (e.g. <https://www.alzforum.org/research-models>) and brain-wide quantitative studies of a few models have recently been conducted (e.g. Whitesell et al. 2018), neuroanatomical characterization of many transgenic lines is still very much incomplete. The limited quantity, quality and reproducibility of morphological data can be ascribed to several challenges:

1. *Large-scale quantitative neuroanatomy requires development of efficient, reproducible pipelines and workflows* for organization, visualization, image analysis, annotation and sharing of huge volumes of image data (Rockland, 2016). So far, few laboratories have access to such infrastructure and workflows, and to date, few brain-wide quantitative mapping studies are available.
2. *Traditional journals have limitations* on the amount of graphical documentation and background research data that can be shared alongside articles.
3. *Disease models are usually created to investigate a specific problem* with experimental focus on selected brain areas, and data outside the immediate scope of a study often remain unanalyzed and unpublished (Schonig et al. 2013).
4. *It is difficult to compare results across lines and interpret reported differences* as data originate from many independent laboratories, using different methods and techniques, and studies are often conducted on a single mouse strain.
5. *Many studies are statistically underpowered* (Jucker, 2010; Button et al. 2013; Nord et al. 2017). Inadequate study design or improper data analysis as factors that limit validity and reproducibility of preclinical studies in which mouse models are used are also addressed by the US National Institute of Health (Collins & Tabak, 2014), further emphasizing the need for high quality baseline data, standardized workflows and quality control.

There are several reasons why preclinical neuroscience should address these challenges and aim towards generation and open sharing of high-quality data. In a broad sense, “making research data widely available to the research community in a timely and responsible manner ensures that these data can be verified, built upon and used to advance knowledge and its application to generate improvements in health” (The Wellcome Trust Policy on Research Data, 2014, www.sanger.ac.uk/legal/assets/policy-and-guidelines.pdf). From an ethical point of view, “scientific findings should be made available to the entire scientific community to allow other researchers to conduct their own analyses and verify the results. Independent replication of research findings is the fundamental mechanism by which scientific evidence accumulates to support a hypothesis” (Merton, 1979). Open data sharing may also reduce the number of research animals that needs to be sacrificed. The concept of “the three R’s” (Replacement, Reduction, Refinement) were introduced by Russell & Burch in 1959 and is included in the laws and regulations on animal welfare in Norway (lovdata.no, forskrift om bruk av dyr i dyreforsøk). Reuse of data may contribute to reduction of duplicate experiments and enable researchers to make more informed choices on which new experiments to conduct. Furthermore, access to a larger pool of data can reveal patterns that are impossible to detect in component data sets, and research data often has inherent value outside the context of the original study.

The potential benefits and current challenges of open data sharing are increasingly recognized by the neuroscience community. Major funding sources, such as the Research Council of Norway, have adopted policies on open access to research data from publicly funded projects (The Research Council of Norway, 2017). The national strategy on access to and sharing of research data by the Norwegian Ministry of Education and Research clearly states that “research data should be shared and reused more widely” (Ministry of Education and Research, 2017). Internationally, over 20 major funders of global health research are connected to The Public Health Research Data Forum that aims to increase the availability and use of health research data (Walport & Brest, 2011). Many journals now encourage, or even require, supporting data to be available from public repositories or to

be published as supplementary material to printed articles (National Institutes of Health, 2017). Recently, representatives from academia, industry, funding agencies, and scholarly publishers designed and endorsed a set of principles referred to as the “FAIR” (Findability, Accessibility, Interoperability, and Reusability) Data Principles, outlining proper collection, curation and conservation of data and metadata with specific emphasis on computerized data mining and data re-use (reviewed by Wilkinson et al. 2016). Implementation of these principles in real-life experimental neuroscience, however, is not a trivial task, and as stated by Silvestri and colleagues: “Contemporary neuroscience is in urgent need of a new generation of neuroanatomical techniques allowing scalable, reliable, specific, and quantitative analysis of macroscopic portions of brain tissue with cellular or sub-cellular resolution” (Silvestri et al. 2015).

Neuroscience is a complex field that includes data from various disciplines, such as anatomy, physiology, genetics, molecular biology, developmental biology and psychology. The challenging enterprise of integrating the increasingly large volumes of diverse data about the brain is a major focus in the field of neuroinformatics. The International Neuroinformatics Coordinating Facility (INCF, www.incf.org), established in 2005, is an independent organization dedicated to promote data sharing by coordinating infrastructure and standards. An important aspect of effective resource sharing is that data, processing methods, workflows, and tools, not only are made publicly available, but that they are made available in a way that ensures reproducibility of published findings (Abrams et al. 2019). Additionally, data should be published with focus on integration and reuse to facilitate new interpretations and extraction of new knowledge (Ferguson et al. 2014). To achieve this, neuroscience needs to adopt common standards for data management and stewardship, such as the FAIR Guiding Principles (Wilkinson et al. 2016), and standards for proper data citation, such as the Joint Declaration of Data Citation Principles (Cousijn et al. 2018).

A number of international neuroanatomy/ neuroinformatics initiatives have been launched during the last decade, dealing with efficient processing and

analysis of large volume datasets, data mining, data visualization and open sharing. Examples include projects concerned with development and maintenance of publicly available image databases containing gene expression data (Heintz, 2004; Lein et al. 2007; Odeh et al. 2011; Smith et al. 2019), high-throughput analysis of such data (e.g. Madisen et al. 2010), development of 3D brain atlases (Dong, 2008; Bowden et al. 2011; Papp et al. 2014a; Kjonigsen et al. 2015; Kuan et al. 2015; Murakami et al. 2018), and projects focused on integrating image data into reference atlases (Sunkin et al. 2013; Amunts et al. 2014; Papp et al. 2014b; Tiesinga et al. 2015; Armit et al. 2017; Bjerke et al. 2018b; Erö et al. 2018; Salinas et al. 2018).

With rapidly developing commercial and open access software solutions, specialized hardware and increasingly faster internet connections, researchers now have the tools to address many of the issues that have limited the quality and volume of available neuroanatomical data from disease models. Nevertheless, with the wide range of different sub-fields, data modalities and new technological possibilities, it is still a challenge to establish, optimize, test and quality control efficient and reliable workflows for data acquisition, organization, analysis, and sharing.

Challenges addressed in this thesis:

The ambition of the present thesis was to address some key challenges for basic neurodegenerative research based on genetically altered mouse models, by use of new tools, infrastructure, and workflows developed in the field of neuroinformatics. We chose to focus specifically on the following challenges:

1. Transgenic mouse models of Alzheimer's disease are increasingly used for experimental interventional studies (Lutz & Osborne, 2013; Gitler et al. 2017; Mullane & Williams, 2019), but empirical evidence about the amount and variability of neuropathological manifestations is frequently scarce (Jucker, 2010; Justice & Dhillon, 2016; Whitesell et al. 2018) and results are often not reproducible (Egan et al. 2016).

2. Selection of the most suitable conditional mouse model for a particular study requires access to detailed empirical data on where in the brain the pharmacologically regulated transgene expression occurs. Presently, however, available neuroanatomical data from different lines are often restricted to some selected brain regions, with limited publicly available documentation of the brain-wide anatomical distribution (Schonig et al. 2013).
3. Several web-accessible data repositories sharing brain-wide histological image data from murine brains are available (e.g. Lein et al. 2007; Bertrand & Nissanov, 2008), including some on transgenic mice (Heintz, 2004; Boy et al. 2006; Odeh et al. 2011), but data available in such repositories are acquired and analyzed with different methods and techniques, and thus difficult to compare across studies.

AIMS AND APPROACH

To address the challenges stated above, we defined our overall objective to be: To establish, optimize, and test workflows for efficient brain-wide evaluation, documentation, and comparison of transgene expression in mouse models of neurodegenerative disease, and to demonstrate how large collections of histological data can be openly shared in accordance with the FAIR Data Principles (Wilkinson et al. 2016).

Specific goals were to:

- Demonstrate how the anatomical location, density and variance of β -amyloid deposits in a transgenic mouse model of Alzheimer's disease can be quantified and used to design interventional studies with adequate statistical power.
- Demonstrate how we can build upon and improve legacy semi-quantitative assessment methods to perform efficient and detailed brain-wide analysis of transgene expression distribution and levels in a tetracycline transactivator driver line frequently used in studies of memory and dementia.
- Demonstrate how novel methods developed in the field of neuroinformatics can be used to map, organize, compare and share data from diverse tetracycline transactivator mouse lines and how such data can be used to address specific neurobiological questions.

Our broad approach was to adopt, refine and improve existing methods for histological evaluation of cellular labeling in rodent brains (Boy et al. 2006; Odeh et al. 2011; Zakiewicz et al. 2011) and apply variations of the resulting workflow in three subprojects in which we analyzed a selection of transgenic mouse models relevant for preclinical neurodegenerative research. In papers I and II, we established efficient methods for brain-wide assessment of the locations, levels and variance of transgene expression. In paper III,

we implemented methods for atlas registration and demonstrated how the anatomical location and levels of transgene expression in mouse brains can be compared across several independent studies by spatially relating microscopic images to a common 3D reference space, and how the atlas-integrated image data could be visualized online and openly shared in agreement with the FAIR Guiding Principles for scientific data management and stewardship.

METHODS

To achieve the stated aims, we first chose to study an Alzheimer's disease model relevant for investigations of β -amyloid accumulation, formation, and clearance, as well as interventional studies evaluating drug effects on β -amyloid plaque load (tg-ArcSwe; paper I). We utilized immunohistochemistry to visualize β -amyloid deposits and optimized digital image analysis techniques to quantify the β -amyloid load in major brain regions (fig. 3). The statistical variance of deposited β -amyloid was calculated and used to estimate appropriate group sizes to achieve adequate statistical power in interventional studies using this model.

For our second sub-project, we chose a tetracycline transactivator (tTA) driver line with reported transgene expression limited to the entorhinal and subicular areas, that had been used in several studies of the entorhinal-hippocampal network and for investigations of transsynaptic spread of pathological proteins in Alzheimer's disease (Nop-tTA; paper II). Since proper interpretation of findings from this model to a large degree relies on the tTA dependent expression to be spatially restricted to specific brain regions, we needed to apply methods with high anatomical granularity. We utilized colorimetric detection of the lacZ gene product β -galactosidase to visualize reporter expression in serial brain sections and applied both brightfield and fluorescence staining methods to reveal the underlying cytoarchitecture for identification of anatomical brain regions. Since the main objective of this study was to establish efficient and reliable methods for anatomical assessment of transgene expression distribution and levels in the entire mouse brain with high anatomical fidelity, it was judged too time consuming to use the image analysis techniques applied in paper I. We therefore refined methods for semi-quantitative evaluation from earlier projects (Boy et al. 2006; Odeh et al. 2011) and developed a visual guide system for scoring labeling densities in brain regions defined by cytoarchitectonic criteria (fig. 4).

In the third sub-project, we wanted to build upon the experiences gained throughout the first two studies and establish an efficient, practical and

generic workflow for brain-wide analysis of transgene expression in mouse models of neurodegenerative disease. We chose to improve and expand upon the semi-quantitative analysis protocol introduced in paper II and optimized the workflow for comparison of different tTA promoter lines. To evaluate the robustness of our methods, we chose to include both newly generated promoter-reporter constructs and legacy data from tTA lines downloaded from the rodent brain workbench (rbwb.org). We utilized recently developed neuroinformatics tools (Puchades et al. 2017) to register all section images to the well-established Allen Mouse Brain Common Coordinate Framework (Oh et al. 2014) and performed a brain-wide assessment of transgene expression distribution and levels in five tTA promoter lines. Atlas plates specifically tailored to fit individual sections were used as visual aids to identify anatomical regions, and expression levels were scored semi-quantitatively using methods derived from paper II. To ease anatomical navigation and facilitate comparison between lines, we broadened the functionality of the online repositories presented in the first two studies by sharing all the histological data with semi-transparent atlas overlays. To ensure that the data were findable, accessible, interoperable and reusable, they were distributed both via the rbwb.org web page and through curated and sustainable services offered by the EU Human Brain Project (www.humanbrainproject.eu).

In the following section, we briefly state the ethical considerations of the present project and outline the workflow for brain-wide evaluation and sharing of neuroanatomical gene expression data from the mouse brain. Second, we provide a brief summary of the most relevant transgenic mouse lines. Third, we detail the individual steps in the workflow, i.e. the animal and operational procedures and the methods employed for image data acquisition, organization, atlas registration, analysis and online sharing.

ETHICAL CONSIDERATIONS

All animal procedures were performed in accordance with the National Institutes of Health Guide for the care and use of laboratory animals and approved by local institutional animal welfare committees associated with the University of Oslo (paper I), Baylor College of Medicine (papers II and III) or the University of Tübingen (paper III). Animal data were acquired in accordance with European Union and International legislation regarding use of animal subjects. For data shared by the Human Brain Project, verification of compliance with European legal and regulatory requirements is provided with the original article (paper III).

WORKFLOW

Based on experience gained throughout this project, we established a generic workflow for efficient brain-wide processing, organization, analysis and sharing of expression data in histochemically labeled sections from mouse models of brain disease. In the following flow chart of experimental design, each black box represents a procedure, while the white boxes represent physical or digital objects. The first block (A) represents all pre-imaging procedures, including generation of genetic models, breeding and housing, experimental procedures (e.g. surgical procedures or pharmacological intervention), tissue processing and histochemistry. Each procedure generates a new physical or digital object, and descriptive metadata. Description of parameters, such as genetic background (animal), sacrifice procedure and tissue fixation methods (tissue), sampling frequency and staining protocols (section) are stored in Navigator3 as metadata and linked to the corresponding image data.

Blocks B and C represent post-histology image acquisition and informatics procedures. In summary, all sections are scanned, and high-resolution images of the sections are organized in the Navigator3 database. Various tools can be applied to perform analyses (e.g. quantitative image analysis or semi-quantitative evaluation of labeling density and distribution) and to facilitate registration of section images to a 3D atlas reference space. Image data, descriptive and positional metadata, and analysis results can be

shared online via an html interface (e.g. rbwb.org) or through external resources such as the EU Human Brain Project data storage facility (www.humanbrainproject.eu).

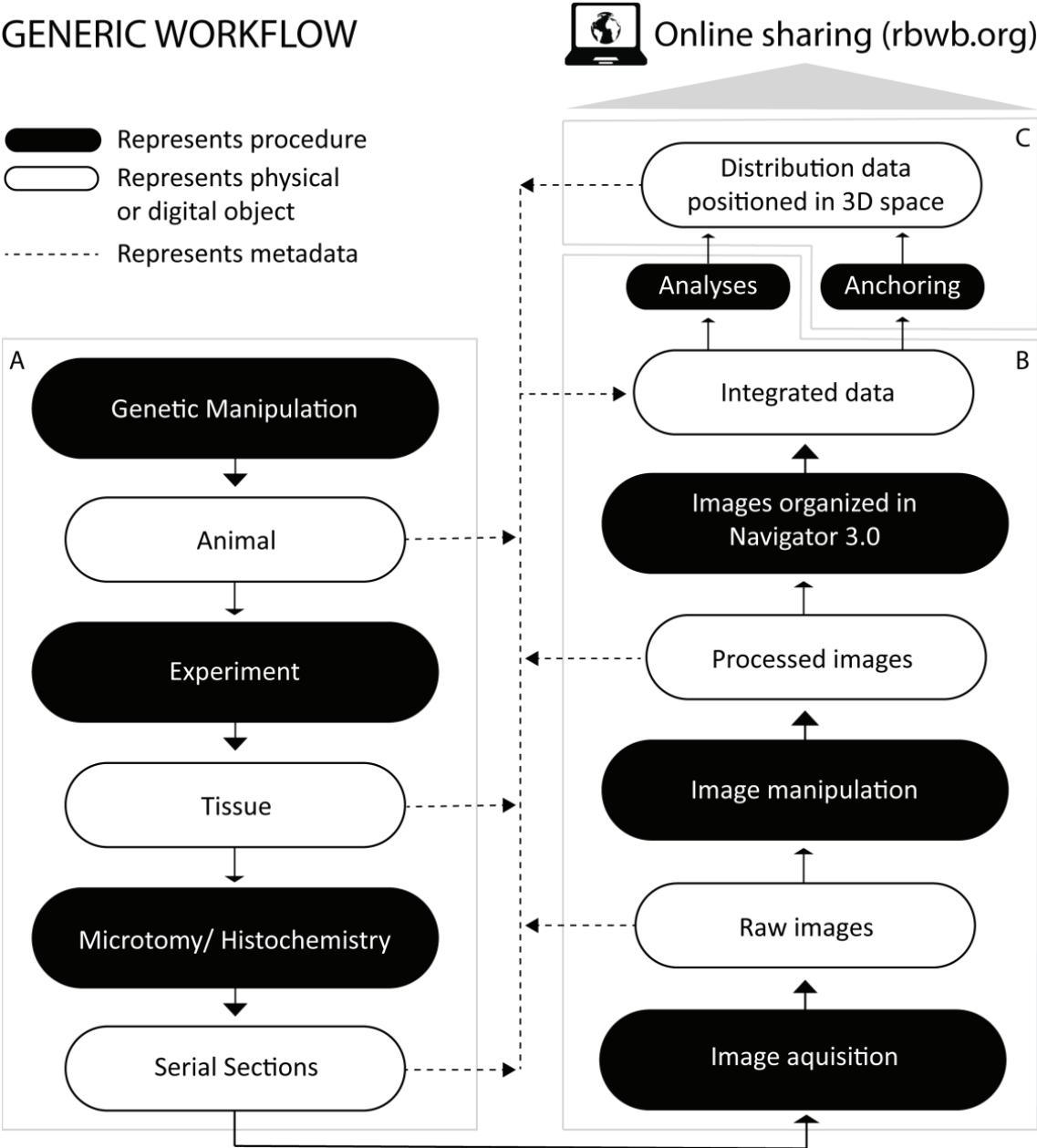


Figure 2 | Workflow. A generic workflow for projects utilizing neuroinformatics to organize, analyze and share gene expression data derived from digital images of histological sections from the mouse brain. Block A and B are relevant for paper I-III, while block C (anchoring) was only applied in paper III.

Disease models and tTA driver lines evaluated in this thesis:

tg-ArcSwe (Lord et al. 2006): The tg-ArcSwe Alzheimer's disease model carries both the Arctic and the Swedish APP mutations. Inclusion of the Swedish mutation triggers pathological changes at an earlier age than models using the Arctic mutation alone. The tg-ArcSwe model has a marked phenotype with early age-dependent intraneuronal β -amyloid accumulation (Lord et al. 2006; Philipson et al. 2009b) and insoluble β -amyloid deposits similar to the plaques found in human Alzheimer's disease patients (Philipson et al. 2009a). In recent years, tg-ArcSwe mice have been used e.g. in studies of Alzheimer's disease neuropathology (Yang et al. 2017), early diagnosis (Hultqvist et al. 2017) and immunotherapy (Tucker et al. 2015).

Neuropsin(Nop)-tTA (Yasuda & Mayford, 2006): Also referred to as Klk8-tTA, Prss19-tTA, EC-tTA, and tTA-EC. tTA models utilizing the Nop promoter have been used to study activity-dependent competition in the entorhinal–hippocampal circuitry (Yasuda et al. 2011) and to identify a novel monosynaptic connection between the entorhinal cortex and hippocampal area CA2 (Rowland et al. 2013). Nop-tTA models have also become popular in studies examining the propagation of abnormal protein aggregates in Alzheimer's disease (e.g. Harris et al. 2010; Pickett et al. 2017).

Pituitary homeobox 3(Pitx3)-tTA (Lin et al. 2012): The Pitx3 protein is a transcriptional regulator important for the differentiation and maintenance of meso-diencephalic dopaminergic (mdDA) neurons during development. Pitx3-tTA mice has predominantly been used in studies of Parkinson's disease, for example to evaluate the role of Leucine rich kinase 2 (Liu et al. 2015) and α -synuclein (Lin et al. 2012; Sastry et al. 2015).

Purkinje cell protein 2 (Pcp2)-tTA (Zu et al. 2004; Echigo et al. 2009): Purkinje cell protein 2 is known to be expressed specifically in cerebellar Purkinje cells and retinal cells. The Pcp2-tTA line has earlier been used to drive conditional expression of mutant ataxin-1 in mice models of spinocerebellar ataxia type 1 (Zu et al. 2004) and to examine the role of mutant type β -III spectrin in spinocerebellar ataxia type 5 (Armbrust et al. 2014). Available from Jackson Laboratory, Jax stock # 5625, www.jax.org/strain/005625.

Calmodulin-dependent protein kinase II (Camk2a)-tTA: Also referred to as CamKII-tTA. The Camk2a promoter has earlier been shown to be primarily distributed within the gray matter of the forebrain (Odeh et al. 2011). Camk2a-tTA mice have been used to investigate a number of neurological and psychological conditions, including Huntington's disease (Yamamoto et al. 2000), Parkinson's disease (Nuber et al. 2008), schizophrenia (Pletnikov et al. 2008), and to study how conditional tau suppression affect memory function in Alzheimer's disease (SantaCruz et al. 2005). Available from Jackson Laboratory, Jax stock # 7004, www.jax.org/strain/007004.

Prion protein (Prnp)-tTA (Tremblay et al. 1998): Also referred to as PrP-tTA. High levels of cellular prion protein are mainly distributed in the brainstem and cerebellum, but also in several other brain regions (Boy et al. 2006). The Prnp-tTA line has been used to study a wide range of brain disorders, including prion diseases (Tremblay et al. 1998), dystonia (Goodchild & Dauer, 2004), alcoholism (Choi et al. 2002), and Alzheimer's disease (Melnikova et al. 2016). Available from Jackson Laboratory, Jax stock #18124, www.jax.org/strain/018124.

GENE CONSTRUCTS, TISSUE PROCESSING AND HISTOCHEMISTRY

tg-ArcSwe

The tg-ArcSwe mouse line was initially developed by our collaborators, Lars Nilsson and colleagues (Department of Pharmacology, University of Oslo and Oslo University Hospital, Oslo, Norway). Tissue processing and histochemistry were performed by Reidun Torp and colleagues (Department of Anatomy, Institute of Basic Medical Sciences, University of Oslo, Norway). The model was generated by incorporating human APP cDNA with the Swedish mutation (KM670/671NL) and the Arctic mutation (E693G) into the genome of C57BL/6-CBA-F1 mice, as detailed by Lord and colleagues (Lord et al. 2006).

Sagittal sections from the right brain hemispheres were cut at 25 μm using a freezing microtome. The primary protocol used to visualize β -amyloid deposits is detailed by Phillipson and colleagues (Phillipson et al. 2009a) and in paper I. In brief, sections were incubated with primary antibody A β x-40, secondary antibody biotinylated goat anti-rabbit antibody and streptavidin-biotinylated horseradish peroxidase complex. After histochemical processing, β -amyloid deposits appeared microscopically as intensely stained, dark brown elements contrasting a light brown background (fig. 3). Additionally, ultrathin sections from the cerebral cortex were labeled with A β x-40 and 6E10 antibodies and analyzed with a transmission electron microscope to visualize plaque ultrastructure and verify the specificity of the A β x-40 antibody.

tTA-lines

Our collaborators at the Joanna Jankowsky Laboratory (Departments of Neuroscience, Huffington Center on Aging, Baylor College of Medicine, Houston, TX, USA) were responsible for breeding, tissue processing and histochemical processing of non-legacy tTA mice (paper II and III). In short, mice expressing humanized tTA under control of various promoters (i.e. Nop, Pitx3, and Pcp2) were crossed with reporter mice encoding an in-frame fusion of the *E. coli* lacZ gene with green fluorescent protein (GFP)

under control of the tetO promoter to generate bigenic promoter-tTA/tetO-lacZ-nls-GFP offspring.

Brains were sectioned at 35-45 μm using a freezing-sliding microtome. Both horizontal and coronal series were cut as close as possible to resemble the cutting angles used in the stereotaxic atlas of the mouse brain (Franklin & Paxinos, 2013). A reliable and frequently used β -galactosidase assay (Cepko et al. 1998) was chosen as our primary method for expression analyses. The β -galactosidase enzyme is the gene product of the lacZ gene and cleaves lactose into glucose and galactose. β -galactosidase also cleaves X-gal, a lactose analog, into galactose and 5-bromo-4-chloro-3-hydroxyindole. The latter spontaneously dimerizes and is oxidized into an insoluble, intensely blue, product (5,5'-dibromo-4,4'-dichloro-indigo). In this way, the assay visualized brain tissue where tTA dependent β -galactosidase activity occurred (fig. 4). The X-gal/ β -galactosidase assay was applied together with counterstains (Neutral Red, Nuclear Fast Red or Cresyl Violet) to reveal the underlying cytoarchitecture.

To exclude possible interference from endogenous β -galactosidase, sections adjacent to those used for X-gal staining were processed to detect the co-expressed green fluorescent protein (GFP) reporter. 4',6-diamidino-2-phenylindole (DAPI) was used as counterstain for fluorescence microscopy. Amyloid plaques in Nop-APP mice were visualized with Campbell-Switzer silver stain. Finally, tyrosine hydroxylase and calbindin immunohistochemistry was used to identify dopaminergic cells in Pitx3-tTA mice and Purkinje cells in Pcp2-tTA mice respectively.

IMAGE ACQUISITION, ORGANIZATION AND ONLINE SHARING

Whole slide imaging

In the present work, two generation of slide scanners and commercial software were used to generate high-resolution brightfield and fluorescence digital slides; a Mirax Scan slide scanner (Carl Zeiss MicroImaging, Jena, Germany) running Panoramic Viewer software (3DHistec, Budapest, Hungary) was replaced by an Axio Scan Z1 (Carl Zeiss MicroImaging, Jena, Germany) running Zen software (Carl Zeiss MicroImaging, Jena, Germany). Slides were scanned using 20X objectives, and the digital slides were stored as tagged image format (TIFF) files.

The Navigator3 platform

The Navigator3 platform, developed by the Neural Systems Laboratory (NeSys, University of Oslo, Norway), is an image management system used for organizing and serving collections of large histological images (Moene et al. 2011). The platform provides web-microscopy viewer functionality and integrated tools, including the in-house LocaliZoom tool with functionalities for displaying microscopic images with atlas overlays, annotation functionality, and a viewer tool for three-dimensional (3D) visualization of annotated points of interest together with 3D surface models of the Allen Mouse Brain Atlas. Digital images are imported via file transfer protocol (FTP) and converted to Deep Zoom image files (using open source Bio-Formats libraries; www.openmicroscopy.org) and low-resolution Portable Network Graphics (.png) preview images. The Deep Zoom format allows users to interactively pan and zoom high-resolution images in a web browser. Images are stored at servers hosted by the Norwegian Neuroinformatics Node, University of Oslo, with all preprocessing performed server-side. Both the original and preview images are available for download. In filmstrip viewer mode, series of digital slides are numerically organized by filename with thumbnail (preview) images of each slide in a “filmstrip”, allowing users to navigate efficiently between slides (fig. 3a).

Spatial registration (anchoring)

Image registration is a key step in a variety of biomedical imaging. It refers to the ability to geometrically align one dataset with another, and is essential for comparing datasets across subjects, imaging modalities, and over time. Image registration algorithms may facilitate data pooling and comparison of experimental findings across different laboratories, construction of population-based brain atlases, and the creation of systems to detect group patterns in imaging data. In the context of the present work, we refer to “anchoring” as the process of registering a two-dimensional image to a three-dimensional reference space using only linear transformations.

Images were anchored to a volumetric version of the Allen Mouse Common Coordinate Framework (CCF) version 2 (Oh et al. 2014; available from mouse.brain-map.org) using the QuickNII software tool for registration of section images (Puchades et al. 2017). This semiautomatic tool provided custom mouse brain atlas plates cut at angles of orientation matching the experimental images, which could compensate for variations in tissue cutting angle. The custom atlas plates were interactively tuned to match the spatial position of the histological sections, superimposed on section images, and linearly transformed to establish a global match with anatomical landmarks (fig. 4c). After a satisfying global match in one section was achieved, spatial transformation parameters were propagated across series of sections. Each custom atlas plate was subsequently adjusted manually to match the corresponding section image. Vectors describing the spatial relation between a section and the 3D atlas space were stored in Navigator3 as metadata. The spatial positions of points of interest could be recorded as xyz-coordinates within the CCF using the annotation tool in the LocaliZoom viewer and co-visualized together with atlas structures in a 3D viewer.

Data and custom code availability

Image data repositories from the first two studies (papers I and II) were made publicly available through The Rodent Brain Workbench (www.rbwb.org), a webpage that serves as a portal to several collections of

brain mapping and atlas resources. The Rodent Brain Workbench is developed and maintained by the Neural Systems Laboratory, University of Oslo. For our third project (paper III), image data, analysis results and metadata were additionally shared through services for data storage, management, and data curation offered by the EU Human Brain Project (HBP; www.humanbrainproject.eu; Amunts et al. 2016) to make data publicly available in accordance with the FAIR guiding principles (Wilkinson et al. 2016) as data that are Findable, Accessible, Interoperable, and Reusable. The HBP curation service offers DataCite (<https://datacite.org>) DOIs for each data set, structured metadata describing basic parameters on data provenance, compliance with regulations on ethical conduct, conditions and license for data sharing, as well as validated location metadata defining the location of data in the Allen Mouse Common Coordinate Framework. The primary image data in the repositories are shared in standard Tagged Image File Format (TIFF) that can be viewed and analyzed with a range of other tools. The software used to register images to atlas (QuickNII) is shared via the Human Brain Project Collaboratory platform for sharing of tools and workflows, which is available from the HBP webpage following registration.

DISTRIBUTION AND DENSITY ANALYSES

Quantitative image analyses and statistics

From each tg-ArcSwe animal, three sagittal sections from the right hemisphere were used for image analysis. Sections were selected at corresponding distances from the midline in all animals; each including parts of our main regions of interest (ROIs), the cerebral cortex, the hippocampus, and the thalamus.

The β -amyloid plaque load in the hippocampus, the thalamus and the cerebral cortex was evaluated quantitatively. In each section, the outlines of these regions were manually delineated based on predefined anatomical criteria using Image J 1.46r (<http://imagej.nih.gov/ij>). Within each ROI, images were binarized (converted to black and white) by selecting a threshold value in Image J which yielded plaque boundary definitions best

corresponding to the observed, expert-evaluated, plaque boundaries (fig. 3c). The ROI areas and the labeled areas were calculated, and β -amyloid plaque load was subsequently calculated as area fraction (the area of labeled objects within a ROI divided by the ROI area). For each animal, the mean area fractions of three sections were used for analysis of variability and statistical power. Statistical analyses were performed using InStat (GraphPad Software, San Diego, CA, USA).

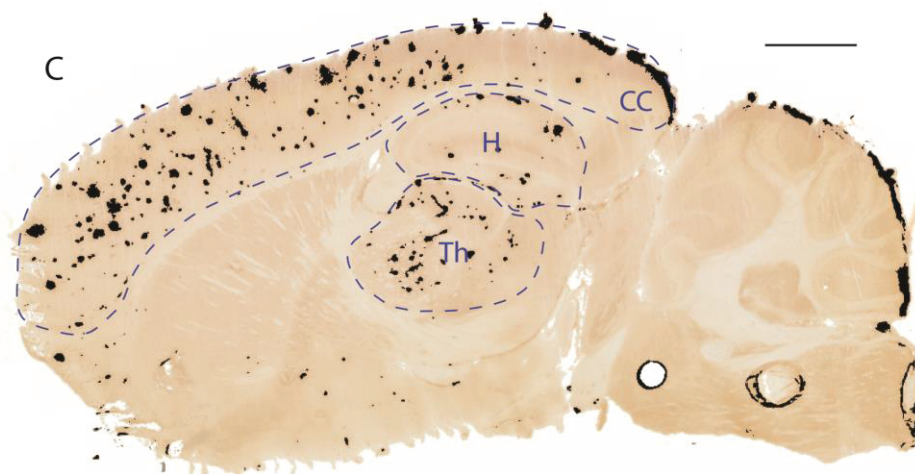
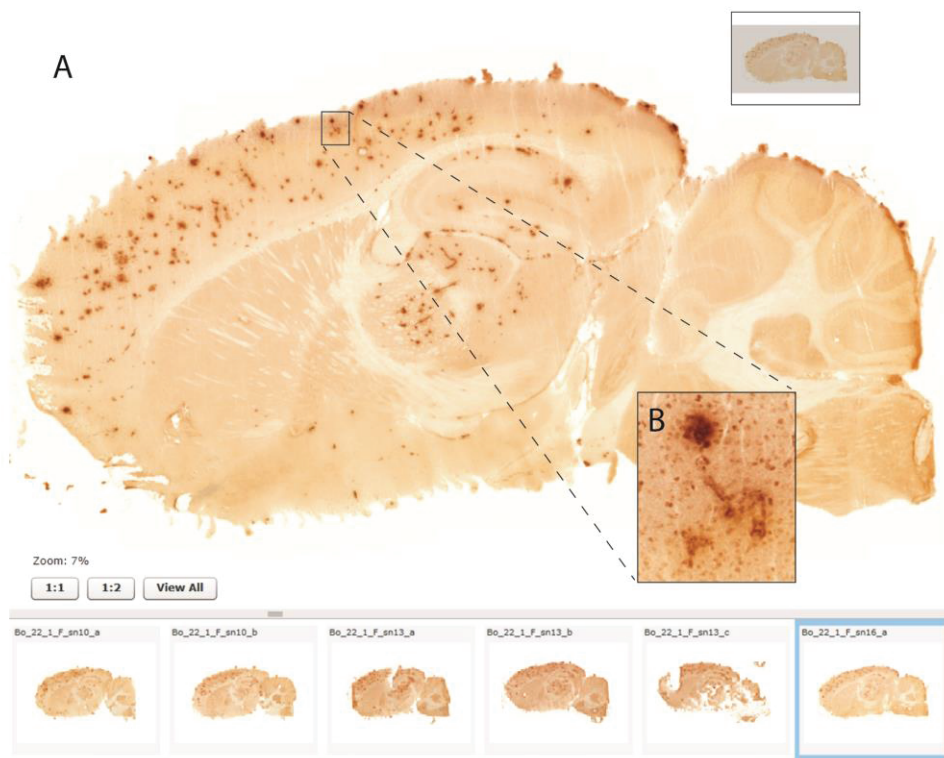


Figure 3 | *Navigator3 graphical user interface / quantitative image analysis. A:* A sagittal A β x-40 labeled section as displayed in the online filmstrip viewer repository. Labeled β -amyloid appears dark brown on a light brown background. The main image can be zoomed and panned, and the preview images can be used to navigate between sections. **B:** High-resolution inset showing a dense β -amyloid plaque and looser β -amyloid deposits. All parts of the section can be interactively zoomed to similar resolution with the online viewer tool. **C:** Principle illustration of the quantitative image analysis procedures. The main regions of interest (ROIs), the cerebral cortex (CC), the Hippocampus (H), and the Thalamus (Th), were manually delineated based on anatomical criteria. Labeled β -amyloid (here visualized as black elements) was separated from the background with a thresholding algorithm, and β -amyloid load calculated as are fraction (labeled area divided with ROI area). *Scale bar 1 mm.*

Semi-quantitative assessment

Earlier studies from the NeSys group have evaluated tTA dependent transgene expression in the Prnp-tTA (Boy et al. 2006) and the Camk2a-tTA (Odeh et al. 2011) lines. In these studies, the anatomical granularity was tailored to the specific lines, with greater anatomical detail in areas with much labeling and lower fidelity in areas where labeling was sparse. A similar approach was chosen for the analysis of the Nop-tTA line (paper II), where the main focus was to evaluate whether promoter expression was strictly limited to the entorhinal cortex and the pre-/parasubiculum as reported in earlier studies. The need for high anatomical granularity was therefore highest in these and surrounding brain areas. Each region was carefully delineated based on cytoarchitectonic criteria. Labeling densities, reflecting β -galactosidase activity, were assessed using a grading system from 0 to 4. To facilitate fast and reproducible analyses, we developed a visual guide with defined criteria for each density category (fig. 4e).

A similar semi-quantitative approach was chosen in paper III, where the aim was to perform a brain-wide comparison of reporter distribution and density for five different tTA promoter lines (Nop, Pitx3, Pcp2, Camk2a, and Prnp) with highly diverging expression patterns. Since manual delineation of all sections with high anatomical fidelity were considered to be very time consuming and inefficient, we developed a workflow where section images

were first anchored to a downscaled version of the 3D Allen Mouse Brain Reference Atlas with ~200 distinct brain regions. After anchoring, semi-transparent custom atlas plates were superimposed on section images to identify each anatomical brain region, and the density of X-gal labeling in each brain area was evaluated and scored according to the visual guide.

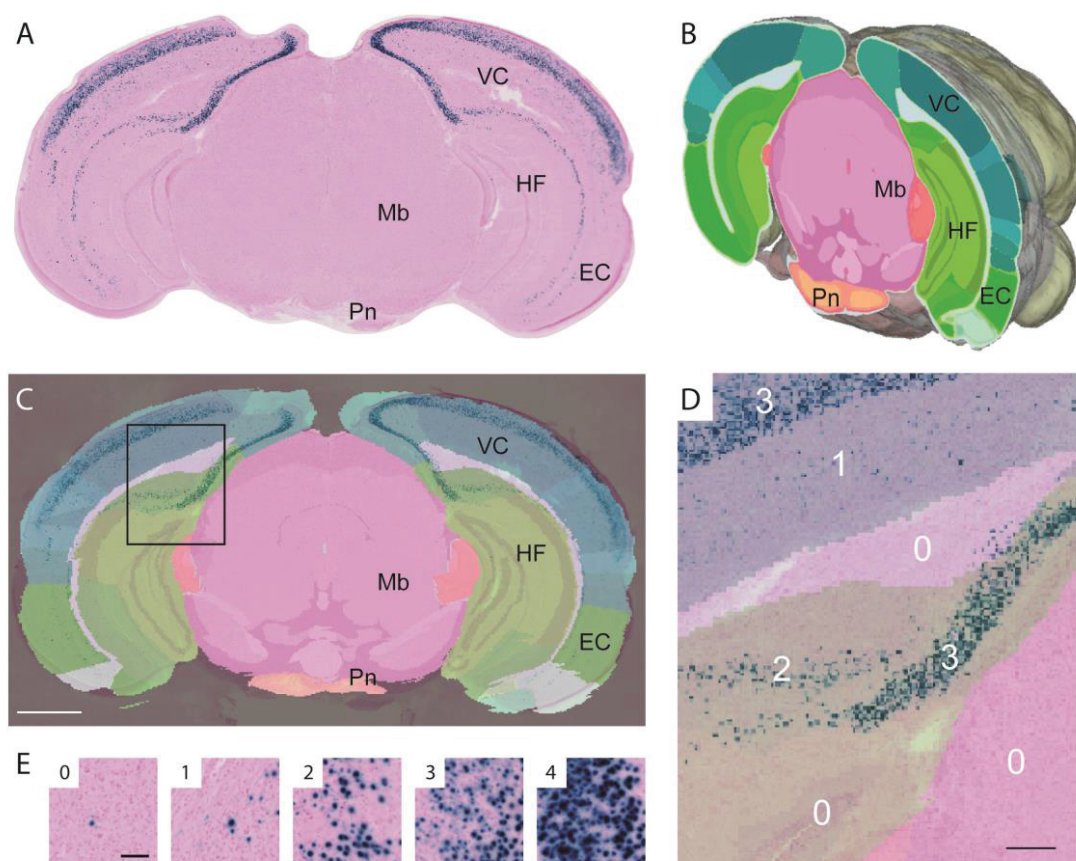


Figure 4 | *Atlas registration and semi-quantitative analysis.* **A:** Coronal X-gal and Nuclear Fast Red stained section from a Nop-tTA-lacZ mouse. Cells with tTA dependent β -galactosidase activity appear as dark blue spots on a pink background. **B:** A corresponding custom atlas cut from the 3D Allen Mouse Brain Reference Atlas. **C:** The custom atlas plate is superimposed on the original section image to match global anatomical landmarks. **D:** Individual brain regions are scored according to the grading system shown in E. Anatomical segmentation is aided by the atlas overlay. **E:** Visual guide for semi-quantitative density analysis (adapted from paper II). Abbreviations: EC, entorhinal cortex; Mb, midbrain, HF, hippocampal formation; Pn, pontine nuclei, VC, visual cortex. *Scale bar* 1 mm (**a,c**), 200 μ m (**d**), 100 μ m (**e**)

RESULTS

SUMMARY OF PAPERS I-III

PAPER I

Brainwide distribution and variance of amyloid-beta deposits in tg-ArcSwe mice.

Lillehaug S*, Syverstad GH*, Nilsson LN, Bjaalie JG, Leergaard TB, Torp R.

Neurobiology of Aging 35:556-64, 2014.

DOI: [10.1016/j.neurobiolaging.2013.09.013](https://doi.org/10.1016/j.neurobiolaging.2013.09.013)

PMID: 24126157

*These authors contributed equally to this work

There are currently many mouse models available featuring different aspects of Alzheimer's disease, but no single model can reproduce the full spectrum of histological and biochemical changes seen in humans. Selecting an appropriate model and estimating the number of specimens needed for a specific experimental setting is challenging and relies on the availability of high-quality empirical data describing the models different phenotypes.

The tg-ArcSwe double APP transgenic mouse is considered a promising model for investigations of intraneuronal β -amyloid accumulation in Alzheimer's disease, as well as formation and clearance of amyloid plaques. Our first ambition with this study was to establish a workflow for quantitative assessment of β -amyloid load in immunolabeled sections and apply this workflow to provide empirical data on the spatial distribution, amount, and variability of accumulated β -amyloid in major brain regions (i.e. the cerebral cortex, the thalamus and the hippocampus) in adult male and female tg-ArcSwe mice. Second, we aimed to utilize the quantitative data to estimate suitable group sizes for future interventional studies using changes in β -amyloid load as endpoint. Third, we wanted to assess plaque morphology qualitatively and perform a brain-wide, semi-quantitative evaluation of β -amyloid distribution and load using virtual microscopy techniques. Finally, we aimed to share the high-resolution image data in a

publicly available online repository to facilitate external evaluation and reanalysis of the morphological characteristics and spatial distribution of β -amyloid in the tg-ArcSwe mouse brain.

In this publication we presented:

- Quantitative analysis of the area fraction occupied by β -amyloid in the cerebral cortex, the thalamus and the hippocampus, showing that β -amyloid plaque deposits are consistently present in these regions.
- Brain-wide, semi-quantitative assessment of β -amyloid distribution, demonstrating that β -amyloid deposits were variably present in all major brain regions.
- Qualitative assessment of plaque morphology with particular focus on vessel-related amyloid deposits.
- Statistical analyses showing no significant differences in β -amyloid load in male and female mice.
- Statistical power analyses indicating that group sizes needed for reliable results in interventional trials using changes in β -amyloid load as endpoint is higher than commonly used.
- An online image repository containing high-resolution serial section images from two representative animals (one male and one female) and a selection of additional images exemplifying interesting morphological phenomena.

The tg-ArcSwe image repository is available through the Rodent Brain Workbench web portal (rbwb.org: tg-ArcSwe Atlas)

PAPER II

Transgene expression in the Nop-tTA driver line is not inherently restricted to the entorhinal cortex.

Yetman MJ*, Lillehaug S*, Bjaalie JG, Leergaard TB, Jankowsky JL.

Brain Structure and Function 221:2231-49, 2016.

DOI: 10.1007/s00429-015-1040-9

PMID: 25869275

*These authors contributed equally to this work

The entorhinal cortex is important for episodic memory and is one of the earliest brain regions to be affected by Alzheimer's disease. Conditional regulation of transgene expression in this region is therefore an important tool for researchers studying memory function and dementia. To achieve this, several studies have used a transgenic line where the tetracycline transactivator (tTA) is controlled by the neuropsine (Nop) promoter. The Nop-tTA line was initially developed by Yasuda and Mayford (Yasuda & Mayford, 2006) and was reported to display conditional transgene expression restricted to the enthorhinal cortex and the pre-/parasubiculum. Although interpretation of results from experiments using this driver line depends on the spatial specificity of the promoter, no detailed brain-wide neuroanatomical evaluation of tTA depend transgene expression had been conducted.

Our ambition was to perform such an assessment, after developing a reliable experimental design for comprehensive, brain-wide evaluation of the spatial distribution and levels of transgene expression based on colorimetric detection of the lacZ gene product β -galactosidase (reflecting tTA promoter activity). Since we aimed to perform a brain-wide evaluation of labeling densities with high anatomical granularity, we chose to adapt semi-quantitative assessment methods used in earlier studies (Boy et al. 2006; Odeh et al. 2011) and implemented a novel visual guide system to

improve efficiency and reproducibility. We also wanted to make the complete set of histological image data publicly available as a resource for scientists currently using, or planning to use, the Nop-tTA driver line their research.

The main findings in this study were:

- Reproducible, semi-quantitative assessment of the spatial distribution and density of labeled elements covering the entire brain can be performed relatively fast and with high anatomical fidelity by scoring each brain region aided by a visual guide system.
- The highest density of tTA dependent reporter expression was found in the entorhinal cortex and pre-/parasubiculum, but there was also considerable expression in several other cortical areas.
- Ectopic transgene expression may account for the appearance of pathological protein aggregates outside the entorhinal cortex in tTA models of Alzheimer's disease utilizing the neuropsin promoter. Our results suggest caution when designing experiments that depend on precise localization of gene products controlled by the Nop promoter or other spatially restrictive transgenic drivers.
- Publicly sharing the complete data behind analyses facilitates transparency and reproducibility and may provide valuable reference data to external researchers.

The Nop-tTA image repository is available through the Rodent Brain Workbench web portal (rbwb.org: tTA/TetOff Atlas: Nop).

PAPER III

Brain-wide distribution of reporter expression in five transgenic tetracycline-transactivator mouse lines.

Lillehaug S, Yetman MJ, Puchades MA, Checinska MM, Kleven H, Jankowsky JL, Bjaalie JG, Leergaard TB.

Scientific Data 6:190028, 2019

DOI: [10.1038/sdata.2019.28](https://doi.org/10.1038/sdata.2019.28)

PMID: 30806643

A number of tTA transgenic mouse lines with expression in the brain have been generated for various experimental purposes. Detailed information about where in the brain and to what extent the transgenes are expressed is important for selecting suitable driver lines when studying specific brain regions, brain circuits, or pathological conditions. Despite this need, comparison of expression patterns between different lines has historically been difficult because of varying methods used to locate transgene expression as well as considerable variation in spatial granularity and scope of analyses.

To address the challenges of cross-model comparison, we aimed to develop a generic workflow for analysis of transgene expression distribution and levels in histological mouse brain sections, utilizing atlas registration and semi-quantitative analysis techniques. Second, we wanted to apply this workflow to analyze two new promoter-reporter crosses with presumably spatially restrictive transgene expression, and further verify the utility of the workflow by re-analyzing three previously published datasets from tTA mice with highly diverging expression patterns. Finally, we aimed to present the results in a way that facilitated comparison of expression patterns across the five driver lines (Nop, Pitx3, Pcp2, Prnp, and Camk2a), and share the complete data in accordance with the FAIR guiding principles for scientific data management and stewardship (Wilkinson et al. 2016).

In the article we presented:

- An atlas of X-gal labeled serial microscopic images showing tTA dependent reporter expression in five frequently used promoter lines, with all images spatially registered to the Allen Mouse Common Coordinate Framework and presented with semi-transparent overlays of custom atlas plates.
- Image data, metadata, and tools shared via the EU Human Brain Project (HBP) services for data storage, management, and data curation, making the data findable, accessible, interoperable, and reusable.
- A tabular interpretation of transgene expression distribution and levels in 245 distinct brain regions, semi-quantitatively scored from 0-4 aided by a visual guide and atlas overlays.
- Proof of concept of how 3D atlas registration facilitates easy identification of large numbers of anatomical regions in histological mouse brain sections and examples demonstrating how histological data registered to a common reference space may be utilized to address specific neurobiological questions.
- Evidence of spatially and cell-type specific lacZ/GFP reporter expression under control of the Pitx3 and Pcp2 promoters, confirming earlier reports from these driver lines based on other promoter-reporter constructs.

The tTA atlas is available through the Rodent Brain Workbench web portal (rbwb.org: Brain Atlas of tTA driver lines). High-resolution images and associated metadata are also shared via the web page of the EU Human Brain Project (www.humanbrainproject.eu).

DISCUSSION

Our main ambitions with this work was to establish, optimize, and test workflows for brain-wide evaluation of transgene expression in mouse models of neurodegenerative disease, and to demonstrate how large collections of histological data can be openly shared in accordance with the FAIR Data Principles (Wilkinson et al. 2016). To this aim, we optimized and refined methods for brain-wide (semi-)quantitative assessment of the locations, levels and variance of transgene expression and used these methods in analyses of the tg-ArcSwe and Nop-tTA mouse lines. The different methods were organized in a streamlined workflow and applied to datasets from five tetracycline transactivator mouse lines, demonstrating how the anatomical location of cellular labeling in mouse brains can be compared across several studies by spatially relating microscopic images to a common mouse brain reference atlas. Image data were openly shared through services for data storage, management, and data curation offered by the EU Human Brain Project (www.humanbrainproject.eu) and/or the Rodent Brain Workbench web portal (rbwb.org). In the following section, we discuss the validity of the applied methods, the implications of the main findings and the scientific impact of the present work.

VALIDITY OF METHODS

Quantitative image analysis

The quantitative image analysis procedure used in paper I was based on methods outlined by Papp and colleagues (Papp et al. 2016) and adapted to suit the A β x-40 stained sections from tg-ArcSwe mouse brains (fig. 3). The method relies on computerized separation of signal (labeled elements) from noise (background and artifacts). This separation can be based on differences in shape, size, color or contrast. In the A β x-40 labeled sections from tg-ArcSwe mouse brains, both labeled β -amyloid and background were colored brown, but the amyloid deposits stained more intensely. We utilized this difference to separate labeling from background and calculate the area

occupied by β -amyloid within our regions of interest (the hippocampus, the thalamus, and the cerebral cortex) by applying a thresholding algorithm in Image J 1.46r (<http://imagej.nih.gov/ij>). Several factors might have influenced the results of the quantitative image analyses; 1) the exact threshold value was determined based on microscopic expert evaluation, and thus involved some degree of subjective interpretation. 2) The anatomical delineations of the regions of interest were performed manually. To some extent this also involved subjective evaluation but was judged unlikely to account for much variation since the boundaries of the selected regions were clearly visible in the sections and defined by robust anatomical criteria. 3) The histochemical processing may also have affected the results of the quantitative image analysis. Although we carefully used the same protocol across all specimens, we found that the background in some sections stained slightly darker than in others. To compensate for these differences, we applied a normalization filter (Sedgewick, 2008) with an A β x-40 stained section from a wild-type mouse without any amyloid plaques as reference. Still, differences in staining intensity might have marginally contributed to variation between specimens.

Atlas integration and semi-quantitative analysis

Although quantitative methods generally are preferable, there are currently limitations to where methods such as the quantitative image analysis described in the previous paragraph are applicable. Unless computer algorithms can be applied to perform automatic segmentation of brain regions, such analyses are very time consuming to perform with high anatomical fidelity across the entire mouse brain. For the current project, automatic delineation using computerized atlas registration procedures was a theoretical option for paper II and III, but the methods available at the time were considered too unprecise to yield reliable results. It was feasible to manually delineate a selection of brain regions in few sections, or few regions in many sections, while brain-wide manual delineation of numerous regions in a large number of sections were considered too time consuming to be a realistic option. We also considered applying unbiased stereology methods, but this would also require considerable manual involvement (i.e.

anatomical delineations, protocol setup and counting for ~200 brain regions).

Since we aimed to achieve a brain-wide and efficient interpretation of the spatial distribution and levels of transgene expression with high granularity (paper II-III), we chose to build upon earlier work (Boy et al. 2006; Odeh et al. 2011) to create a workflow for semi-quantitative analysis using custom atlas overlays to define anatomical regions, and a novel visual guide system (fig. 4e) for scoring expression levels in individual brain regions. Two factors in this semi-quantitative assessment procedure were influenced by subjective interpretation. First, the anchoring procedure, where custom atlas slices were superimposed onto section images and linearly transformed to match anatomical landmarks, would never be performed exactly the same by two different operators, and could thus introduce small variations in the boundaries of anatomical regions. Second, the evaluation of labeling density using the semi-quantitative grading scale was to some degree subjective, especially in areas where the labeling density did not clearly correspond to a certain category and in areas with varying expression levels.

To evaluate whether these factors influenced the reproducibility of our results, we performed a pilot study where three different individuals with little prior experience with the method were asked to analyze the complete series of sections from one Nop-tTA mouse. One post-doctoral neuroscientist, one master degree researcher, and one master student, each spent 3-5 hours analyzing 171 regions in 45 sections. They used the QuickNII software tool for registration of section images (Puchades et al. 2017) to adapt custom atlas plates to corresponding sections and scored the labeling density within each anatomical region from 0-4 aided by a visual guide (fig. 4). The three pilot testers scored 126 areas equally, and 43 regions had scores varying with ± 1 . In only two regions did the score vary with more than ± 1 . The scoring of areas with very sparse labeling (scored 0 or 1) varied the most. This may be due to slight variations in atlas anchoring or difficulties in interpreting the “less than 1 per 0.01 square millimeters” criteria. Overall, we concluded that the semi-quantitative analysis pipeline was adequately reproducible, and it emerged as a relatively fast way to

produce meaningful interpretations of the spatial distribution and levels of transgene expression in our material.

Workflow

The selection and interpretation of genetically altered disease models requires comprehensive and detailed background data about e.g. genetic background, behavioral alterations, and the neuroanatomical phenotypes occurring in each model. Especially for experiments with conditional models, where restriction of transgene expression to specific cell types or brain regions at specific developmental stages often are key elements, having access to detailed data describing where in the brain and at what level the transgenes of interest are expressed can be crucial for experimental success. Our workflow, although producing meaningful interpretations of expression levels and anatomical distributions, still has room for further optimization and refinement when it comes to the speed and precision of serial section analysis.

Basic biological factors, such as animal breeding time, are difficult to influence. We found, however, that optimizing the histochemical processing protocol significantly reduced the degree of manual involvement needed during steps further down the workflow. In traditional, microscopy-based, microanatomy, factors such as mounting angle, number of sections per slide, minor artifacts, background homogeneity etc., plays little role since the human brain is able to ignore most noise. In a digital environment, variations have to be corrected manually or by custom computer algorithms. Either way, such corrections are tedious and time consuming when working with terabyte-sized images. We found that investing a little extra time in mounting fewer sections per slide, detailed labeling of slides, taking care in always mounting sections in the same order from top to bottom on a slide etc. was more than compensated for by the reduced time needed for digital image processing and organization.

The image acquisition process was improved by upgrading from a relatively slow Mirax Scan slide scanner to a more advanced Axioscan Z1. Some time and expertise were needed to configure prescan software parameters, but

with the new technology, slide scanning was no longer a rate-limiting step in the workflow. Whole Slide Imaging solutions will presumably continue to improve in both quality and efficiency in years to come.

The greatest potential for workflow improvements lies on the software side. During this project, development of specialized software solutions for image processing, image analysis and atlas registration were still in an early phase. Many steps in the atlas anchoring procedure had to be performed semi-automatically or manually. For example, although generated bitmap custom atlas plates were valuable aids during semi-quantitative analysis, they could not automatically be used to delineate regions of interest for digital image analysis. Improvements to the procedure presented in this work have already been explored, such as workflows utilizing custom made atlas plates as masks to produce atlas coordinates for individual objects sorted according to brain regions (Bjerke et al. 2018a; Bjerke et al. 2018b; Yates, 2018). Methods for automatic neuroanatomical segmentation based on atlas registration have also recently been introduced in a quantitative study of APP transgenic Alzheimer's disease models (Whitesell et al. 2018).

An ideal software solution, and the goal of future projects, would be a pipeline where section images, after slide scanning, automatically were integrated in a neuroinformatics infrastructure (e.g. Navigator3) and registered to a chosen 3D reference space by means of automatic, non-linear warping and 2D to 3D atlas registration (Gefen et al. 2008). The density of histochemically labeled elements within each ROI would be quantified by means of digital image analysis, and spatial coordinates recorded within a 3D reference atlas framework. The development of such generic, automated tools, however, is associated with many challenges. The largest obstacle is, perhaps, the loss of 3D information during sectioning. When the spatial relationship between sections disappears, reconstructing this information section by section is a both time consuming and not completely reliable. This obstacle could be overcome by using serial block-face scanning technology (Denk & Horstmann, 2004) that maintains the 3D information during sectioning. When the volumetric information is intact, there are several well-proven methods for nonlinear 3D to 3D atlas registration (Klein et al. 2009). A serial block-face scanning microscope is, however, an

expensive investment and currently not available for most neuroscientists. Furthermore, block face information is not available for all the brains already sectioned and processed. As the research community recognizes the value and opportunities of atlas registration and volumetric information, new facilitating technologies will likely emerge to improve existing workflows.

EVALUATION OF MAIN FINDINGS AND SCIENTIFIC IMPACT

β -amyloid in tg-ArcSwe mice

Numerous mouse models of Alzheimer's disease have been developed over the last decades. The Alzheimer Forum (www.alzforum.org/) has created a comprehensive, searchable database that contains detailed information about the different models, genes of interest, and related publications. Currently over 160 different AD models are listed, of which about fifty percent are APP transgenic models (Alzforum; Retrieved March 30, 2019, from <http://www.alzforum.org/research-models>). Such a resource is of tremendous value when navigating the complex landscape of Alzheimer's disease modeling, but for many purposes, additional data are needed. For most models, quantitative data and comprehensive image data from multiple specimens are unavailable. Our approach when evaluating the tg-ArcSwe model has several advantages. First, quantitative image analysis of β -amyloid in major brain regions of several specimens allowed us to empirically estimate suitable group sizes for interventional studies using changes in β -amyloid load as endpoint. Second, publicly releasing high-resolution image data online gives interested researchers the opportunity to re-evaluate our results, analyze regions of interest in more detail, or use our data as reference material in their studies. Potentially, this could reduce the number of animals needed to be sacrificed and reduce both time consume and cost of future studies utilizing the tg-ArcSwe model.

Our analysis of tg-ArcSwe mice demonstrated that the load and distribution of β -amyloid were largely consistent with earlier studies using different methods, although the overall β -amyloid burden were measured slightly higher (Lord et al. 2006; Philipson et al. 2009a). This might be accounted

for by the methodological factors discussed earlier or may be a result of genetic drift of phenotypes in the colony at Oslo University compared with the original colony at Uppsala University (Lord et al. 2006). The statistical power analysis suggested that group sizes of at least 16 mice ($\pi = 0.80$) or 27 mice ($\pi = 0.95$) are needed to detect a difference of 25% ($\alpha = 0.05$) in interventional studies using our methods for measuring changes in β -amyloid load. This is more than commonly used in preclinical studies. The measured coefficient of variation (CV) in the cerebral cortex (22%) and in the hippocampus (25%) were smaller than in most other models, for example the frequently used Tg2576 (Citron et al. 1992) and tg-Swe (Lord et al. 2011). The modest phenotype variability in in these regions, in terms of both anatomical distribution and density of deposits, means that relatively few tg-ArcSwe mice are needed to gain statistical power when evaluating novel therapeutics affecting β -amyloid load.

Transgene expression in Nop-tTA mice

Most Tet-Off models are constructed to express a specific gene product, for example a disease-causing protein such as mutant APP or tau, in certain tissues or cell types regulated by the specificity of the promoter that initiates tTA transcription. For a tTA-model to successfully replicate a human neurodegenerative condition, it is necessary that the pathological gene product is expressed in the same brain regions or cell types as the neuropathological changes occur in human patients.

The Nop-tTA line was originally reported to display tTA dependent transgene expression restricted to the entorhinal cortex (EC) and the pre-/parasubiculum (Yasuda & Mayford, 2006). Since we found a more widespread expression of the reporter genes compared to the original publication, we searched for possible explanations. To explore whether different staining protocols could account for the promiscuous expression observed, we stained additional sections using the methods described in the original characterization of the line (Yasuda & Mayford, 2006). We found, however, that the higher concentration of X-gal in their developing solution actually made the cortical expression more pronounced rather than less. The lack of widespread labeling in the Pcp2-tTA and the Pitx3-tTA animals

using the same protocols as for the Nop-tTA mice also points to an explanation within the Nop-tTA model itself rather than differences in the staining protocol. To investigate if the ectopic expression was unique to the lacZ reporter, we crossed the Nop-tTA mice with another tet-responsive reporter line expressing green fluorescent protein (GFP). This reporter displayed more limited expression outside the entorhinal and subicular areas, but GFP-positive cells could still be found in the hippocampus, the thalamus and in cortical regions outside the entorhinal area. We noticed, however, that the Nop-GFP mice displayed significant transgene expression in the reticular nucleus of the thalamus. Labeling in this region was much less prominent in the Nop-lacZ animals, a finding that indicates that two responders may behave differently when crossed to the same driver. We also wanted to explore whether the widespread expression was influenced by animal age or gender. Our initial findings were based on 2-2.5 months old male mice. We therefore analyzed male and female mice of 7-9 months of age, two of which were included in the online repository. We found no significant sex difference, and the expression patterns in these animals were similar to those found in the younger mice. Although there were subtle differences between responder lines, the core expression pattern in all the analyzed Nop-tTA mice was largely consistent over time, between genders, and with different reporter crosses. We therefore concluded that no methodological or individual factors could explain the widespread labeling, and that the most likely explanation for the observed differences from previous reports was a change in the strain background on which the transgene was expressed (detailed in paper II).

Our findings of promoter leakiness in Nop-tTA mice emphasize that comprehensive re-analyses of established models, with well-known reporters and neuroanatomical methods with high level of detail, might reveal expression patterns that diverge from the original findings. The ectopic expression we observed in Nop-tTA mice could influence interpretation of several past studies that depended on this line to have transgene expression strictly limited to the EC and the pre-/ parasubiculum. In particular, this applies to a series of papers where the Nop-tTA line was used to evaluate potential trans-synaptic spread of pathological proteins in

models of Alzheimer's disease (Harris et al. 2010; de Calignon et al. 2012; Liu et al. 2012). In these studies, the Nop-tTA line was used to drive expression of mutant protein (APP or tau), and later tested for presence of these proteins in synaptically connected brain regions. All three studies described pathological proteins in the EC, followed months later by their presence in the dentate gyrus and in the hippocampus, and at still later ages in cortical regions further down the synaptic pathways. These findings were interpreted as evidence for trans-synaptic spread of pathological proteins from the EC to connected brain regions. However, definitive proof of trans-synaptic spread requires that the tTA driven expression of the mutant proteins is strictly limited. Our analysis indicates that the Nop-tTA line, especially after many generations, might not meet this requirement. We argue that tTA dependent expression in some promoter-tTA lines might change over time, and, whenever spatial localization is important, transgene expression should be verified with well-characterized reporters prior to use.

Online tTA resource

In paper III, we streamlined the methods developed throughout the first two studies and applied the resulting workflow to establish an online resource containing data, metadata, and analysis results from five tTA promoter lines. The animals included in the repository vary with respect to age and sex, but to our knowledge, variation in promoter activity as a function of age and sex in the included mouse lines has not been described, at least not at the light-microscopic level used in our study. We recognize, however, the possibility for genetic drift, age and sex difference, and that different promoter-reporter crosses can display varying expression levels. Variations in these parameters may be relevant in certain settings and should be taken into account when interpreting results.

Nevertheless, our results demonstrate how disparate data collected over a decade can be mapped to a common reference atlas and compared. As such, our study presents the first detailed brain-wide comparison of commonly used tTA promoter mouse lines with known expression in the brain. Inclusion of data from more driver lines, with more specimens, and preferably also at multiple age points, would increase the scientific value of

the collection. Such an expansion of the data repository, however, was beyond the scope of the present thesis and would require substantial efforts over time by several laboratories. The present work paves the way for such efforts by demonstrating how image collections from different sources can be compared in spite of their essential differences. We established a robust workflow for brain-wide assessment of transgene expression in tTA mice at a cellular level and demonstrated the generic value of the workflow by including diverse datasets not specifically tailored for the purpose.

In its present state, we believe that the online tTA repository and the tabular overview of reporter expression distribution and levels may serve as a valuable resource to guide empirically based decisions on which model to choose for a particular purpose. Having access to the complete datasets also provides the opportunity to evaluate regions of interest in more detail and facilitates re-use of data in contexts outside the present project.

Image data, metadata, analysis results and software tools were made publicly available through services for data storage, management, and data curation offered by the EU Human Brain Project (HBP: www.humanbrainproject.eu) in accordance with the FAIR guiding principles (Wilkinson et al. 2016) as data that are Findable, Accessible, Interoperable, and Reusable. The HBP infrastructure offers services for mapping additional data to the same anatomical reference space to become directly comparable to our data. Researchers working with tet-regulatable animals are therefore greatly encouraged to share their datasets and contribute to expand the present collection.

Scientific Impact

The scientific value of the tg-ArcSwe atlas has been recognized by the Alzheimer Forum, which links directly to the atlas url (www.alzforum.org/research-models/tg-arcswe), and the results have been used as reference material in an interventional study (Nuruddin et al. 2014) and in several recent neuroanatomy-related projects (Carlred et al. 2016; Sehlin et al. 2017; Syvänen et al. 2017; Zhang & Wang, 2018). Furthermore, adaptations of the quantitative image analysis procedures used to calculate β -amyloid

plaque load has been utilized and cited in several subsequent studies (e.g. Nuruddin et al., 2014; Subaiea et al. 2014).

Our demonstration of ectopic reporter expression outside the entorhinal cortex and the pre-/parasubiculum in Nop-tTA mice (paper II) has been recognized by the tTA community and lead to more careful interpretation of findings in subsequent studies utilizing this promoter line (e.g. Baker & Gotz, 2016; Fu et al. 2016; Mudher et al. 2017). Our concerns regarding the neuroanatomical specificity of the neuropsin promoter are also taken into account in an upcoming review article on propagation of protein aggregation in neurodegenerative diseases; “Two reports cast doubt on propagation in this mouse model. The first study found that activity of the neuropsin promoter, which was used to drive the Tet-Off factor, may not be anatomically restricted to the entorhinal cortex and that it expresses tau more widely over time, especially within the hippocampus” (Vaquer-Alicea & Diamond, 2019).

Our method for semi-quantitative assessment of the distribution and density of labeled cells in different brain regions aided by a visual guide system has been adapted and used in a recent study of malignant glioma (Mughal et al. 2018). Paper III is the first publication where datasets are shared via the Human Brain Project (HBP) neuroinformatics infrastructure with HBP DataCite digital object identifiers (DOI's) and will hopefully pave the way for many more projects utilizing this framework to distribute and integrate data.

CONCLUSIONS

With large variety, accessibility, and increasing number, transgenic mouse models of neurodegenerative disease are an invaluable resource with huge potential for novel discoveries. Selecting and interpreting findings from appropriate models, however, requires access to comprehensive data describing where in the brain and at what level the transgene expression occurs. Although efforts have been made to compile post hoc data in online databases (e.g. www.alzforum.org/research-models; Schonig et al. 2013), the morphological characterization of models is still often limited by technological or logistical issues, publication restrictions, narrow scope of analysis, lack of standardization or reluctance to openly share data.

The main contribution of this work is to demonstrate how new methodologies developed in the field of neuroinformatics can be utilized to establish workflows for efficient and reproducible neuroanatomical characterization of transgene expression in mouse models of neurodegenerative disease, and how large collections of histological image data from the mouse brain can be acquired, organized, compared, and openly shared in accordance with the FAIR Guiding Principles for scientific data management (Wilkinson et al. 2016).

More specifically, we have addressed topics including:

- How morphological features can be systematically mapped brain-wide and data openly shared to facilitate re-use of data outside the immediate scope of a study.
- How neuroinformatics methods can be utilized to overcome the limitations in data sharing typical for traditional publication channels.
- How assessment and comparison of transgene expression distribution and levels can be facilitated by registering histological mouse brain data to a 3D atlas framework.

- How quantitative analyses of neuropathological features can be used to shed light on specific neurobiological questions and design interventional studies with adequate statistical power.
- How detailed, brain-wide analysis of promoter activity in conditional mouse models utilizing well-known reporters may yield results affecting interpretation of experimental results from studies using these models.

Some major challenges, such as standardizations of data and metadata formats and legal/ ethical frameworks for data ownership, stewardship, and sharing, remain unresolved and require a unified effort from the international neuroscience community. Current projects like the European Human Brain Project (HBP, www.humanbrainproject.eu) and the USA Brain Research through Advancing Innovative Neurotechnologies (BRAIN, www.braininitiative.nih.gov/) are addressing these issues, and will possibly contribute to solutions in the years to come.

In the last decade, our understanding of the complex brain systems involved in neurodegenerative diseases has consistently been expanded by world-leading laboratories (e.g. Fyhn et al. 2007; Høydal et al. 2019), elaborating upon the importance of 3D information. Improved models, more closely resembling human neurodegenerative conditions, are expected to become available as a result of such insights, and also by recent technological advances (e.g. high throughput sequencing and CRISPR/Cas9 genome editing). Systematic characterization of transgenic mouse models and a centralized database of data, metadata, and findings would be a huge asset for the neurodegenerative research community, assisting researchers in selecting the most suitable lines based on experimental needs. Recent large-scale collaborative efforts have potential to make progress toward this goal, at least for newly developed mouse models (e.g. MODEL-AD, <https://model-ad.org/>). The workflows, tools, and methods compiled in this work may be applied to existing or novel models, and the online resource expanded with data from animals with varying age, gender and genetic background. Alternatively, selected elements from our work may be refined,

adapted and implemented in collaborative efforts to standardize morphological characterization of neurodegenerative disease models.

While past experimental research on mouse models of neurodegenerative disorders have had limited translational value (Mullane & Williams, 2019), efforts such as the present work, with increased focus on systematic generation, organization, quantitation and sharing of high-quality morphological data, will hopefully contribute to increase the predictive validity of future studies.

REFERENCES

- Abbott A (2010) **Neuroscience: The rat pack.** *Nature*, 465, 282-283. DOI: 10.1038/465282a
- Abrams M, Bjaalie JG, Das S, Egan GF, Ghosh SS, Goscinski WJ, Grethe JS, Kotaleski JH, Ho ETW, Kennedy DN, Lanyon LJ, Leergaard TB et al. (2019) **A standards organization for Open and FAIR neuroscience: the International Neuroinformatics Coordinating Facility.** [Preprint] DOI: 10.31219/osf.io/3rt9b
- Alrafiah AR (2018) **From mouse models to human disease: An approach for amyotrophic lateral sclerosis.** *In vivo*, 32, 983-998. DOI: 10.21873/invivo.11339
- Alves-Cruzeiro JMDC, Mendonça L, Pereira de Almeida L & Nóbrega C (2016) **Motor dysfunctions and neuropathology in mouse models of spinocerebellar ataxia type 2: A comprehensive review.** *Frontiers in neuroscience*, 10, 572. DOI: 10.3389/fnins.2016.00572
- Amunts K, Ebell C, Muller J, Telefont M, Knoll A & Lippert T (2016) **The Human Brain Project: Creating a European research infrastructure to decode the human brain.** *Neuron*, 92, 574-581. DOI: 10.1016/j.neuron.2016.10.046
- Amunts K, Hawrylycz MJ, Van Essen DC, Van Horn JD, Harel N, Poline JB, De Martino F, Bjaalie JG et al. (2014) **Interoperable atlases of the human brain.** *NeuroImage*, 99, 525-532. DOI: 10.1016/j.neuroimage.2014.06.010
- Angelis MHd, Michel D, Wagner S, Becker S & Beckers J (2007) Chapter 12 - **Chemical mutagenesis in mice.** In Fox JG, Davisson MT, Quimby FW, Barthold SW, Newcomer CE, Smith AL (eds) *The Mouse in Biomedical Research (Second Edition)*. Academic Press, Burlington, pp. 225-260. ISBN: 9780080467719
- Armbrust KR, Wang X, Hathorn TJ, Cramer SW, Chen G, Zu T, Kangas T, Zink AN, Öz G, Ebner TJ & Ranum LPW (2014) **Mutant β -III spectrin causes mGluR1 α mislocalization and functional deficits in a mouse model of spinocerebellar ataxia type 5.** *The Journal of neuroscience*, 34, 9891-9904. DOI: 10.1523/JNEUROSCI.0876-14.2014
- Armit C, Richardson L, Venkataraman S, Graham L, Burton N, Hill B, Yang Y & Baldock RA (2017) **eMouseAtlas: An atlas-based resource for understanding mammalian embryogenesis.** *Developmental biology*, 423, 1-11. DOI: 10.1016/j.ydbio.2017.01.023

- Baker S & Gotz J (2016) **A local insult of okadaic acid in wild-type mice induces tau phosphorylation and protein aggregation in anatomically distinct brain regions.** *Acta neuropathologica communications*, 4, 32. DOI: 10.1186/s40478-016-0300-0
- Beach TG (2017) **A review of biomarkers for neurodegenerative disease: Will they swing us across the valley?** *Neurology and therapy*, 6, 5-13. DOI: 10.1007/s40120-017-0072-x
- Bertrand L & Nissanov J (2008) **The Neuroterrain 3D mouse brain atlas.** *Frontiers in neuroinformatics*, 2, 3-3. DOI: 10.3389/neuro.11.003.2008
- Bjerke IE, Ovsthus M, Andersson KA, Blixhavn CH, Kleven H, Yates SC, Puchades MA, Bjaalie JG & Leergaard TB (2018a) **Navigating the murine brain: Toward best practices for determining and documenting neuroanatomical locations in experimental studies.** *Frontiers in neuroanatomy*, 12, 82. DOI: 10.3389/fnana.2018.00082
- Bjerke IE, Ovsthus M, Papp EA, Yates SC, Silvestri L, Fiorilli J, Pennartz CMA, Pavone FS, Puchades MA, Leergaard TB & Bjaalie JG (2018b) **Data integration through brain atlas: Human Brain Project tools and strategies.** *European psychiatry*, 50, 70-76. DOI: 10.1016/j.eurpsy.2018.02.004
- Bowden DM, Johnson GA, Zaborsky L, Green WDK, Moore E, Badea A, Dubach MF & Bookstein FL (2011) **A symmetrical Waxholm canonical mouse brain for NeuroMaps.** *Journal of neuroscience methods*, 195, 170-175. DOI: 10.1016/j.jneumeth.2010.11.028
- Boy J, Leergaard TB, Schmidt T, Odeh F, Bichelmeier U, Nuber S, Holzmann C, Wree A, Prusiner SB, Bujard H, Riess O & Bjaalie JG (2006) **Expression mapping of tetracycline-responsive prion protein promoter: digital atlas for generating cell-specific disease models.** *NeuroImage*, 33, 449-462. DOI: 10.1016/j.neuroimage.2006.05.055
- Brandner S & Jaunmuktane Z (2017) **Prion disease: experimental models and reality.** *Acta neuropathologica*, 133, 197-222. DOI: 10.1007/s00401-017-1670-5
- Button KS, Ioannidis JP, Mokrysz C, Nosek BA, Flint J, Robinson ES & Munafò MR (2013) **Power failure: why small sample size undermines the reliability of neuroscience.** *Nature reviews neuroscience*, 14, 365-376. DOI: 10.1038/nrn3475
- Carlred L, Michno W, Kaya I, Sjøvall P, Syvanen S & Hanrieder J (2016) **Probing amyloid-beta pathology in transgenic Alzheimer's disease (tgArcSwe) mice using MALDI imaging mass spectrometry.** *Journal of neurochemistry*, 138, 469-478. DOI: 10.1111/jnc.13645

- Carlsson A, Lindqvist M & Magnusson T (1957) **3,4-Dihydroxyphenylalanine and 5-hydroxytryptophan as reserpine antagonists.** *Nature*, 180, 1200. DOI: 10.1038/1801200a0
- Cepko C, Ryder E, Fekete DM & Bruhn S (1998) **Detection of beta-galactosidase and alkaline phosphatase activities in tissue.** In Spector DL, Goldman RD, Leinwand LA (eds) *Laboratory manual volume 3: Subcellular Location of Genes and Their Products*. Cold Spring Harbor Laboratory Press, Cold Spring Harbor. ISBN: 0-87969-521-8
- Choi DS, Wang D, Dadgar J, Chang WS & Messing RO (2002) **Conditional rescue of protein kinase C epsilon regulates ethanol preference and hypnotic sensitivity in adult mice.** *The Journal of neuroscience*, 22, 9905-9911. DOI: 10.1523/JNEUROSCI.22-22-09905.2002
- Citron M, Oltersdorf T, Haass C, McConlogue L, Hung AY, Seubert P, Vigo-Pelfrey C, Lieberburg I & Selkoe DJ (1992) **Mutation of the beta-amyloid precursor protein in familial Alzheimer's disease increases beta-protein production.** *Nature*, 360, 672-674. DOI: 10.1038/360672a0
- Collins FS & Tabak LA (2014) **NIH plans to enhance reproducibility.** *Nature*, 505, 612-613. PMID: 24482835
- Cousijn H, Kenall A, Ganley E, Harrison M, Kernohan D, Lemberger T, Murphy F, Polischuk P, Taylor S, Martone M & Clark T (2018) **A data citation roadmap for scientific publishers.** *Scientific data*, 5, 180259. DOI: 10.1038/sdata.2018.259
- Dawson TM, Golde TE & Lagier-Tourenne C (2018) **Animal models of neurodegenerative diseases.** *Nature neuroscience*, 21, 1370-1379. DOI: 10.1038/s41593-018-0236-8
- de Calignon A, Polydoro M, Suárez-Calvet M, William C, Adamowicz DH, Kopeikina KJ, Pitstick R, Sahara N, Ashe KH, Carlson GA, Spires-Jones, TL & Hyman BT (2012) **Propagation of tau pathology in a model of early Alzheimer's disease.** *Neuron*, 73, 685-697. DOI: 10.1016/j.neuron.2011.11.033
- Denk W & Horstmann H (2004) **Serial block-face scanning electron microscopy to reconstruct three-dimensional tissue nanostructure.** *PLoS biology*, 2, e329. DOI: 10.1371/journal.pbio.0020329
- Dong HW (2008) **The Allen reference atlas: A digital color brain atlas of the C57BL/6J male mouse.** John Wiley & Sons Inc. DOI: 10.1111/j.1601-183X.2009.00552.x
- Doyle A, McGarry MP, Lee NA & Lee JJ (2012) **The construction of transgenic and gene knockout/knockin mouse models of human disease.** *Transgenic research*, 21, 327-349. DOI: 10.1007/s11248-011-9537-3

- Drechsler S, Lynch MA, Novella S, González-Navarro H, Hecimovic S, Barini E, Tucci V, Castro RE, Vandenbroucke RE, Osuchowski M & Potter PK (2016) **With mouse age comes wisdom: A review and suggestions of relevant mouse models for age-related conditions.** *Mechanisms of ageing and development*, 160, 54-68. DOI: 10.1016/j.mad.2016.07.005
- Echigo R, Nakao K, Fukaya M, Watanabe M & Aiba A (2009) **Generation of L7-tTA knock-in mice.** *Kobe journal of medical sciences*, 54, E272-278. PMID: 19628968
- Egan KJ, Vesterinen HM, Beglopoulos V, Sena ES & Macleod MR (2016) **From a mouse: systematic analysis reveals limitations of experiments testing interventions in Alzheimer's disease mouse models.** *Evidence-based preclinical medicine*, 3, e00015. DOI: 10.1002/ebm2.15
- Elder GA, Gama Sosa MA & De Gasperi R (2010) **Transgenic mouse models of Alzheimer's disease.** *The Mount Sinai journal of medicine*, 77, 69-81. DOI: 10.1002/msj.20159
- Ellenbroek B & Youn J (2016) **Rodent models in neuroscience research: is it a rat race?** *Disease models & mechanisms*, 9, 1079-1087. DOI: 10.1242/dmm.026120
- Ericsson AC, Crim MJ & Franklin CL (2013) **A brief history of animal modeling.** *Missouri medicine*, 110, 201-205. PMID: 23829102
- Erö C, Gewaltig MO, Keller D & Markram H (2018) **A cell atlas for the mouse brain.** *Frontiers in neuroinformatics*, 12, 84-84. DOI: 10.3389/fninf.2018.00084
- Esquerda-Canals G, Montoliu-Gaya L, Guell-Bosch J & Villegas S (2017) **Mouse models of Alzheimer's disease.** *Journal of Alzheimers disease*, 57, 1171-1183. DOI: 10.3233/JAD-170045
- Ferguson AR, Nielson JL, Cragin MH, Bandrowski AE & Martone ME (2014) **Big data from small data: data-sharing in the 'long tail' of neuroscience.** *Nature neuroscience*, 17, 1442-1447. DOI: 10.1038/nn.3838
- Ferrante RJ (2009) **Mouse models of Huntington's disease and methodological considerations for therapeutic trials.** *Biochimica et biophysica acta*, 1792, 506-520. DOI: 10.1038/nn.3838
- Franklin KBJ & Paxinos G (2013) **Paxinos and Franklin's The mouse brain in stereotaxic coordinates.** Academic Press, an imprint of Elsevier, Amsterdam. ISBN: 9780123910578

- Fu H, Hussaini SA, Wegmann S, Profaci C, Daniels JD, Herman M, Emrani S, Figueroa HY, Hyman BT, Davies P & Duff KE (2016) **3D visualization of the temporal and spatial spread of tau pathology reveals extensive sites of tau accumulation associated with neuronal loss and recognition memory deficit in aged tau transgenic mice.** *PLoS One*, 11, e0159463. DOI: 10.1371/journal.pone.0159463
- Fyhn M, Hafting T, Treves A, Moser MB & Moser EI (2007) **Hippocampal remapping and grid realignment in entorhinal cortex.** *Nature*. 446(7132), 190-4. DOI: 10.1038/nature05601
- Games D, Adams D, Alessandrini R, Barbour R, Berthelette P, Blackwell C, Carr T, Clemens J, Donaldson T, Gillespie F et al. (1995) **Alzheimer-type neuropathology in transgenic mice overexpressing V717F beta-amyloid precursor protein.** *Nature*, 373, 523-527. DOI: 10.1038/373523a0
- Gefen S, Kiryati N & Nissanov J (2008) **Atlas-based indexing of brain sections via 2-D to 3-D image registration.** *IEEE Transactions on biomedical engineering*, 55, 147-156. DOI: 10.1109/TBME.2007.899361
- Gitler AD, Dhillon P & Shorter J (2017) **Neurodegenerative disease: models, mechanisms, and a new hope.** *Disease models & mechanisms*, 10, 499-502. DOI: 10.1242/dmm.030205
- Goate A, Chartier-Harlin MC, Mullan M, Brown J, Crawford F, Fidani L, Giuffra L, Haynes A, Irving N, James L et al. (1991) **Segregation of a missense mutation in the amyloid precursor protein gene with familial Alzheimer's disease.** *Nature*, 349, 704-706. DOI: 10.1038/349704a0
- Goodchild RE & Dauer WT (2004) **Mislocalization to the nuclear envelope: an effect of the dystonia-causing torsinA mutation.** *Proc Natl Acad Sci USA*, 101, 847-852. PMID: 14711988
- Gordon JW & Ruddle FH (1981) **Integration and stable germ line transmission of genes injected into mouse pronuclei.** *Science*, 214, 1244-1246. DOI: 10.1126/science.6272397
- Gossen M & Bujard H (1992) **Tight control of gene expression in mammalian cells by tetracycline-responsive promoters.** *Proc Natl Acad Sci USA*, 89, 5547-5551. DOI: 10.1073/pnas.89.12.5547
- Götz J, Bodea LG & Goedert M (2018) **Rodent models for Alzheimer disease.** *Nature reviews neuroscience*, 19, 583-598. DOI: 10.1038/s41583-018-0054-8

- Harris JA, Devidze N, Verret L, Ho K, Halabisky B, Thwin MT, Kim D, Hamto P, Lo I, Yu GQ, Palop JJ, Masliah E & Mucke L (2010) **Transsynaptic progression of amyloid-beta-induced neuronal dysfunction within the entorhinal-hippocampal network.** *Neuron*, 68, 428-441. DOI: 10.1016/j.neuron.2010.10.020
- Heemels MT (2016) **Neurodegenerative diseases.** *Nature*, 539, 179. DOI: 10.1038/539179a
- Heintz N (2004) **Gene Expression Nervous System Atlas (GENSAT).** *Nature neuroscience*, 7, 483. DOI: 10.1038/nn0504-483
- Hultqvist G, Syvänen S, Fang XT, Lannfelt L & Sehlin D (2017) **Bivalent brain shuttle increases antibody uptake by monovalent binding to the transferrin receptor.** *Theranostics*, 7, 308-318. DOI: 10.7150/thno.17155
- Høydal ØA, Skytøen ER, Andersson SO, Moser MB & Moser EI (2019) **Object-vector coding in the medial entorhinal cortex.** *Nature* [Preprint] DOI: 10.1038/s41586-019-1077-7
- Jankowsky JL & Zheng H (2017) **Practical considerations for choosing a mouse model of Alzheimer's disease.** *Molecular neurodegeneration*, 12, 89. DOI: 10.1186/s13024-017-0231-7
- Jucker M (2010) **The benefits and limitations of animal models for translational research in neurodegenerative diseases.** *Nature medicine*, 16, 1210. DOI: 10.1038/nm.2224
- Justice MJ & Dhillon P (2016) **Using the mouse to model human disease: increasing validity and reproducibility.** *Disease models & mechanisms*, 9, 101-103. DOI: 10.1242/dmm.024547
- Karch CM, Cruchaga C & Goate AM (2014) **Alzheimer's disease genetics: from the bench to the clinic.** *Neuron*, 83, 11-26. DOI: 10.1016/j.neuron.2014.05.041
- Kjonigsen LJ, Lillehaug S, Bjaalie JG, Witter MP & Leergaard TB (2015) **Waxholm Space atlas of the rat brain hippocampal region: Three-dimensional delineations based on magnetic resonance and diffusion tensor imaging.** *NeuroImage*, 108, 441-449. DOI: 10.1016/j.neuroimage.2014.12.080
- Klein A, Andersson J, Ardekani BA, Ashburner J, Avants B, Chiang MC, Christensen GE, Collins DL, Gee J, Hellier P, Song JH et al. (2009) **Evaluation of 14 nonlinear deformation algorithms applied to human brain MRI registration.** *NeuroImage*, 46, 786-802.

- Kuan L, Li Y, Lau C, Feng D, Bernard A, Sunkin SM, Zeng H, Dang C, Hawrylycz M & Ng L (2015) **Neuroinformatics of the Allen mouse brain connectivity atlas**. *Methods*, 73, 4-17. DOI: 10.1016/j.neuroimage.2008.12.037
- Lee VM, Goedert M & Trojanowski JQ (2001) **Neurodegenerative tauopathies**. *Annual review of neuroscience*, 24, 1121-1159. DOI: 10.1146/annurev.neuro.24.1.1121
- Lein ES, Hawrylycz MJ, Ao N, Ayres M, Bensinger A, Bernard A, Boe AF, Boguski MS, Brockway KS, Byrnes EJ et al. (2007) **Genome-wide atlas of gene expression in the adult mouse brain**. *Nature*, 445, 168-176. DOI: 10.1038/nature05453
- Lin X, Parisiadou L, Sgobio C, Liu G, Yu J, Sun L, Shim H, Gu XL, Luo J, Long CX, Ding J, Mateo Y, Sullivan PH, Wu LG, Goldstein DS, Lovinger D & Cai H (2012) **Conditional expression of Parkinson's disease-related mutant alpha-synuclein in the midbrain dopaminergic neurons causes progressive neurodegeneration and degradation of transcription factor nuclear receptor related 1**. *The Journal of neuroscience*, 32, 9248-9264. DOI: 10.1523/JNEUROSCI.1731-12.2012
- Liu G, Sgobio C, Gu X, Sun L, Lin X, Yu J, Parisiadou L, Xie C, Sastry N, Ding J, Lohr KM, Miller GW, Mateo Y, Lovinger DM & Cai H (2015) **Selective expression of Parkinson's disease-related Leucine-rich repeat kinase 2 G2019S missense mutation in midbrain dopaminergic neurons impairs dopamine release and dopaminergic gene expression**. *Human molecular genetics*, 24, 5299-5312. DOI: 10.1093/hmg/ddv249
- Liu L, Drouet V, Wu JW, Witter MP, Small SA, Clelland C & Duff K (2012) **Trans-synaptic spread of tau pathology *in vivo***. *PLoS One*, 7, e31302. DOI: 10.1371/journal.pone.0031302
- Lord A, Kalimo H, Eckman C, Zhang XQ, Lannfelt L & Nilsson LN (2006) **The Arctic Alzheimer mutation facilitates early intraneuronal Abeta aggregation and senile plaque formation in transgenic mice**. *Neurobiology of aging*, 27, 67-77. DOI: 10.1016/j.neurobiolaging.2004.12.007
- Lord A, Philipson O, Klingstedt T, Westermarck G, Hammarström P, Nilsson KPR & Nilsson LNG (2011) **Observations in APP bitransgenic mice suggest that diffuse and compact plaques form via independent processes in Alzheimer's disease**. *The American journal of pathology*, 178, 2286-2298. DOI: 10.1016/j.ajpath.2011.01.052
- Lutz CM & Osborne MA (2013) **Optimizing mouse models of neurodegenerative disorders: are therapeutics in sight?** *Future neurology*, 9, 67-75. DOI: 10.2217/fnl.13.66

- Madisen L, Zwingman TA, Sunkin SM, Oh SW, Zariwala HA, Gu H, Ng LL, Palmiter RD, Hawrylycz MJ, Jones AR, Lein ES & Zeng H (2010) **A robust and high-throughput Cre reporting and characterization system for the whole mouse brain.** *Nature neuroscience*, 13, 133-140. DOI: 10.1038/nn.2467
- Melnikova T, Park D, Becker L, Lee D, Cho E, Sayyida N, Tian, J, Bandeen-Roche K, Borchelt DR & Savonenko AV (2016) **Sex-related dimorphism in dentate gyrus atrophy and behavioral phenotypes in an inducible tTA:APPsi transgenic model of Alzheimer's disease.** *Neurobiology of disease*, 96, 171-185. DOI: 10.1016/j.nbd.2016.08.009
- Menalled LB & Chesselet MF (2002) **Mouse models of Huntington's disease.** *Trends in pharmacological sciences*, 23, 32-39. DOI 10.1016/S0165-6147(00)01884-8:
- Merton RM (1979) **The Sociology of Science – Theoretical and Empirical Investigations.** University of Chicago Press, Chicago, USA. ISBN: 0226520927
- Ministry of Education and Research (2017) **National strategy on access to and sharing of research data.** URL: www.regjeringen.no/contentassets/3a0ceea1c9b4611a1b86fc5616abde7/en-gb/pdfs/national-strategy-on-access_summary.pdf
- Moene I, Darine D, Leergaard T, Bjaalie JG et al. (2011) **Rodent Brain Navigator: database and atlas system for microscopy and imaging data.** *Abstract: 4th INCF Congress of Neuroinformatics*, Boston, United States.
- Moore DJ & Dawson TM (2008) **Value of genetic models in understanding the cause and mechanisms of Parkinson's disease.** *Current neurology and neuroscience reports*, 8, 288-296. PMID: 18590612
- Mudher A, Colin M, Dujardin S, Medina M, Dewachter I, Naini SMA, Mandelkow EM, Mandelkow E, Buée L, Goedert M & Brion JP (2017) **What is the evidence that tau pathology spreads through prion-like propagation?** *Acta neuropathologica communications*, 5, 99. DOI: 10.1186/s40478-017-0488-7
- Mughal AA, Zhang L, Fayzullin A, Server A, Li Y, Wu Y, Glass R, Meling T, Langmoen IA, Leergaard TB & Vik-Mo EO (2018) **Patterns of invasive growth in malignant gliomas - The hippocampus emerges as an invasion-spared brain region.** *Neoplasia*, 20, 643-656. DOI: 10.1016/j.neo.2018.04.001
- Mullane K & Williams M (2019) **Preclinical models of Alzheimer's disease: Relevance and translational validity.** *Current protocols in pharmacology*, 84, e57. DOI: 10.1002/cpph.57

- Murakami TC, Mano T, Saikawa S, Horiguchi SA, Shigeta D, Baba K, Sekiya H, Shimizu Y, Tanaka KF, Kiyonari H, Iino M, Mochizuki H, Tainaka K & Ueda HR (2018) **A three-dimensional single-cell-resolution whole-brain atlas using CUBIC-X expansion microscopy and tissue clearing.** *Nature neuroscience*, 21, 625-637. DOI: 10.1038/s41593-018-0109-1
- Murrell J, Farlow M, Ghetti B & Benson MD (1991) **A mutation in the amyloid precursor protein associated with hereditary Alzheimer's disease.** *Science*, 254, 97-99. DOI: 10.1126/science.1925564
- National Institutes of Health (2017) **Principles and guidelines for reporting preclinical research.** URL: www.nih.gov/research-training/rigor-reproducibility/principles-guidelines-reporting-preclinical-research
- Nord CL, Valton V, Wood J & Roiser JP (2017) **Power-up: A reanalysis of 'Power Failure' in neuroscience using mixture modeling.** *The Journal of neuroscience*, 37, 8051-8061. DOI: 10.1523/JNEUROSCI.3592-16.2017
- Nuber S, Petrasch-Parwez E, Winner B, Winkler J, von Horsten S, Schmidt T, Boy J, Kuhn M, Nguyen HP et al. (2008) **Neurodegeneration and motor dysfunction in a conditional model of Parkinson's disease.** *The Journal of neuroscience*, 28, 2471-2484. DOI: 10.1523/JNEUROSCI.3040-07.2008
- Nuruddin S, Syverstad GH, Lillehaug S, Leergaard TB, Nilsson LN, Ropstad E, Krogenaes A, Haraldsen IR & Torp R (2014) **Elevated mRNA-levels of gonadotropin-releasing hormone and its receptor in plaque-bearing Alzheimer's disease transgenic mice.** *PLoS One*, 9, e103607. DOI: 10.1371/journal.pone.0103607
- Odeh F, Leergaard TB, Boy J, Schmidt T, Riess O & Bjaalie JG (2011) **Atlas of transgenic Tet-Off Ca²⁺/calmodulin-dependent protein kinase II and prion protein promoter activity in the mouse brain.** *NeuroImage*, 54, 2603-2611. DOI: 10.1016/j.neuroimage.2010.11.032
- Oh SW, Harris JA, Ng L, Winslow B, Cain N, Mihalas S, Wang Q, Lau C, Kuan L, Henry AM, Mortrud MT, Ouellette B, Nguyen TN et al. (2014) **A mesoscale connectome of the mouse brain.** *Nature*, 508, 207. DOI: 10.1038/nature13186
- Onos KD, Sukoff Rizzo SJ, Howell GR & Sasner M (2016) **Toward more predictive genetic mouse models of Alzheimer's disease.** *Brain research bulletin*, 122, 1-11. DOI: 10.1016/j.brainresbull.2015.12.003
- Orban PC, Chui D & Marth JD (1992) **Tissue- and site-specific DNA recombination in transgenic mice.** *Proc Natl Acad Sci U S A*, 89, 6861-6865. DOI: 10.1073/pnas.89.15.6861

- Pankevich DE, Wizemann TM, Mazza AM & Altevogt BM (2012) **International Animal Research Regulations: Impact on Neuroscience Research: Workshop Summary**. The National Academies Press, Washington, DC. ISBN-10: 0-309-25208-3
- Papp EA, Leergaard TB, Calabrese E, Johnson GA & Bjaalie JG (2014a) **Waxholm Space atlas of the Sprague Dawley rat brain**. *NeuroImage*, 97, 374-386.
- Papp EA, Leergaard TB, Csucs G & Bjaalie JG (2016) **Brain-wide mapping of axonal connections: Workflow for automated detection and spatial analysis of labeling in microscopic sections**. *Frontiers in neuroinformatics*, 10, 11. DOI: 10.1016/j.neuroimage.2014.04.001
- Papp EA, Leergaard TB, Csucs G, Darine DA & Bjaalie JG (2014b) **Workflow for integration and analysis of histological data in rodent brain Waxholm Space**. *Abstract: Neuroinformatics 2014*, Leiden, Netherlands.
- Perrin S (2014) **Preclinical research: Make mouse studies work**. *Nature*, 507, 423-425. DOI: 10.1038/507423a
- Philipson O, Hammarstrom P, Nilsson KP, Portelius E, Olofsson T, Ingelsson M, Hyman BT, Blennow K, Lannfelt L, Kalimo H & Nilsson LN (2009a) **A highly insoluble state of Abeta similar to that of Alzheimer's disease brain is found in Arctic APP transgenic mice**. *Neurobiology of aging*, 30, 1393-1405. DOI: 10.1016/j.neurobiolaging.2007.11.022
- Philipson O, Lannfelt L & Nilsson LN (2009b) **Genetic and pharmacological evidence of intraneuronal Abeta accumulation in APP transgenic mice**. *FEBS letters*, 583, 3021-3026. DOI: 10.1016/j.febslet.2009.08.009
- Pickett EK, Henstridge CM, Allison E, Pitstick R, Pooler A, Wegmann S, Carlson G, Hyman BT & Spires-Jones TL (2017) **Spread of tau down neural circuits precedes synapse and neuronal loss in the rTgTauEC mouse model of early Alzheimer's disease**. *Synapse*, 71, e21965. DOI: 10.1002/syn.21965
- Pihlstrøm L, Wiethoff S & Houlden H (2018) **Genetics of neurodegenerative diseases: an overview**. In Kovacs GG, Alafuzoff I (eds) *Handbook of Clinical Neurology*. Elsevier, 309-323. DOI: 10.1016/B978-0-12-802395-2.00022-5
- Pletnikov MV, Ayhan Y, Nikolskaia O, Xu Y, Ovanesov MV, Huang H, Mori S, Moran TH & Ross CA (2008) **Inducible expression of mutant human DISC1 in mice is associated with brain and behavioral abnormalities reminiscent of schizophrenia**. *Molecular psychiatry*, 13, 173-186. DOI: 10.1038/sj.mp.4002079

- Puchades MA, Csucs G, Checinska M, Øvsthus M, Bjerke IE, Andersson K, Leergaard TB & Bjaalie JG (2017) **QuickNII: Neuroinformatics tool and workflow for anchoring of serial histological images in rodent brain 3D space.** *Abstract: Society for Neuroscience 2017*, Washington DC., United States.
- Querfurth HW & LaFerla FM (2010) **Alzheimer's Disease.** *The New England journal of medicine*, 362, 329-344. DOI: 10.1056/NEJMra0909142
- Ray P, Tang W, Wang P, Homer R, Kuhn C, Flavell RA & Elias JA (1997) **Regulated overexpression of interleukin 11 in the lung. Use to dissociate development-dependent and -independent phenotypes.** *The Journal of clinical investigation*, 100, 2501-2511. DOI: 10.1172/JCI119792
- Roberson ED (2012) **Mouse models of frontotemporal dementia.** *Annals of neurology*, 72, 837-849. DOI: 10.1002/ana.23722
- Rockland KS (2016) **Lighting up Neuroanatomy.** *Frontiers in neuroscience*, 10, 293. DOI: 10.3389/fnins.2016.00293
- Rowland DC, Weible AP, Wickersham IR, Wu H, Mayford M, Witter MP & Kentros CG (2013) **Transgenically targeted rabies virus demonstrates a major monosynaptic projection from hippocampal area CA2 to medial entorhinal layer II neurons.** *The Journal of neuroscience*, 33, 14889-14898. DOI: 10.1523/JNEUROSCI.1046-13.2013
- Salinas CBG, Lu TTH, Gabery S, Marstal K, Alanentalo T, Mercer AJ, Cornea A, Conradsen K, Hecksher-Sørensen J, Dahl AB, Knudsen LB & Secher A (2018) **Integrated brain atlas for unbiased mapping of nervous system effects following liraglutide treatment.** *Scientific reports*, 8, 10310. DOI: 10.1038/s41598-018-28496-6
- SantaCruz K, Lewis J, Spires T, Paulson J, Kotilinek L, Ingelsson M, Guimaraes A, DeTure M, Ramsden M, McGowan E et al. (2005) **Tau suppression in a neurodegenerative mouse model improves memory function.** *Science*, 309, 476-481. DOI: 10.1126/science.1113694
- Sastry N, Zheng W, Liu G, Wang H, Chen X, Cai M, Contractor P, Sgobio C, Sun L, Xie C & Cai H (2015) **No apparent transmission of transgenic α -synuclein into nigrostriatal dopaminergic neurons in multiple mouse models.** *Translational neurodegeneration*, 4, 23. DOI: 10.1186/s40035-015-0046-9
- Schonig K, Freundlieb S & Gossen M (2013) **Tet-Transgenic Rodents: a comprehensive, up-to date database.** *Transgenic research*, 22, 251-254. DOI: 10.1007/s11248-012-9660-9

- Sedgewick J (2008) **Scientific imaging with Photoshop: Methods, measurement, and output.** Peachpit Press, California. ISBN: 0321514335
- Sehlin D, Fang XT, Meier SR, Jansson M & Syvänen S (2017) **Pharmacokinetics, biodistribution and brain retention of a bispecific antibody-based PET radioligand for imaging of amyloid- β .** *Scientific reports*, 7, 17254. DOI: 10.1038/s41598-017-17358-2
- Shimizu S, Hirose D, Hatanaka H, Takenoshita N, Kaneko Y, Ogawa Y, Sakurai H & Hanyu H (2018) **Role of Neuroimaging as a Biomarker for Neurodegenerative Diseases.** *Frontiers in neurology*, 9, 265-265. DOI: 10.3389/fneur.2018.00265
- Shulman JM, De Jager PL & Feany MB (2011) **Parkinson's disease: genetics and pathogenesis.** *Annual review of pathology*, 6, 193-222. DOI: 10.1146/annurev-pathol-011110-130242
- Silvestri L, Paciscopi M, Soda P, Biamonte F, Iannello G, Frasconi P & Pavone FS (2015) **Quantitative neuroanatomy of all Purkinje cells with light sheet microscopy and high-throughput image analysis.** *Frontiers in neuroanatomy*, 9, 68. DOI: 10.3389/fnana.2015.00068
- Smith CM, Hayamizu TF, Finger JH, Bello SM, McCright IJ, Xu J, Baldarelli RM, Beal JS, Campbell J, Corbani LE et al. (2019) **The mouse Gene Expression Database (GXD): 2019 update.** *Nucleic acids research*, 47, D774–D779. DOI: 10.1093/nar/gky922
- Subaiea G, Ahmed A, Adwan L & Zawia N (2014) **Reduction of amyloid- β deposition and attenuation of memory deficits by tolfenamic acid.** *Journal of Alzheimers disease*, 43, 425-33. DOI: 10.3233/JAD-132726
- Sunkin SM, Ng L, Lau C, Dolbeare T, Gilbert TL, Thompson CL, Hawrylycz M & Dang C (2013) **Allen Brain Atlas: an integrated spatio-temporal portal for exploring the central nervous system.** *Nucleic acids research*, 41, D996-D1008. DOI: 10.1093/nar/gks1042
- Syvänen S, Edén D & Sehlin D (2017) **Cationization increases brain distribution of an amyloid-beta protofibril selective F(ab')₂ fragment.** *Biochemical and biophysical research communications*, 493, 120-125. DOI: 10.1016/j.bbrc.2017.09.065
- The Research Council of Norway (2017) **Open Access to Research Data.** URL: www.forskningradet.no/globalassets/publikasjoner/1254032622112.pdf
- Tiesinga P, Bakker R, Hill S & Bjaalie JG (2015) **Feeding the human brain model.** *Current opinion in neurobiology*, 32, 107-114. DOI: 10.1016/j.conb.2015.02.003

- Trancikova A, Ramonet D & Moore DJ (2011) Chapter 11 - **Genetic mouse models of neurodegenerative diseases**. In Chang KT, Min KT (eds) *Progress in Molecular Biology and Translational Science*. Academic Press, 419-482. DOI: 10.1016/B978-0-12-384878-9.00012-1
- Tremblay P, Meiner Z, Galou M, Heinrich C, Petromilli C, Lisse T, Cayetano J, Torchia M, Mobley W, Bujard H, DeArmond SJ & Prusiner SB (1998) **Doxycycline control of prion protein transgene expression modulates prion disease in mice**. *Proc Natl Acad Sci USA*, 95, 12580-12585. DOI: 10.1073/pnas.95.21.12580
- Tucker S, Moller C, Tegerstedt K, Lord A, Laudon H, Sjodahl J, Soderberg L, Spens E, Sahlin C, Waara ER, Satlin A, Gellerfors P, Osswald G & Lannfelt L (2015) **The murine version of BAN2401 (mAb158) selectively reduces amyloid-beta protofibrils in brain and cerebrospinal fluid of tg-ArcSwe mice**. *Journal of Alzheimers disease*, 43, 575-588. DOI: 10.3233/JAD-140741
- Vaquer-Alicea, J & Diamond MI (2019) **Propagation of protein aggregation in neurodegenerative diseases**. *Annual review of biochemistry* [Preprint] DOI: 10.1146/annurev-biochem-061516-045049
- Walport M & Brest P (2011) **Sharing research data to improve public health**. *Lancet*, 377, 537-539. DOI: 10.1016/S0140-6736(10)62234-9
- Whitesell JD, Buckley AR, Knox JE, Kuan L, Graddis N, Pelos A, Mukora A, Wakeman W, Bohn P, Ho A, Hirokawa KE & Harris JA (2018) **Whole brain imaging reveals distinct spatial patterns of amyloid beta deposition in three mouse models of Alzheimer's disease**. *The Journal of comparative neurology* [Preprint] DOI: 10.1002/cne.24555
- Wilkinson MD, Dumontier M, Aalbersberg IJ, Appleton G, Axton M, Baak A, Blomberg N, Boiten JW, da Silva Santos LB, Bourne PE et al. (2016) **The FAIR Guiding Principles for scientific data management and stewardship**. *Scientific data*, 3, 160018. DOI: 10.1038/sdata.2016.18
- Yamamoto A, Lucas JJ & Hen R (2000) **Reversal of neuropathology and motor dysfunction in a conditional model of Huntington's disease**. *Cell*, 101, 57-66. DOI: 10.1016/S0092-8674(00)80623-6
- Yang J, Zhang R, Shi C, Mao C, Yang Z, Suo Z, Torp R & Xu Y (2017) **AQP4 Association with amyloid deposition and astrocyte pathology in the tg-ArcSwe mouse model of Alzheimer's disease**. *Journal of Alzheimers disease*, 57, 157-169. DOI: 10.3233/JAD-160957
- Yasuda M, Johnson-Venkatesh EM, Zhang H, Parent JM, Sutton MA & Umemori H (2011) **Multiple forms of activity-dependent competition refine hippocampal circuits in vivo**. *Neuron*, 70, 1128-1142. DOI: 10.1016/j.neuron.2011.04.027

Yasuda M & Mayford MR (2006) **CaMKII activation in the entorhinal cortex disrupts previously encoded spatial memory.** *Neuron*, 50, 309-318. DOI: 10.1016/j.neuron.2006.03.035

Yates SC (2018) **Workflow for automated quantification and spatial analysis of labeling in microscopic rodent brain sections.** *Abstract: Society for Neuroscience 2017*, San Diego, United States.

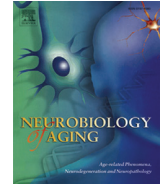
Zhang Y & Wang P (2018) **Age-related increase of insulin-degrading enzyme is inversely correlated with cognitive function in APP^{swe}/PS1^{dE9} mice.** *Medical science monitor: International medical journal of experimental and clinical research*, 24, 2446-2455. DOI: 10.12659/MSM.909596

Zu T, Duvick LA, Kaytor MD, Berlinger MS, Zoghbi HY, Clark HB & Orr HT (2004) **Recovery from polyglutamine-induced neurodegeneration in conditional SCA1 transgenic mice.** *The Journal of neuroscience*, 24, 8853-8861. DOI: 10.1523/JNEUROSCI.2978-04.2004

PAPERS

Contents lists available at [ScienceDirect](http://www.sciencedirect.com)

Neurobiology of Aging

journal homepage: www.elsevier.com/locate/neuaging

Brainwide distribution and variance of amyloid-beta deposits in tg-ArcSwe mice

Sveinung Lillehaug^a, Gry H. Syverstad^a, Lars N.G. Nilsson^{b,c}, Jan G. Bjaalie^a, Trygve B. Leergaard^{a,*}, Reidun Torp^a^a Department of Anatomy, Institute of Basic Medical Sciences, University of Oslo, Oslo, Norway^b Department of Pharmacology, University of Oslo and Oslo University Hospital, Oslo, Norway^c Department of Public Health and Caring Sciences/Molecular Geriatrics, Uppsala University, Rudbeck Laboratory, Uppsala, Sweden

ARTICLE INFO

Article history:

Received 15 May 2013

Received in revised form 3 September 2013

Accepted 7 September 2013

Available online 12 October 2013

Keywords:

Amyloidosis

Alzheimer's disease

Digital brain atlas

Disease model

Immunohistochemistry

Power analysis

ABSTRACT

Transgenic mice carrying the Arctic (E693G) and Swedish (KM670/6701NL) amyloid- β precursor protein (A β PP) develop amyloid-beta (A β) deposits in the brain that resemble Alzheimer's disease neuropathology. Earlier studies of this model have documented morphologic features in selected parts of the cerebral cortex and hippocampus, but the spatial distribution within the brain and variance of A β deposits within a group of tg-ArcSwe mice is unknown. Using immunohistochemistry and brainwide microscopic analysis of 12-month-old tg-ArcSwe mice, we show that A β x-40 plaque deposits are consistently present in the cerebral cortex, hippocampus, and thalamus and variably present in other regions. Using quantitative image analysis, we demonstrated that the average A β burden in the cortex and hippocampus is similar across animals, with coefficients of variance of 22% and 25%, respectively. This indicates that interventional studies of tg-ArcSwe mice are feasible using region-of-interest comparisons and that interventional trials require larger group sizes than commonly used. We also present an online atlas providing access to images showing the detailed characteristics and spatial distribution patterns of A β x-40 labeling.

© 2014 Elsevier Inc. All rights reserved.

1. Introduction

Alzheimer's disease (AD) is a neurodegenerative disorder characterized by premature cognitive decline and excessive formation of amyloid plaques and neurofibrillary tangles in the brain (Holtzman et al., 2011). With rising incidence in an increasingly elderly population, AD stands out as one of the largest current challenges in neurology. There is urgent need for improved diagnostic tools, better understanding of the genetic and molecular basis of the disease, and new interventions. To this end, genetic animal models represent powerful tools for experimental investigations of pathogenic processes, new diagnostic markers, and identification and evaluation of potential new therapeutic strategies.

Several gene mutations associated with familial AD (Schellenberg and Montine, 2012) have been used to create transgenic mouse models. The first genetic animal model reflecting important characteristics of AD was the platelet-derived growth factor β -driven APP (PDAPP) model carrying the Indiana mutation (p.V717F) (Games et al., 1995). Since then a range of other models

have emerged, and there is a considerable number of genetic mouse models available that mimic various aspects of the disease (Philipson et al., 2010). However, no animal model can reproduce the full spectrum of histologic and biochemical changes seen in AD patients (Duyckaerts et al., 2009), and the selection of appropriate models for different experimental investigations is a considerable challenge but critical for investigational outcomes. The use and interpretation of genetic models for AD therefore requires comprehensive and detailed knowledge about the genetic background, behavioral alterations, and neuropathologic phenotypes occurring in various models. Moreover, in context of intervention trials comparing the effects of experimental treatment versus placebo in groups of animals, suitable quantitative biometric parameters are needed to measure the effect of intervention. For studies of AD models, this typically involves parameters reflecting hallmarks of disease, such as the amount, density, size, and detailed morphology of amyloid plaques or neurofibrillary tangles (Philipson et al., 2010). The variance of such quantitative morphometric parameters naturally occurring within a group of animals is one of several critical parameters for the planning of interventional studies and estimation of the statistical power needed to detect effects of a certain magnitude (Jucker, 2010).

The transgenic tg-ArcSwe mouse model (Lord et al., 2006; Philipson et al., 2009a) stands out as a particularly promising

S.L. and G.H.S. contributed equally to this work.

* Corresponding author at: Department of Anatomy, Institute of Basic Medical Sciences, University of Oslo, Box 1105, Blindern, N-0317 Oslo, Norway. Tel.: +47 22851052; fax: +47 22851278.

E-mail address: t.b.leergaard@medisin.uio.no (T.B. Leergaard).

0197-4580/\$ – see front matter © 2014 Elsevier Inc. All rights reserved.

<http://dx.doi.org/10.1016/j.neurobiolaging.2013.09.013>

model for investigations of intraneuronal A β accumulation as well as formation and clearance of amyloid plaques because of their biochemically resilient structure resembling AD brain. The transgene carries both the Arctic mutation (p. E693G), which is located within the A β domain of the amyloid- β precursor protein (A β PP) gene and facilitates A β protofibril formation (Nilsberth et al., 2001; Philipson et al., 2012), and the Swedish mutation (p. KM670/671NL), which is coupled to increased generation of A β peptides (Citron et al., 1992; Mullan et al., 1992). Inclusion of the Swedish A β PP mutation accelerates age of onset in the animal model compared with using the Arctic mutation alone (Lord et al., 2006; Rönnbäck et al., 2011). Among dozens of amyloid- β precursor protein (A β PP) transgenic models, the tg-ArcSwe model is unique because of its marked phenotype with age-dependent intraneuronal A β accumulation occurring several months before the onset of extracellular plaque formation (Lord et al., 2006; Philipson et al., 2009b). Intraneuronal A β has also been observed in post-mortem human AD brains (Gouras et al., 2000). Morphologic investigations have revealed progressive structural changes of plaque formation from age 6 months, accompanied by dynamic response in surrounding tissue including swollen and distorted dendrites and synaptic nerve endings and inflammatory reactions in tissue, with microgliosis and profound upregulation of certain inflammatory markers (Lord et al., 2006; Philipson et al., 2009a). Although these earlier reports have documented morphologic features of A β deposits in the hippocampus and cerebral cortex, the detailed spatial distribution and density of A β deposits across the entire brain is less well characterized. More important, variance in the amount and anatomic distribution of neuropathology within a group of tg-ArcSwe mice is not well described.

The aim of the present study was thus to contribute to the characterization of the morphologic phenotype of tg-ArcSwe mice by (1) mapping the distribution of A β plaque across the entire brain in adult male and female tg-ArcSwe mice and (2) determining the amount and variability of A β deposits in these mice. Here we report the detailed morphologic characteristics, brainwide distribution, and statistical variance of immunolabeled A β plaques. Our comprehensive immunohistochemical mapping and quantitative results are subsequently used for statistical power analysis and discussed in terms of how this model can be used in future interventional investigations. Finally, we provide a publicly available online atlas of high-resolution images of the histologic material, facilitating inspection and reanalysis of the morphologic characteristics and spatial distribution of A β plaques across the brain. The atlas, available through the Rodent Brain WorkBench (www.rbwb.org), includes a series of section images from a representative male and female mouse and selected example images illustrating key morphologic features.

2. Methods

2.1. Animals

Ten mice carrying a human A β PP cDNA with the Arctic (p. E693G) and Swedish (p. KM670/671NL) mutations were investigated for histologic characterization at light microscopic level, and additional samples from 2 tg-ArcSwe animals from our electron microscopy (EM)-tissue repository were investigated for immunohistochemistry at the ultrastructural level. Mice were housed under standard conditions (12-hour dark-light cycles) with unrestricted access to food and water. All mice were sacrificed at 12 months of age. All animal procedures were in accordance with the National Institutes of Health Guide for the care and use of laboratory animals and approved by the Biological Research Ethics Committee in Norway.

2.2. Tissue processing

Animals were anesthetized using Isofluran Baxter (IsoFlo, Abbot Laboratories, Abbott Park, IL, USA) before being sacrificed by decapitation. Brains were extracted, and the hemispheres were divided and frozen using Nordfjord cool spray (Norden Olje, Ski, Norway) and dry ice and stored at -80°C . Only the right hemispheres were used in this study; the left hemispheres were preserved for other analysis.

2.3. Electron microscopy

The animals used for electron microscopy were anesthetized with Equithesin (0.02 mL/g), transcardially perfused with 4% formaldehyde and 0.1% glutaraldehyde in phosphate buffer pH 7.4 and postfixed in the same solution overnight, and stored in 1/10 fixative at 4°C until further preparation. Pieces from cerebral cortex ($1.0 \times 0.5 \times 0.5\text{mm}^3$) were dissected and embedded in Lowicryl HM20 following our laboratory's standard protocol (Takumi et al., 1999). There are 2 main steps in this procedure, cryoprotection and cryosubstitution. Cryoprotection was done by immersing the tissues into phosphate-buffered glucose followed by increasing concentrations (10%, 20%, and 30%) of glycerol before plunging the tissue specimens into liquid propane at -190°C in a liquid nitrogen-cooled cryofixation unit KF80 (Reichert, Vienna, Austria). Cryosubstitution was undertaken in 0.5% uranyl acetate in anhydrous methanol at -90°C for 24 hours in a cryosubstitution unit (Leica EM AFS, Leica Microsystems GmbH, Wien, Austria). The temperature was stepwise increased to -45°C , and Lowicryl HM20 was gradually substituted for methanol. The specimens were polymerized under ultraviolet light for 48 hours at -45°C . Ultrathin sections were cut and placed on Formvar-coated single-hole grids. Postembedding immunohistochemistry with antibodies A β x-40 and 6E10 (epitope 5-10 in A β) was used to identify amyloid deposits. Electron micrographs were obtained digitally from a transmission electron microscope (Tecnaï 12, Philips Electron Optics BV, Eindhoven, The Netherlands).

2.4. Immunohistochemistry

Sagittal sections from the right hemisphere were cryosectioned (Leica CM3050 S) at $25\ \mu\text{m}$, postfixed with 4% formaldehyde for 5 minutes and pretreated with 80% (w/v) formic acid for 2 minutes and then in 2% H_2O_2 for 7 minutes. From each animal, 3 sections from the right brain hemisphere were selected for image analysis. These sections were selected at corresponding distances from the midline in all animals, each including parts of the cerebral cortex, the hippocampus, and the thalamus. After washing with 10 mM phosphate-buffered saline (PBS), sections were immersed in a preincubation solution (10% normal goat serum [NGS], 1% bovine serum albumin (BSA), and 0.5% Triton X-100 in 10 mM PBS) for 30 minutes at room temperature. Afterward, sections were incubated with the primary antibody A β x-40 (Philipson et al., 2012) (0.5 μm /mL with 3% NGS, 1% BSA, 0.5% Triton X-100 in 10 mM PBS) at 4°C overnight. After repeated washing, sections were incubated with secondary biotinylated goat anti-rabbit antibody (BA-1000, Vector Laboratories, CA, USA) diluted 1:300 in 3% NGS, 1% BSA, 0.5% Triton X-100 in 10 mM PBS, washed in 10 mM PBS, and then incubated with Streptavidin-biotinylated horseradish peroxidase complex (RPN 1051, GE Healthcare, Little Chalfont, UK) diluted 1:100 in 0.5% Triton X-100 in 10 mM PBS for 1 hour at room temperature. After washing with 10 mM PBS, all sections were incubated with 3,3'-diaminobenzidine tetrahydrochloride (Sigma, St Louis, MO, USA) for 5 minutes before 0.1% H_2O_2 was added to a 10 mL 3,3'-diaminobenzidine tetrahydrochloride solution and applied onto the

sections until proper labeling was achieved (3 minutes). The sections were briefly rinsed in water before mounting with glycerine-gelatin (Chemi Teknik, Oslo, Norway).

2.5. Image acquisition, virtual microscopy, and creation of online repository

High-resolution images of sections were acquired using an automated slide scanner system (Mirax Scan, Carl Zeiss Micro-Imaging, Jena, Germany), yielding TIFF images with a spatial resolution of 0.23 $\mu\text{m}/\text{pixel}$. Images were inspected by virtual microscopy and exported 1:2 using Panoramic Viewer software (3DHISTECH, Budapest, Hungary). Exported TIFF images were uploaded in a database system built on a technological platform outlined in (Bjaalie et al., 2005; Moene et al., 2007). The resource uses a web interface (<http://www.rbwb.org/>, select “tg-ArcSwe atlas”) providing access to a customized virtual microscopy tool based on Open Zoom technology (www.openzoom.org) for viewing and navigating within and across section images. All labeled sections from 2 representative animals, 1 male (case M3) and 1 female (case F1), were included in the repository. In addition, we included selected sections from other animals illustrating key morphologic phenomena.

2.6. Quantitative image analysis

Images were first scaled 1:16 (to a spatial resolution of 3.28 $\mu\text{m}/\text{pixel}$) using the export functionality of the Panoramic Viewer. Second, to compensate for different background color intensities following immunohistochemistry, all image histograms were normalized using the match-color algorithm in Adobe Photoshop CS6 with a photomicrograph of a wild-type section as reference (Sedgewick, 2008). Quantitative image analysis was then performed in 3 regions of interest (ROIs) using Image J 1.46r (<http://imagej.nih.gov/ij/>). In each section, the outline of the cerebral cortex, thalamus, and hippocampus were manually delineated. The cerebral cortex was anteriorly delineated by a line connecting the rhinal fissure and anterior tip of the external capsule, dorsally by the external surface of the brain, ventrally by the external capsule, and posteriorly by the dorsal subiculum. The anterior, ventral, and dorsal boundaries of the thalamus were defined by the surrounding white matter in the fimbria, internal capsule and cerebral peduncle, and the hippocampus, and the posterior boundary was approximated by connecting the brachium of the superior colliculus and cerebral peduncle with a curved line encompassing geniculate nucleus. The delineation of the hippocampus included the 3 cornu ammonis subfields (CA1, CA2, CA3), the dentate gyrus, and subiculum and was defined anteriorly against the fimbria, dorsally and posteriorly against the external capsule, and ventrally against the thalamus. Within each ROI, images were binarized by selecting a threshold value in Image J, which yielded boundary definitions best corresponding to the observed plaque boundaries, such that the core and surrounding halo of labeling were included; weakly stained areas in the periphery of the plaque formations and background staining were excluded. The same threshold value was used for all sections. The area of each ROI and the area of labeled objects within each ROI were calculated, and the results were expressed as labeled area fraction in percent (labeled area/ROI area \times 100) as a measure of A β plaque load. For each animal, the mean area fractions of 3 sections were used for the final analysis of group variation and standard deviation. Statistical analyses were performed using InStat (GraphPad Software, San Diego, CA, USA).

3. Results

3.1. Structural and ultrastructural morphology

To confirm that the antibody against A β x-40 yielded the same labeling pattern in tg-ArcSwe mice as an antibody detecting all C-terminally truncated variants of A β , we incubated consecutive ultrathin sections from the prefrontal cerebral cortex with antibodies A β x-40 and 6E10 (epitope A β 5-10). Both antibodies specifically recognized amyloid fibrils within the same plaque, showing that the antibody directed against the C-terminus of A β x-40 gave the same overall labeling pattern as the 6E10 (Fig. 1). This confirmed previous control experiments performed at light microscopic level (Lord et al., 2009, see their supplementary Fig. 1). The EM images also showed plaque deposits associated with necrotic structures, filled with inclusion bodies (Fig. 1A, asterisk). In addition to the typical plaque formation, we consistently observed a considerable fraction of vascular deposits in all cases. Both at the light microscopic and EM level A β x-40 labeling were observed around the endothelium of small to medium-sized vessels (Fig. 2).

3.2. Brainwide spatial distribution of A β x-40 plaques

To map the spatial distribution of A β x-40 plaques across the brain, we evaluated high-resolution digital images of immunostained sections from all 10 animals to determine the presence, size, and morphologic characteristics of A β x-40 stained plaque formations. The amount of A β x-40 plaques was consistently high in the cerebral cortex and hippocampus in all cases. In most cases, substantial amounts of plaque were found in the thalamus, whereas the occurrence of plaque varied more in other brain regions (Fig. 3, Table 1). The highest density of amyloid plaques was consistently found in the cerebral cortex, hippocampus, and, to a lesser extent, thalamus (Table 1). Within the cerebral cortex, there was a clear trend toward higher plaque load in the prefrontal areas compared with parietal and occipital cortical regions (Fig. 3). Notably, amyloid depositions associated with vessels were more prominent in the prefrontal cortex. In the hippocampus, the amyloid deposits were particularly concentrated in CA1 and subiculum (Fig. 4C). Vessel-associated amyloid deposits were also observed in the hippocampus of some animals, but to a lesser degree than in the prefrontal cortex and thalamus. In the thalamus, amyloid plaques were distributed across several thalamic subnuclei (Fig. 3). The size of amyloid plaques varied considerably (Fig. 4), but we observed a trend toward smaller plaque size in the thalamus compared with the cerebral cortex and hippocampus. As in the prefrontal cortex, many of the observed amyloid deposits in the thalamus were associated with vessels (Fig. 2A). In other brain regions, the amount of amyloid plaque varied across animals (Table 1). In some cases, modest amounts of labeling were observed in the olfactory bulb, superior colliculus, cerebellum, and brainstem.

3.3. Quantification of A β plaque load and variance

The amount of A β x-40 labeling was determined in ROIs (Fig. 4A) by image analysis (Fig. 4B and 4C). In this cohort of 12-month-old tg-ArcSwe mice ($n = 10$), the A β -burden was estimated to be $4.1\% \pm 0.3\%$ (SEM) in the cerebral cortex, $4.1\% \pm 0.3\%$ in the hippocampus, and $3.1\% \pm 0.6\%$ in the thalamus. Amyloid- β plaque load ranged from 2.9% to 5.9% in the cerebral cortex and 2.5% to 5.4% in the hippocampus, whereas the greatest variation in amyloid- β plaque load was found in the thalamus, ranging from 0.5% to 6.2%. Coefficient of variance (CV) was 22% in the cerebral cortex, 25% in the hippocampus, and 64% in the thalamus. Fig. 5 provides an overview of the amount of A β x-40 labeling measured.

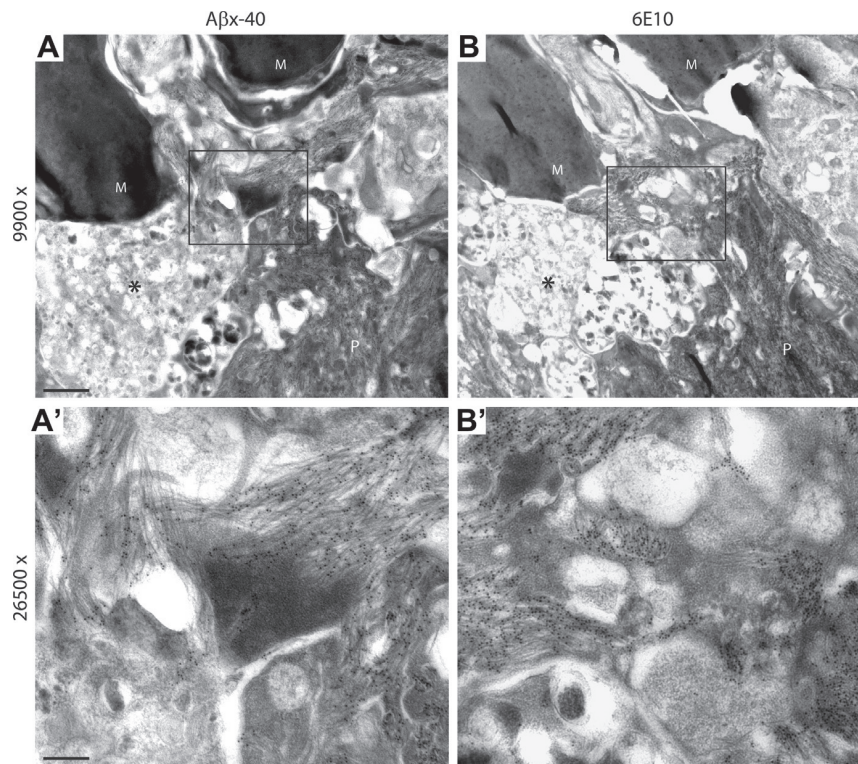


Fig. 1. Amyloid plaque morphology and ultrastructure. Electron micrographs showing the same plaque (P) with amyloid fibrils surrounded by microglia (M) and necrotic patches (asterisk) in consecutive ultrathin sections incubated with antibodies recognizing the C-terminal of A β x-40 (A, A'), or the 6E10 antibody recognizing the N-terminal part of A β (B, B'). Frames in panels A and B indicate the positions of the enlarged images (A' and B'). In all sections, the amyloid fibrils are decorated with dark gold particles indicating presence of A β x-40 (A') or 6E10 (B'). The intensity of A β x-40 labeling in panel A' is comparable to the 6E10 labeling seen in panel B. The images demonstrate that the 2 antibodies allow specific identification of amyloid fibrils in the same plaque. Scale bars: A and B = 1 μ m; A' and B' = 0.1 μ m.

3.4. Gender differences

Two-tailed *t* tests between male ($n = 6$) and female ($n = 4$) mice showed no significant gender difference in plaque load in the cerebral cortex ($p = 0.29$) or thalamus ($p = 0.39$) but indicated that plaque load in the hippocampus was lower in the female group ($p < 0.01$).

4. Discussion

We have mapped the spatial distribution A β -40 deposits in 12-month-old tg-ArcSwe mice and quantified the amount of plaques in 3 ROIs. Our analyses demonstrated that A β x-40 plaque deposits are consistently present in the cerebral cortex, hippocampus, and thalamus and variably present in several other regions. Our ROI-based

quantification of plaque load showed relatively similar A β -burden in the 3 regions, with CVs of 22%, 25%, and 63%, respectively. Gender comparison indicates lower plaque load in the hippocampus of female mice, whereas no differences were found in the other regions.

4.1. Antibody specificity

Several antibodies specific for different A β epitopes are available. The A β x-40-antibody used here detects a neo-epitope and was generated, affinity-purified, and tested for specificity in vitro using enzyme-linked immunosorbent assay as reported earlier (Näslund et al., 2000). We previously demonstrated a single homogenous population of cored A β -plaques in the tg-ArcSwe model that stains with antibodies recognizing N- or C-terminal epitopes in A β (Lord et al., 2009). Thus, in tg-ArcSwe mice the 6E10, A β x-40 or A β x-42

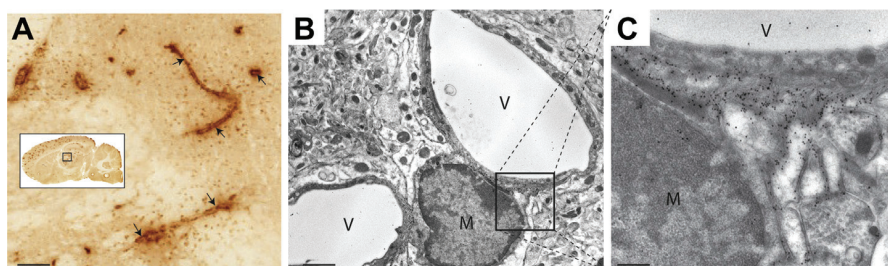


Fig. 2. Vessel associated A β x-40 deposits. (A) Light microscopic image showing thalamic vessels (arrows) surrounded by amyloid (from animal F3). (B) Electron microscopic image showing a section immunostained with 6E10-antibody labeled with gold particles detecting A β in close contact with the vessel endothelium (V). The frame in panel B is enlarged in panel C. Note the electron-dense gold particles decorating the fibrils. Scale bars: A = 100 μ m, B = 3 μ m, and C = 0.3 μ m. Abbreviations: V, vessel; M, microglia.

Table 1
Semiquantitative assessment of A β x-40 distribution across the brain in all animals investigated

	F1	F2	F3	F4	M1	M2	M3	M4	M5	M6
Brain region										
Olfactory bulb	NA	–	NA	+	–	NA	–	NA	NA	NA
Cerebral cortex	+++	+++	+++	+++	+++	+++	+++	+++	+++	+++
Hippocampus	++	++	+++	+++	+++	+++	++	++	++	+++
Striatum	–	–	+	+	–	+	+	–	–	–
Thalamus	+++	+	+++	+	+++	++	+	+++	+	+++
Hypothalamus and amygdala	–	–	+	–	–	+	–	+	–	++
Tectum	–	–	–	–	++	+	+	–	–	++
Brain stem	–	–	+	+	+	–	–	–	–	–
Cerebellum	–	++	–	+	+	–	++	+	+	+

Key: F1–F4: female mice; M1–M6: male mice; NA, = material not available. Density of A β x-40 labeling: –, no plaques or plaque fragments without visible core; + = 1–5 plaques; ++ = 6–20 plaques; +++ \geq 20 plaques.

antibodies will produce the same labeling pattern and indicate the same A β burden, at least at the light-microscopic level used here. This is due to the Arctic A β PP mutation, which makes all A β -peptides including A β 1–40 far more aggregation prone (Nilsberth et al., 2001). Theoretically, a minor fraction of A β -deposits may not be detected with the 6E10 antibody, but because the concentration of N-terminal and modified peptides is low in mice carrying the Swedish mutation (Philipson et al., 2009a), this will, if anything, have only a negligible effect on the plaque loads measured in the present study and be of no relevance for the group comparisons performed. Although N-truncated peptide species dominate in the human brain (Philipson et al., 2012), the concentration of such peptides is low in tg-ArcSwe mice, likely because of the Swedish A β PP mutation and other species differences in A β PP-processing. Additional evidence of the specificity of A β x-40-antibody was provided by an earlier investigation of tg-Swe mice, in which we demonstrated 2 plaque populations, 1 consisting of diffuse wild-type A β plaques that are only A β 42-immunopositive and a second type of cored plaques that stains with A β 40- and A β 42-specific antibodies (Lord et al., 2011). It should also be noted that antibody 6E10, unlike an A β x-40 antibody, binds to both A β PP and sAPP β . However, pretreatment of sections with formic acid as in the present study, will dramatically lower signals from A β PP and enhance detection of aggregated and fibrillized A β (Christenson et al., 2009; Philipson et al., 2009b).

4.2. Impact of transgene-dependent A β -biology on phenotypes

Our transgene mouse colony followed a breeding protocol in which the human A β PP gene was inherited only from male mice. The expression of the proteins was more uniform, and phenotypes were thus found to be less variable compared with random carriers (R. Torp, L.N.G. Nilsson, unpublished results). Amyloid deposition will depend on A β -synthesis (i.e., expression and endoproteolytic processing of the human A β PP transgene) as well as factors influencing A β -transport and deposition. A β PP-expression in the tg-ArcSwe mouse model is regulated by a Thy-1 promoter cassette in which lymphoid expression has been eliminated by deleting the third intron in the murine Thy-1 gene (Vidal et al., 1990). Apart from the Arctic mutation, our model differs from the APP23-model (Sturchler-Pierrat et al., 1997) in 2 aspects: the A β PP695 isoform was inserted and the cDNA extended until 3252 (SmaI) instead of 3026 (HindIII) in 3'UTR untranslated sequences. A shorter 3'UTR increased and widened anatomic transgene-expression in brain (Andra et al., 1996), but the insertion site also plays a major role in transgene expression.

4.3. On the character, morphology, and spatial distribution of A β -deposits

The first reports of this model (Lord et al., 2006; Philipson et al., 2009b) described intraneuronal A β -aggregates in the cerebral

cortex and hippocampus that were visible until 9 months, whereas with advancing age, deposits with amyloid cores were found primarily at extracellular locations. Our current findings indicate dystrophic elements surrounding the plaque areas in tg-ArcSwe mice, with membrane inclusions and filled core vesicles suggestive of dystrophic neurites and most likely cell death. This is noticeable considering the scarcity or absence of neurodegenerative phenotypes in most A β PP transgenic mouse models.

Here we report amyloid deposits that varied considerably in size and density, distributed in cerebral cortex, hippocampus, and thalamus and frequently also in the olfactory bulb, striatum, tectum, amygdala, hypothalamus, brainstem, and cerebellum. The finding of a high plaque load in the prefrontal cortex and a low density of amyloid plaques in the occipital cortex is interesting. We speculate that it relates to default activity (Buckner et al., 2005), but a different level of transgene expression could also play a role. Old tg-ArcSwe mice (aged 24 months) displayed even more widespread A β -deposition than reported here. Deposits were found in striatum and brainstem (Magnusson et al., 2013), which were seldom afflicted in 12-month-old mice.

Although A β PP expression is known to be low in the thalamus (Lord et al., 2006), thalamic plaque deposits were observed in all animals, albeit with more variance than in the cerebral cortex and hippocampus. Axonal transport is of relevance to accumulation of extracellular A β deposits because fiber transection of the perforant pathway markedly reduces A β accumulation in the limbic system of A β PP transgenic mice (Lazarov et al., 2002; Sheng et al., 2002). The importance of neuronal connections is illustrated in our study by the abundance of A β deposition in thalamus, despite low transgene A β PP expression in this region. Reciprocal connections between the cerebral cortex and thalamus (Hoogland et al., 1987; Welker et al., 1988) are crucial for relay and modulation of information between these regions (Sherman and Guillery, 1996), and cortico-thalamic oscillations are linked to absence seizures and sleep spindles. Interestingly, enhanced seizure activity in association with altered hippocampal circuitry was observed in transgenic human A β PP mice (Palop et al., 2007), and AD is a known risk factor for epileptic discharges.

We also noticed considerable amounts of perivascular amyloid deposits in cortical areas and in the thalamus. Perivascular drainage pathways through which extracellular and soluble A β -peptides transport and adhere along arteries and capillaries resulting in amyloid angiopathy and other A β deposits could also have contributed to A β deposits remote from the location of A β production (Weller et al., 2009). This morphologic feature makes the model attractive for investigation of interactions between amyloid and proteins of the vascular unit. Vascular plaques were studied in relation to aquaporin 4 (AQP4) in a recent study from our group (Yang et al., 2011) using an antibody recognizing total A β .

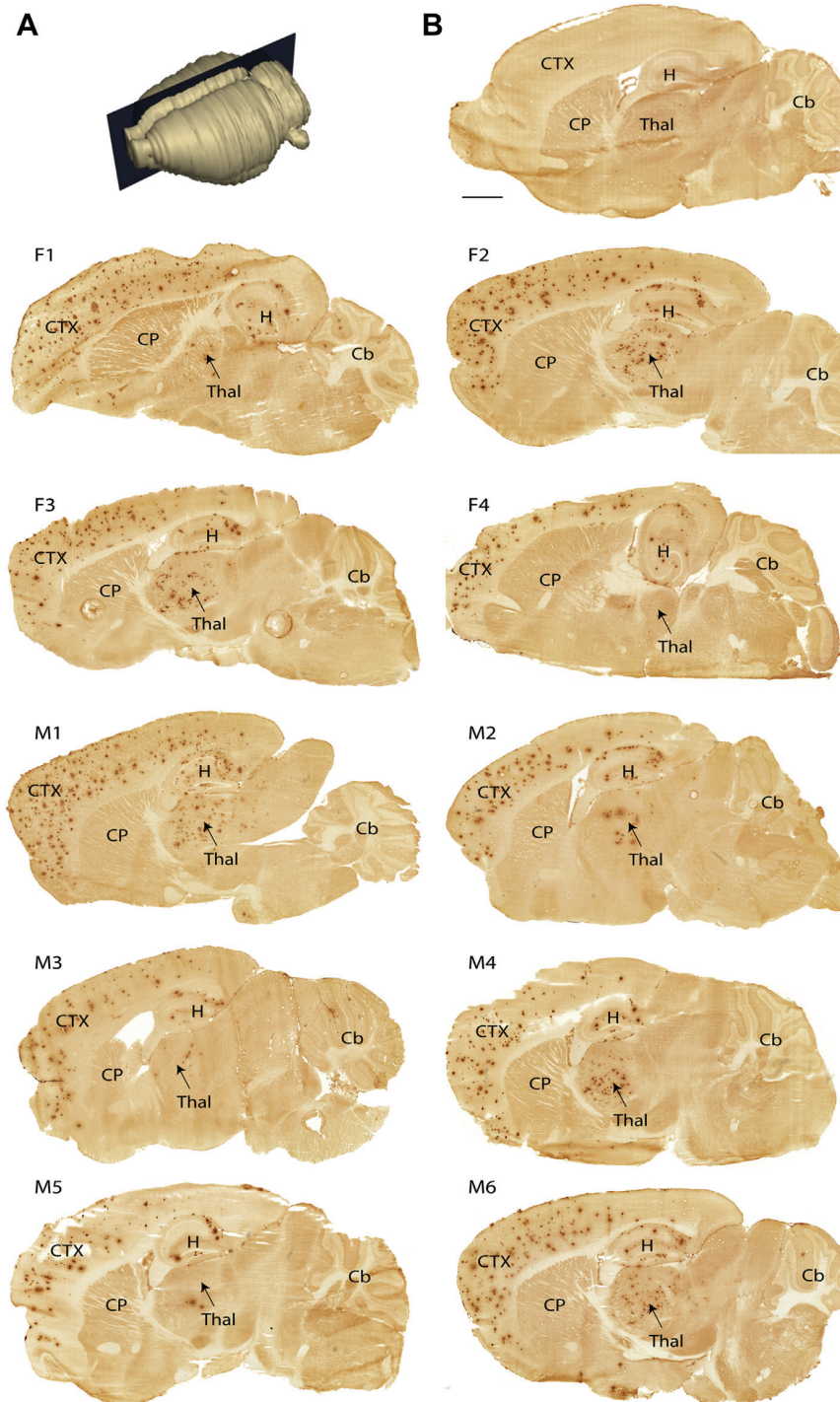


Fig. 3. Spatial distribution of A β x-40 labeling across the brain. Images of A β x-40 immunostained sagittal sections from each of the 10 mice (females F1–F4; males M1–M6) investigated, showing the spatial distribution of A β x-40 in various brain regions. (A) The approximate plane of sectioning. (B) For comparison, an immunostained control section from a wild-type mouse. Scale bar: 1000 μ m. Abbreviations: Cb, cerebellum; CP, caudate putamen complex; CTX, cerebral cortex; H, hippocampus; Thal, thalamus.

The A β -burden measured in this study is somewhat higher than in other studies with tg-ArcSwe (Lord et al., 2009; Philipson et al., 2009a), which might relate to experimental procedures (larger area examined, better signal-noise-ratio of immunostaining, or the threshold chosen) or genetic drift of phenotypes in this new colony at Oslo University compared with the original one at Uppsala

University (Lord et al., 2006). The difference in age-dependent plaque development is modest compared, for example, with the 3xTg-AD model, which has also been bred at different locations (Mastrangelo and Bowers, 2008; Oddo et al., 2003). Senile plaque formation is seed-dependent with an extreme kinetics and thus is partly a stochastic process (Jarrett and Lansbury, 1993). Therefore, a

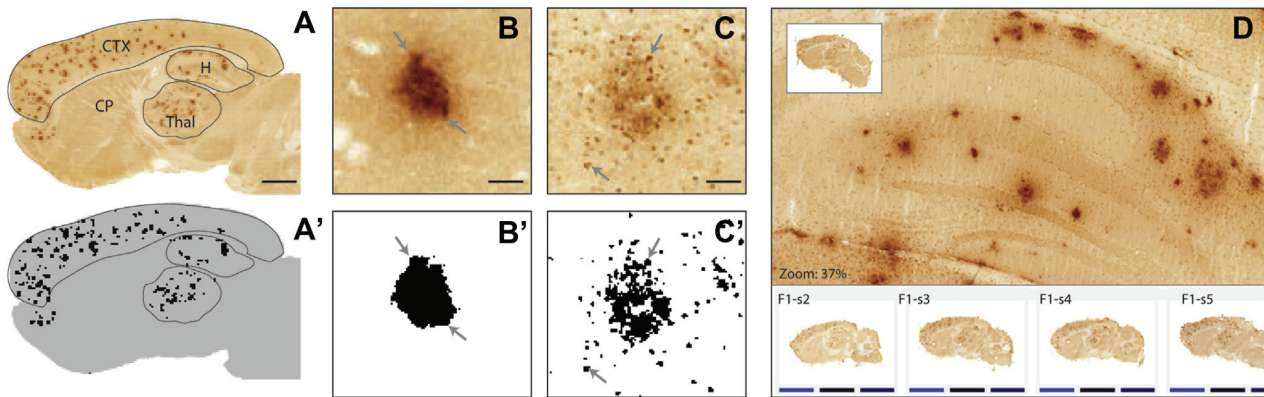


Fig. 4. Morphology and quantification of A β x-40 labeled plaques. (A) Image of a sagittal section from mouse F1 in which 3 regions of interest (cerebral cortex, hippocampus, and thalamus) are outlined. (A'): Binarized version of the same image after applying a threshold value separating labeled A β x-40 from background. The area fraction of black pixels within each region of interest was calculated and used as a measure of plaque load. The gray background indicates the outline of the brain. (B) Magnified images showing a representative dense plaque from the prefrontal cortex (mouse M1). (B') Binarized version of panel B. (C) Magnified image exemplifying a more loosely organized plaque surrounded by scattered labeling in the prefrontal cortex (mouse M1). (C') Binarized version of panel C. Arrows in panels B and C indicate corresponding locations in (B') and (C'). (D) Screenshot showing the graphical user interface of the Virtual Microscopy viewer of the online image repository (<http://www.rbwb.org>). Scale bars: A = 1000 μ m; B and C = 100 μ m. Abbreviations: CP, caudate putamen complex; CTX, cerebral cortex; H, hippocampus; Thal, thalamus.

certain amount of variability is to be expected across brain regions, even in siblings. A β -deposition in thalamus, where little human A β is synthesized, also depends on unknown biological mechanisms that likely differ between animals. Differences in activity of signaling in corticothalamic connections or in A β -drainage may play a role in this regard.

4.4. Gender differences

In line with previous studies with tg-ArcSwe (Lord et al., 2009; Philipson et al., 2009a), we were not able to find gender-dependent differences in the cerebral cortex. Our finding that male tg-ArcSwe mice have a higher hippocampal A β -burden may reflect a region-dependent or random effect. Given the small group size used for this comparison, replication is needed to confirm this finding. Nevertheless, our findings clearly indicate that the gender-specific tendency for development of amyloid deposits is different in tg-ArcSwe model compared with female transgenic mice, with only the Swedish mutation consistently having more amyloid deposits than male siblings (Callahan et al., 2001; L.N.G. Nilsson, unpublished data).

4.5. Variability and power analysis

A β PP transgenic models are often used to determine efficacy of new therapeutic strategies or to evaluate value of nutritional

supplements. Studies suggest that surprisingly diverse types of substances are able to lower A β -deposition in A β PP transgenic mice (Blennow et al., 2006). A CV \approx 25% means that groups of 7 mice would be needed to detect altered cortical A β -deposition of 50% ($\alpha = 0.05$; power (π) = 0.95), that is, it would be as likely that such a study would fail to detect a true therapeutic effect of 50% as to report an untrue effect by coincidence. A CV of approximately 25% in tg-ArcSwe is rather low. Judging from the literature and our own studies, CV of approximately 40%–50% in less aggressive A β PP models such as tg2576 (Callahan et al., 2001) or tg-Swe (Lord et al., 2011). With 40% variability, a group size of 10 animals which is more than typically used in published intervention studies with A β PP transgenic mice, should in theory usually lead to failure in detecting effects of approximately 50% ($\pi = 0.80$) (Jucker, 2010). Thus, misuse and selective reporting of positive studies with A β PP transgenic mice coupled with publication bias likely explain why there are so many successful trials in the literature. Using tg-ArcSwe mice, power analyses suggest that a group size of at least 16 mice ($\pi = 0.80$) or 27 mice ($\pi = 0.95$) is needed to detect a difference of 25% ($\alpha = 0.05$).

4.6. Web-based image repository of A β x-40 burden in tg-ArcSwe mice

Choice of appropriate animal models is critical to the outcome of experimental investigations and requires detailed knowledge not

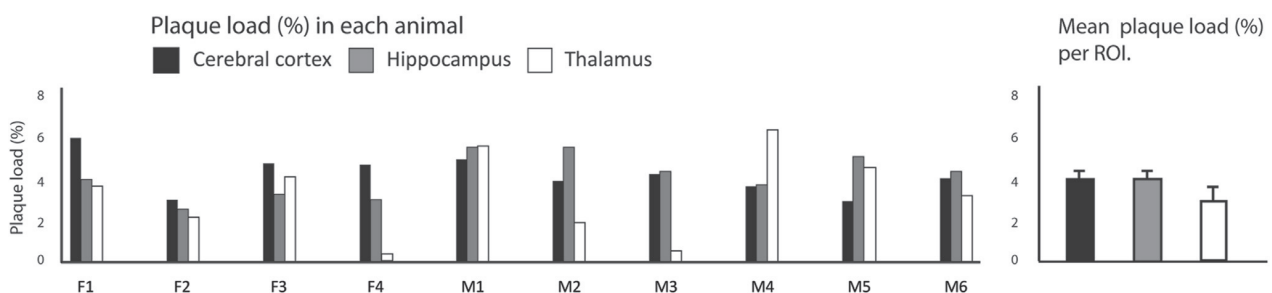


Fig. 5. Total and regional area fraction of A β x-40 labeling. Graphs showing plaque areas measured in the 3 regions of interest (ROI) for each case and average areas per ROI for all animals (n = 10) with SEM.

only about the genetic background of animals but also the morphologic expression of disease-specific neuropathology. In this context, the publicly available web atlas of images from the histologic sections produced in this study represents a valuable source of information that could not be communicated in journal-article format. With the virtual microscopy tool embedded in the web application (Fig. 4C), the user can browse section images across the brain and select any image for detailed inspection of the A β x-40 immunolabeling. We believe that by providing comprehensive information about transgenic animal models available through this type of neuroinformatics resource (Boy et al., 2006; Odeh et al., 2011), it will be possible to make more informed decisions on choice of animal model and study design.

4.7. Concluding remarks

The tg-ArcSwe mouse model is practical to use considering the early onset of extracellular plaque formation. Senile plaques appear in the brain at age 5 to 6 months (Lord et al., 2006) and become highly abundant in regions where the A β PP-transgene is expressed at 12 months, but are also present in other brain regions. Importantly, A β deposits better resemble AD brain in terms of resilience to biochemical extraction with sodium dodecyl sulfate (SDS; Philipson et al., 2009a). Compared with other models, for example, the commonly used Tg2576, phenotype variability among tg-ArcSwe mice is modest in terms of both anatomic distribution and density of deposits in the cerebral cortex and hippocampus. This means that fewer mice are needed to gain statistical power when evaluating novel therapeutics. The smaller CV presumably relates to the strong genetic effect of 2 AD mutations but also to tg-ArcSwe mice being bred on a pure genetic background. The model is expected to be suitable for behavioral studies because it can be maintained on a pure genetic background of C57Bl/6J, which in theory should reduce the variability of all phenotypes (including behavior). Also, many tasks are thought to depend on vision, and thus C57Bl/6J is a preferred inbred strain for behavioral studies because it is one of few inbred strains that are devoid of visual deficits (Brown, 2007). Moreover, given that the Arctic mutation results in amyloid deposition around and within vessels, the tg-ArcSwe model also stands out as a valuable tool for studying A β drainage and clearance at an early stage.

Disclosure statement

L.N.G.N. is stock owner in BioArctic Neuroscience AB, which owns the patent to the tg-ArcSwe mouse model. The other authors report no conflicts of interest.

Acknowledgements

This work was supported by the Letten Centre, University of Oslo to RT, Anders Jahres stiftelse, Helse Sør-Øst, and Swedish Research Council (#2009–4389) to LNGN, and The Research Council of Norway to JGB. The authors thank Grazyna Babinska for expert histotechnical assistance and Dmitri Darine for expert technical assistance related use and adaptation of neuroinformatics infrastructure. Professor Lars Lannfelt and the Uppsala University Transgenic Facility are acknowledged for their support in developing the tg-ArcSwe mouse model.

Author contributions: study concept and design: R.T., T.B.L., L.N.G.N., S.L., G.H.S.; animal breeding, immunohistochemistry: G.H.S., R.T.; electron microscopy: R.T.; microscopy and morphologic analyses: G.H.S., S.L., T.B.L., R.T.; quantitative image analysis: S.L., G.H.S., T.B.L.; statistical analyses: L.N.G.N., S.L., T.B.L.; neuroinformatics infrastructure and digital image repository: J.G.B., S.L.,

T.B.L.; preparation of figures: S.L., G.H.S., T.B.L., R.T.; preparation of manuscript: S.L., G.H.S., T.B.L., R.T., L.N.G.N., J.G.B.; study supervision: R.T., T.B.L. All authors have read and approved the final manuscript and take responsibility for the integrity of the data and the accuracy of the data analysis.

References

- Andra, K., Abramowski, D., Duke, M., Probst, A., Wiederhold, K.H., Burki, K., Goedert, M., Sommer, B., Staufenbiel, M., 1996. Expression of APP in transgenic mice: a comparison of neuron-specific promoters. *Neurobiol. Aging* 17, 183–190.
- Bjaalie, J.G., Leergaard, T.B., Lillehaug, S., Odeh, F., Moene, I.A., Kjøde, J.O., Darin, D., 2005. Database and tools for analysis of topographic organization and map transformations in major projection systems of the brain. *Neuroscience* 136, 681–695. <http://dx.doi.org/10.1016/j.neuroscience.2005.06.036>.
- Blennow, K., de Leon, M.J., Zetterberg, H., 2006. Alzheimer's disease. *Lancet* 368, 387–403. [http://dx.doi.org/10.1016/S0140-6736\(06\)69113-7](http://dx.doi.org/10.1016/S0140-6736(06)69113-7).
- Boy, J., Leergaard, T.B., Schmidt, T., Odeh, F., Bichelmeier, U., Nuber, S., Holzmann, C., Wree, A., Prusiner, S.B., Bujard, H., Riess, O., Bjaalie, J.G., 2006. Expression mapping of tetracycline-responsive prion protein promoter: digital atlas for generating cell-specific disease models. *Neuroimage* 33, 449–462. <http://dx.doi.org/10.1016/j.neuroimage.2006.05.055>.
- Brown, R.E., 2007. Behavioural phenotyping of transgenic mice. *Can. J. Exp. Psychol.* 61, 328–344. <http://dx.doi.org/10.1037/cjep2007033>.
- Buckner, R.L., Snyder, A.Z., Shannon, B.J., LaRossa, G., Sachs, R., Fotenos, A.F., Sheline, Y.I., Klunk, W.E., Mathis, C.A., Morris, J.C., Mintun, M.A., 2005. Molecular, structural, and functional characterization of Alzheimer's disease: evidence for a relationship between default activity, amyloid, and memory. *J. Neurosci.* 25, 7709–7717. <http://dx.doi.org/10.1523/JNEUROSCI.2177-05.2005>.
- Callahan, M.J., Lipinski, W.J., Bian, F., Durham, R.A., Pack, A., Walker, L.C., 2001. Augmented senile plaque load in aged female beta-amyloid precursor protein-transgenic mice. *Am. J. Pathol.* 158, 1173–1177.
- Christenson, D.Z., Bayer, T.A., Wirths, O., 2009. Formic acid is essential for immunohistochemical detection of aggregated intraneuronal Abeta peptides in mouse models of Alzheimer's disease. *Brain Res.* 1301, 116–125. <http://dx.doi.org/10.1016/j.brainres.2009.09.014>.
- Citron, M., Oltersdorf, T., Haass, C., McConlogue, L., Hung, A.Y., Seubert, P., Vigo-Pelfrey, C., Lieberburg, I., Selkoe, D.J., 1992. Mutation of the beta-amyloid precursor protein in familial Alzheimer's disease increases beta-protein production. *Nature* 360, 672–674. <http://dx.doi.org/10.1038/360672a0>.
- Duyckaerts, C., Delatour, B., Potier, M.C., 2009. Classification and basic pathology of Alzheimer disease. *Acta Neuropathol.* 118, 5–36. <http://dx.doi.org/10.1007/s00401-009-0532-1>.
- Games, D., Adams, D., Alessandrini, R., Barbour, R., Berthelette, P., Blackwell, C., Carr, T., Clemens, J., Donaldson, T., Gillespie, F., Guido, T., Haganian, S., Johnson-Wood, K., Khan, K., Lee, M., Leibowitz, P., Lieberburg, I., Little, S., Masliah, E., McConlogue, L., Montoya-Zavala, M., Mucke, L., Paganini, L., Penniman, E., Power, M., Schenk, D., Seubert, P., Snyder, B., Soriano, F., Tan, H., Vitale, J., Wasdsworth, S., Wolozin, B., Zhan, J., 1995. Alzheimer-type neuropathology in transgenic mice overexpressing V717F beta-amyloid precursor protein. *Nature* 373, 523–527. <http://dx.doi.org/10.1038/373523a0>.
- Gouras, G.K., Tsai, J., Naslund, J., Vincent, B., Edgar, M., Checler, F., Greenfield, J.P., Haroutunian, V., Buxbaum, J.D., Xu, H., Greengard, P., Relkin, N.R., 2000. Intraneuronal Abeta42 accumulation in human brain. *Am. J. Pathol.* 156, 15–20.
- Holtzman, D.M., Morris, J.C., Goate, A.M., 2011. Alzheimer's disease: the challenge of the second century. *Sci. Transl. Med.* 3, 77sr1. <http://dx.doi.org/10.1126/scitranslmed.3002369>.
- Hoogland, P.V., Welker, E., Van der Loos, H., 1987. Organization of the projections from barrel cortex to thalamus in mice studied with Phaseolus vulgaris-leucoagglutinin and HRP. *Exp. Brain Res.* 68, 73–87.
- Jarrett, J.T., Lansbury Jr., P.T., 1993. Seeding "one-dimensional crystallization" of amyloid: a pathogenic mechanism in Alzheimer's disease and scrapie? *Cell* 73, 1055–1058.
- Jucker, M., 2010. The benefits and limitations of animal models for translational research in neurodegenerative diseases. *Nat. Med.* 16, 1210–1214. <http://dx.doi.org/10.1038/nm.2224>.
- Lazarov, O., Lee, M., Peterson, D.A., Sisodia, S.S., 2002. Evidence that synaptically released beta-amyloid accumulates as extracellular deposits in the hippocampus of transgenic mice. *J. Neurosci.* 22, 9785–9793.
- Lord, A., Englund, H., Soderberg, L., Tucker, S., Clausen, F., Hillered, L., Gordon, M., Morgan, D., Lannfelt, L., Pettersson, F.E., Nilsson, L.N., 2009. Amyloid-beta protofibril levels correlate with spatial learning in Arctic Alzheimer's disease transgenic mice. *FEBS J.* 276, 995–1006. <http://dx.doi.org/10.1111/j.1742-4658.2008.06836.x>.
- Lord, A., Kalimo, H., Eckman, C., Zhang, X.Q., Lannfelt, L., Nilsson, L.N., 2006. The Arctic Alzheimer mutation facilitates early intraneuronal Abeta aggregation and senile plaque formation in transgenic mice. *Neurobiol. Aging* 27, 67–77. <http://dx.doi.org/10.1016/j.neurobiolaging.2004.12.007>.
- Lord, A., Philipson, O., Klingstedt, T., Westermark, G., Hammarstrom, P., Nilsson, K.P., Nilsson, L.N., 2011. Observations in APP bitransgenic mice suggest that diffuse and compact plaques form via independent processes in Alzheimer's disease. *Am. J. Pathol.* 178, 2286–2298. <http://dx.doi.org/10.1016/j.ajpath.2011.01.052>.

- Magnusson, K.S.D., Syvänen, S., Svedberg, M.M., Philipson, O., Söderberg, L., Tegerstedt, L., Holmquist, M., Gellerfors, P., Tolmachev, V., Antoni, G., Lannfelt, L., Hall, H., Nilsson, L.N.G., 2013. Specific uptake of an amyloid- β protofibril-binding antibody-tracer in A β PP transgenic mouse brain. *J. Alzheimers Dis.* 37, 29–40.
- Mastrangelo, M.A., Bowers, W.J., 2008. Detailed immunohistochemical characterization of temporal and spatial progression of Alzheimer's disease-related pathologies in male triple-transgenic mice. *BMC Neurosci.* 9, 81. <http://dx.doi.org/10.1186/1471-2202-9-81>.
- Moene, I.A., Subramaniam, S., Darin, D., Leergaard, T.B., Bjaalie, J.G., 2007. Toward a workbench for rodent brain image data: systems architecture and design. *Neuroinformatics* 5, 35–58.
- Mullan, M., Crawford, F., Axelman, K., Houlden, H., Lilius, L., Winblad, B., Lannfelt, L., 1992. A pathogenic mutation for probable Alzheimer's disease in the APP gene at the N-terminus of beta-amyloid. *Nat. Genet.* 1, 345–347. <http://dx.doi.org/10.1038/ng0892-345>.
- Näslund, J., Haroutunian, V., Mohs, R., Davis, K.L., Davies, P., Greengard, P., Buxbaum, J.D., 2000. Correlation between elevated levels of amyloid beta-peptide in the brain and cognitive decline. *JAMA* 283, 1571–1577. <http://dx.doi.org/10.1001/jama.283.12.1571>.
- Nilsberth, C., Westlind-Danielsson, A., Eckman, C.B., Condron, M.M., Axelman, K., Forsell, C., Stenh, C., Luthman, J., Teplow, D.B., Younkin, S.G., Näslund, J., Lannfelt, L., 2001. The "Arctic" APP mutation (E693G) causes Alzheimer's disease by enhanced Abeta protofibril formation. *Nat. Neurosci.* 4, 887–893. <http://dx.doi.org/10.1038/nn0901-887>.
- Oddo, S., Caccamo, A., Shepherd, J.D., Murphy, M.P., Golde, T.E., Kaye, R., Metherate, R., Mattson, M.P., Akbari, Y., LaFerla, F.M., 2003. Triple-transgenic model of Alzheimer's disease with plaques and tangles: intracellular Abeta and synaptic dysfunction. *Neuron* 39, 409–421.
- Odeh, F., Leergaard, T.B., Boy, J., Schmidt, T., Riess, O., Bjaalie, J.G., 2011. Atlas of transgenic Tet-Off Ca²⁺/calmodulin-dependent protein kinase II and prion protein promoter activity in the mouse brain. *Neuroimage* 54, 2603–2611. <http://dx.doi.org/10.1016/j.neuroimage.2010.11.032>.
- Palop, J.J., Chin, J., Roberson, E.D., Wang, J., Thwin, M.T., Bien-Ly, N., Yoo, J., Ho, K.O., Yu, G.Q., Kreitzer, A., Finkbeiner, S., Noebels, J.L., Mucke, L., 2007. Aberrant excitatory neuronal activity and compensatory remodeling of inhibitory hippocampal circuits in mouse models of Alzheimer's disease. *Neuron* 55, 697–711. <http://dx.doi.org/10.1016/j.neuron.2007.07.025>.
- Philipson, O., Hammarstrom, P., Nilsson, K.P., Portelius, E., Olofsson, T., Ingelsson, M., Hyman, B.T., Blennow, K., Lannfelt, L., Kalimo, H., Nilsson, L.N., 2009a. A highly insoluble state of Abeta similar to that of Alzheimer's disease brain is found in Arctic APP transgenic mice. *Neurobiol. Aging* 30, 1393–1405. <http://dx.doi.org/10.1016/j.neurobiolaging.2007.11.022>.
- Philipson, O., Lannfelt, L., Nilsson, L.N., 2009b. Genetic and pharmacological evidence of intraneuronal Abeta accumulation in APP transgenic mice. *FEBS Lett.* 583, 3021–3026. <http://dx.doi.org/10.1016/j.febslet.2009.08.009>.
- Philipson, O., Lord, A., Gumucio, A., O'Callaghan, P., Lannfelt, L., Nilsson, L.N., 2010. Animal models of amyloid-beta-related pathologies in Alzheimer's disease. *FEBS J.* 277, 1389–1409. <http://dx.doi.org/10.1111/j.1742-4658.2010.07564.x>.
- Philipson, O., Lord, A., Lalowski, M., Soliymani, R., Baumann, M., Thyberg, J., Bogdanovic, N., Olofsson, T., Tjernberg, L.O., Ingelsson, M., Lannfelt, L., Kalimo, H., Nilsson, L.N., 2012. The Arctic amyloid-beta precursor protein (AbetaPP) mutation results in distinct plaques and accumulation of N- and C-truncated Abeta. *Neurobiol. Aging* 33. <http://dx.doi.org/10.1016/j.neurobiolaging.2011.10.022>, 1010.e1–13.
- Rönnbäck, A., Zhu, S., Dillner, K., Aoki, M., Lilius, L., Naslund, J., Winblad, B., Graff, C., 2011. Progressive neuropathology and cognitive decline in a single Arctic APP transgenic mouse model. *Neurobiol. Aging* 32, 280–292. <http://dx.doi.org/10.1016/j.neurobiolaging.2009.02.021>.
- Schellenberg, G.D., Montine, T.J., 2012. The genetics and neuropathology of Alzheimer's disease. *Acta Neuropathol.* 124, 305–323. <http://dx.doi.org/10.1007/s00401-012-0996-2>.
- Sedgewick, J., 2008. *Scientific Imaging with Photoshop: Methods, Measurement, and Output*. Peachpit Press, California. ISBN-10: 0321514335.
- Sheng, J.G., Price, D.L., Koliatsos, V.E., 2002. Disruption of corticocortical connections ameliorates amyloid burden in terminal fields in a transgenic model of Abeta amyloidosis. *J. Neurosci.* 22, 9794–9799.
- Sherman, S.M., Guillery, R.W., 1996. Functional organization of thalamocortical relays. *J. Neurophysiol.* 76, 1367–1395.
- Sturchler-Pierrat, C., Abramowski, D., Duke, M., Wiederhold, K.H., Mistl, C., Rothacher, S., Ledermann, B., Burki, K., Frey, P., Paganetti, P.A., Waridel, C., Calhoun, M.E., Jucker, M., Probst, A., Staufenbiel, M., Sommer, B., 1997. Two amyloid precursor protein transgenic mouse models with Alzheimer disease-like pathology. *Proc. Natl. Acad. Sci. U.S.A.* 94, 13287–13292.
- Takumi, Y., Ramirez-Leon, V., Laake, P., Rinovik, E., Ottersen, O.P., 1999. Different modes of expression of AMPA and NMDA receptors in hippocampal synapses. *Nat. Neurosci.* 2, 618–624. <http://dx.doi.org/10.1038/10172>.
- Vidal, M., Morris, R., Grosveld, F., Spanopoulou, E., 1990. Tissue-specific control elements of the Thy-1 gene. *EMBO J.* 9(3): 833–840.
- Welker, E., Hoogland, P.V., Van der Loos, H., 1988. Organization of feedback and feedforward projections of the barrel cortex: a PHA-L study in the mouse. *Exp. Brain Res.* 73, 411–435.
- Weller, R.O., Djuanda, E., Yow, H.Y., Carare, R.O., 2009. Lymphatic drainage of the brain and the pathophysiology of neurological disease. *Acta Neuropathol.* 117, 1–14. <http://dx.doi.org/10.1007/s00401-008-0457-0>.
- Yang, J., Lunde, L.K., Nuntagij, P., Oguchi, T., Camassa, L.M., Nilsson, L.N., Lannfelt, L., Xu, Y., Amiry-Moghaddam, M., Ottersen, O.P., Torp, R., 2011. Loss of astrocyte polarization in the tg-ArcSwe mouse model of Alzheimer's disease. *J. Alzheimers Dis.* 27, 711–722. <http://dx.doi.org/10.3233/JAD-2011-110725>.



SCIENTIFIC DATA

OPEN Data Descriptor: Brain-wide distribution of reporter expression in five transgenic tetracycline-transactivator mouse lines

Received: 20 February 2018
 Accepted: 19 December 2018
 Published: 26 February 2019

Sveinung Lillehaug¹, Michael J. Yetman², Maja A. Puchades¹, Martyna M. Checinska¹, Heidi Kleven¹, Joanna L. Jankowsky^{2,3}, Jan G. Bjaalie¹ & Trygve B. Leergaard¹

The spatial pattern of transgene expression in tetracycline-controlled mouse models is governed primarily by the driver line used to introduce the tetracycline-controlled transactivator (tTA). Detailed maps showing where each tTA driver activates expression are therefore essential for designing and using tet-regulated models, particularly in brain research where cell type and regional specificity determine the circuits affected by conditional gene expression. We have compiled a comprehensive online repository of serial microscopic images showing brain-wide reporter expression for five commonly used tTA driver lines. We have spatially registered all images to a common three-dimensional mouse brain anatomical reference atlas for direct comparison of spatial distribution across lines. The high-resolution images and associated metadata are shared via the web page of the EU Human Brain Project. Images can be inspected using an interactive viewing tool that includes an optional overlay feature providing anatomical delineations and reference atlas coordinates. Interactive viewing is supplemented by semi-quantitative analyses of expression levels within anatomical subregions for each tTA driver line.

Design Type(s)	parallel group design • genetic modification design
Measurement Type(s)	reporter gene assay
Technology Type(s)	light microscopy
Factor Type(s)	genotype
Sample Characteristic(s)	Mus musculus • brain

¹Department of Molecular Medicine, Institute of Basic Medical Sciences, University of Oslo, Oslo, Norway.

²Department of Neuroscience, Baylor College of Medicine, Houston, TX, USA. ³Departments of Molecular and Cellular Biology, Neurology, and Neurosurgery, Huffington Center on Aging, Baylor College of Medicine, Houston, TX, USA. Correspondence and requests for materials should be addressed to T.B.L. (email: t.b.leergaard@medisin.uio.no)

Background & Summary

Transgenic mice in which the expression of specific genes can be pharmacologically regulated are powerful tools for studying brain disease^{1–10}. One common approach for temporally-regulated transgene expression allows transcription to be exogenously controlled by administration of tetracycline or its chemical derivatives^{11–14}. Tetracycline-responsive transcription depends on a bipartite system in which the promoter controlling a transgene of interest is activated exclusively by an artificial fusion protein known as the tetracycline-controlled transactivator (tTA; Fig. 1a,b). The promoter used to restrict tTA expression therefore dictates the spatial distribution of the transgenic protein of interest.

Many different tTA transgenic lines with varying expression patterns have been generated for individual experimental purposes. A database of tet-transgenic rodents lists more than a hundred mouse lines expressing tTA or its tet-inducible counterpart reverse tTA (rtTA), and about one fourth of these are reported to have transgene expression in the brain¹⁴. Detailed information about the expression pattern of tTA is important for selecting a driver line suitable for the circuit or brain region of interest. Despite this need, comparison of expression patterns reported across the myriad tTA/rtTA lines has historically been difficult because of the varying methods used to locate transgene expression compounded by significant variation in spatial granularity and scope of analyses. Some reports describe brain expression patterns at the level of major brain regions^{15–17}, while others focus on selected brain regions with limited documentation of possible expression outside the region of interest^{18,19}.

To the best of our knowledge, only four studies have characterized the expression pattern of tTA driver lines in detail across the entire mouse brain. These studies have mapped reporter expression in tTA driver lines based on the promoters for cellular prion protein (Prnp)⁴, neuropeptide Y receptors Y1 and Y5²⁰, Ca²⁺/calmodulin-dependent protein kinase II α (Camk2a)²¹, and neuropsin (Nop)²². Three of these studies provide web-based virtual microscopy and repositories with series of histological section images spanning the mouse brain. This information is complemented by semiquantitative analyses of expression levels within selected subregions^{4,21,22} and shared via the Rodent Brain Workbench portal (www.rbwb.org). Detailed anatomical comparison of expression patterns between driver lines nevertheless remains challenging due to differences in the reference atlases used, the criteria for identifying anatomical boundaries, and the plane of sectioning of histological material. Only a subset of corresponding sections can be compared side-by-side, as shown by Odeh *et al.*²¹.

To overcome this limitation in cross-model comparison, we present a repository of serial microscopic images showing lacZ reporter activity in five frequently used tTA-expressing transgenic lines (Prnp; Camk2a; Nop; L7/Purkinje cell protein 2, Pcp2; and Pituitary homeobox 3, Pitx3). The repository serves as a resource for neuroscience researchers working with tet-transgenic models. The image data and associated metadata are made available via the web page of the EU Human Brain Project (www.humanbrainproject.eu)²³. All images have all been registered to the Allen Mouse Common Coordinate Framework (CCF) version 2²⁴. For each tTA transgenic line, the density of lacZ reporter expression across the brain is semi-quantitatively scored. All histological images can be interactively examined online by virtual microscopy with superimposed atlas maps or downloaded for off-line comparison with other experimental materials. The image repository is suitable as a benchmark reference for transgenic mouse models with tetracycline-controlled transgene expression in the brain.

Methods

Overview of experimental design

To specify and compare where in the brain conditional gene expression occurs in the most commonly used tTA promoter lines with known brain expression (Prnp, Camk2a, Nop, Pitx3, and Pcp2), we created a repository of microscopic images showing the location of conditional gene expression in five promoter-reporter crosses. In these mice, the transgenic responder line encodes the *lacZ* gene, allowing a β -galactosidase reaction to reveal the spatial distribution of the tTA promoter and thereby indicate where in the brain conditional gene expression occurs. Registration of all histological images to a common mouse brain reference atlas makes it possible to directly compare the regional specificity and amount of expression across the five tTA driver lines. The core workflow is outlined in Fig. 1c.

Mouse strain generation

All animal procedures were performed in accordance with the National Institutes of Health Guide for the care and use of laboratory animals and approved by local institutional animal welfare committees (associated with Baylor College of Medicine, University of Tübingen, or University of Oslo). The tTA image repository holds image data from 12 adult bigenic mice, representing intercrosses between five promoter-tTA driver lines and two tetO-lacZ reporter lines (Table 1). Experimental details about animal constructs are provided below. Microscopic images from Prnp, Camk2a, and Nop driver lines^{4,21,22} were imported from the Rodent Brain Workbench (www.rbwb.org). Data from single transgenic (tetO-lacZ) control animals, excluding the possibility of endogenous β -galactosidase staining, have been reported earlier²². Information on the three strains used to generate Pcp2 and Pitx3 lacZ expression data is provided below.

tetO-nls-lac-CMK (tetO-GFP-nls-lacZ-Camk2a 3'UTR). The lacZ reporter line used for detection of tTA activity in the Pcp2, Nop, and Pitx3 driver lines encoded an in-frame fusion of the *E. coli lacZ* gene

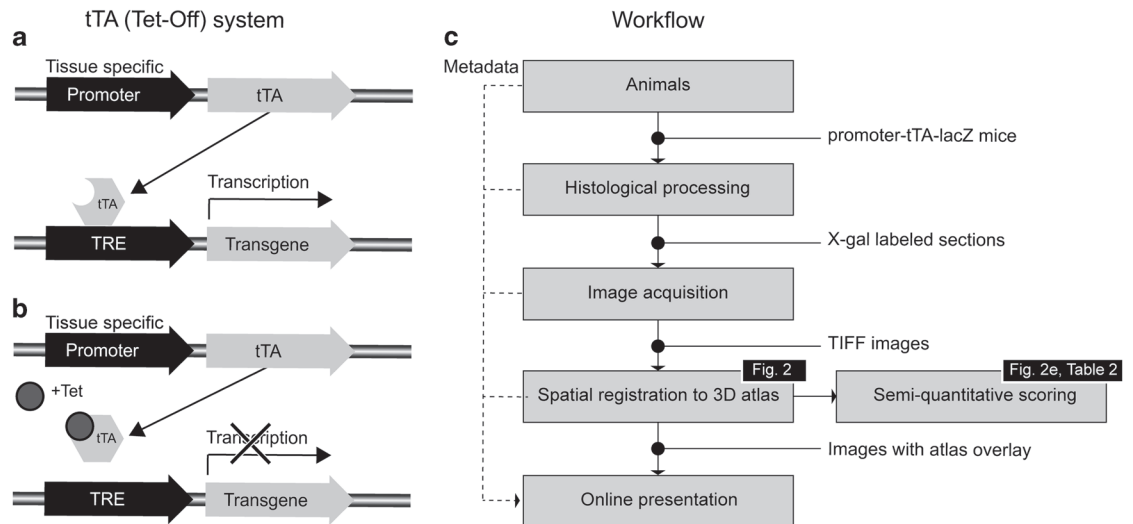


Figure 1. Principle of the tTA/Tet-Off system and workflow. (a,b) Principle of the tetracycline-dependent regulatory (tTA/Tet-Off) system. A tissue-specific promoter drives spatially restricted expression of the tetracycline transactivator protein (tTA) in the desired tissue. In the absence of tetracycline (Tet), the tTA protein binds to a tetracycline responsive element (TRE) which in turn drives expression of the transgene of interest. (b) If tetracycline (Tet) is administered, it prevents tTA from binding to the TRE and activating transgene expression. (c) Outline of the workflow used for collection, analysis and presentation of experimental data.

	Driver line/Reporter line	Animal #	Gender	Age (weeks)	# Images	Orientation
Camk2a	Camk2a-tTA/tetO-lacZ	317.8	female	41	47	coronal
Nop	Nop-tTA/tetO-lacZ-nls-GFP	1952	male	38,5	46	coronal
	Nop-tTA/tetO-lacZ-nls-GFP	2877	male	36	23	horizontal
	Nop-tTA/tetO-lacZ-nls-GFP	2849	female	31	34	coronal
Pcp2	Pcp2-tTA/tetO-lacZ-nls-GFP	1261	male	42,5	41	coronal
	Pcp2-tTA/tetO-lacZ-nls-GFP	3292	female	37	23	horizontal
	Pcp2-tTA/tetO-lacZ-nls-GFP	4340	male	20	33	coronal
Pitx3	Pitx3-tTA/tetO-lacZ-nls-GFP	3435	male	15	42	coronal
	Pitx3-tTA/tetO-lacZ-nls-GFP	5154	female	12,5	16	horizontal
	Pitx3-tTA/tetO-lacZ-nls-GFP	6513	male	9	15	horizontal
	Pitx3-tTA/tetO-lacZ-nls-GFP	6517	female	9	32	coronal
Prnp	Prnp-tTA/tetO-lacZ	388.12	female	5	57	coronal

Table 1. Overview of materials.

with green fluorescent protein (GFP) under control of the first-generation tetO promoter²⁵. The reporter construct also included the nuclear localization signal (nls) from the simian virus 40 (SV40) large T antigen and was followed by the three prime untranslated region (3' UTR) from mouse calcium-calmodulin kinase type II α (Camk2a). It is unclear from the original report whether the tetO-lacZ-nls-GFP animals were generated on a B6CBA F2 or B6SJL F2 background, but in either case the line was eventually maintained by backcross with C57BL/6 (Dr. Mark Mayford, personal communication). This line was obtained from Dr. Mark Mayford (Department of Neuroscience, Scripps Research Institute, La Jolla, CA, USA) in 2010 and backcrossed to C57BL/6 J for another 4 generations before being mated with the Pcp2-tTA and Pitx3-tTA driver lines as described below.

L7/Purkinje cell protein 2 (Pcp2)-tTA/tetO-lacZ-nls-GFP mice (Pcp2-tTA). Mice expressing tTA under control of the mouse L7/Purkinje-cell protein 2 (Pcp2) promoter were created by Dr. Harry T. Orr (Department of Laboratory Medicine and Pathology, University of Minnesota, USA) and obtained from a colony derived from this stock by Dr. David Nelson (Department of Molecular and Human Genetics,

Baylor College of Medicine, USA). The original line was created by injection into FVB/N embryos and maintained on an FVB background. It was received in 2011 and backcrossed to FVB/NJ for another 5 generations before outcrossing to the tetO-lacZ-nls-GFP reporter (see above) for the current studies. The line is available through Jackson Laboratories under strain name FVB-Tg(Pcp2-tTA)³Horrr/J, stock #5625.

Pituitary homeobox 3(Pitx3)-tTA/tetO-lacZ-nls-GFP mice (Pitx3-tTA). Pitx3-tTA mice were generated in the laboratory of Dr. Huaibin Cai (Laboratory of Neurogenetics, National Institute of Aging, Bethesda, MD, USA) by targeted insertion of an IRES2-tTA-loxP-neomycin-loxP cassette in exon 4 of the mouse Pitx3 gene¹⁹. 129/SvJ ES founder males were generated and their offspring were mated with a Cre line to remove the neomycin cassette from the transgene. The line was backcrossed to produce congenic C57BL/6J animals. Animals were obtained from Dr. Mark Mattson (Laboratory of Neurosciences, National Institute of Aging, Baltimore, MD, USA) in 2013 that had been derived from Dr. Huaibin Cai's original colony at the NIH. The mice were bred at Baylor College of Medicine, Houston, TX, USA for one generation with C57BL/6J before outcrossing the offspring with the tetO-lacZ-nls-GFP reporter line for the current study.

Prnp-tTA/tetO-lacZ (Prnp-tTA), Camk2a-tTA/tetO-lacZ (Camk2a-tTA) and Nop-tTA/tetO-lacZ-nls-GFP (Nop-tTA) mice. Description of the construction of Prnp, Camk2a, and Nop-tTA lines are provided in previous publications^{4,21,22}. In brief, *Prnp-tTA/tetO-lacZ* and *Camk2a-tTA/tetO-lacZ* mice were generated by crossing a Prnp promoter line (Prnp-tTA, line F959²⁵) or Camk2a promoter line²⁶ with a responder line transgenic for a bidirectional reporter gene construct containing the *E. coli* derived LacZ reporter gene encoding β -galactosidase^{27,28}, and the *Luciferase* gene from *Photinus pyralis* (not used in the present study) (Luc-tetO-lacZ). *Nop-tTA* mice were generated by backcrossing the Nop-tTA mouse line provided by Dr. Mark Mayford (Line tTA-EC²⁹; also known as Klk8-tTA; MMRRC strain # 031780) to C57BL/6J for 1–3 generations before outcrossing to the responder *E. coli* lacZ and green fluorescent protein (GFP) responder line listed above (tetO-lacZ-nls-GFP)²⁶.

Tissue fixation

The procedures described below pertain to tissue from the Pcp2-tTA, and Pitx3-tTA, and tetO-lacZ-nls-GFP mice. The histological procedures used for previously published strains are very similar, but for details see the original publications (Prnp-tTA⁴; Camk2a-tTA²¹; Nop-tTA²²).

The animals were overdosed with pentobarbital and transcardially perfused with cold phosphate-buffered saline (PBS) containing 10 U/ml of heparin followed by 4% paraformaldehyde (PFA) in PBS. Brains were extracted and post-fixed by immersion for 3 h at 4 °C in 4% PFA/PBS before being cryo-protected by immersion in 30% sucrose/PBS for 48 h at 4 °C.

Brain dissection and sectioning

After removal of the skull, brains were rinsed in PBS before being incubated for 2 h in PBS containing 5% gelatin at 37 °C (Sigma, G2500) followed by 2 h in 11% gelatin/PBS at 37 °C. Tissue blocks were placed flat-face down onto a 3–4 mm thick layer of solidified 11% gelatin inside a plastic mold and flooded with liquid 11% gelatin solution until the tissue was completely submerged. Blocks were allowed to harden at room temperature for 30–60 min. Gelatin blocks were then released from their molds and immersed in 4% PFA/PBS for 4 h at 4 °C. The blocks were then placed in PBS containing 10% sucrose for 24 h at 4 °C, followed by 30% sucrose/PBS for at least 48 h (and up to 7 d) at 4 °C before they were sectioned.

Cryoprotected gelatin blocks were marked with a razor blade to indicate orientation and placed in a peel-away plastic mold (Polysciences, Inc., 18646A-1) filled with pre-warmed 37 °C PBS containing 3% gelatin. The block was then flash frozen by slowly lowering the mold into isopentane (Sigma, M32631) that had been chilled to –60 °C. After 30 min in isopentane, the block was recovered and the plastic mold removed so that the tissue could be mounted with PBS onto the stage of a freezing-sliding microtome and sectioned at 45 μ m. Sections were stored in cryoprotectant (0.1 M phosphate buffer pH 7.4, 30% ethylene glycol, 25% glycerol) at –20 °C until use. Sections were sampled to cover the entire brain; from each brain 32–61 coronal sections or 16–23 horizontal sections were sampled.

β -galactosidase staining and counterstaining

The lacZ gene product (β -galactosidase) was identified using X-gal (5-bromo-4-chloro-3-indolyl- β -D-galactopyranoside) as a substrate. Enzymatic cleavage of X-gal gives rise to an insoluble indigo-blue compound^{30,31}. Sections were mounted onto Superfrost Plus slides (Fisher, 12-550-15) from tris-buffered saline (TBS) and air-dried for 48 h before use. Slides were rehydrated in running tap water for 5 min and rinsed for 15 min at room temperature in PBS containing 2 mM MgCl₂. The slides were then incubated in pre-warmed 0.1 M phosphate buffer containing 2 mM MgCl₂, 0.2% NP-40, and 0.1% sodium deoxycholate for 10 min at 37 °C before being transferred to a solution of the same composition plus 5 mM ferrocyanide (Sigma, P3289), 5 mM ferricyanide (Sigma, 455946), and 1.5 mM of 5-bromo-4-chloro-3-indolyl- β -D-galactoside (X-Gal, 5Prime, 2500040) for 90 min. The reaction was stopped by washing 3 times at room temperature with 1x HEPES buffered saline containing 0.1% Triton X-100 and 1 mM EDTA. Sections were then fixed for 1 h at 4 °C in 4% PFA/PBS and washed several times in PBS before being counterstained as described below.

After stopping the β -galactosidase stain, the slides were defatted by dehydration into xylene and then rehydrated in tap water. Slides were counterstained for 1 min at room temperature with a 1-to-3 dilution of nuclear fast red stock solution (0.1% nuclear fast red Kernechtrot; Fluka, 60700) and 5% aluminum sulfate hydrate (Mallinckrodt, 3208) until the sections attained a light pink color. The slides were then rinsed in running tap water and dehydrated into xylene before being coverslipped with Permount (Fischer Scientific, S70104). Sections from Prnp-tTA mice were counterstained with Neutral red, while the sections from Camk2a-tTA mice were counterstained with Cresyl Violet, as described in the original publications^{4,21}.

Immunohistochemistry for validation of Pitx3 and Pcp2 staining

To validate the cellular identity of X-gal positive cells in the midbrain of Pitx3-tTA and cerebellum of Pcp2-tTA animals, a limited selection of sections adjacent to those used in the primary X-gal analysis from Pitx3-tTA (Mouse 6513) and Pcp2-tTA (Mouse 4340) animals were co-immunostained for β -galactosidase alongside specific markers for tyrosine hydroxylase or calbindin (see below). Prior to immunostaining, brain tissue from each section was carefully separated from the gelatin matrix with iridectomy scissors before being washed in TBS. Sections were blocked for 1 h at room temperature with TBS containing 0.1% Triton-X and 5% normal goat serum before being incubated overnight at 4 °C in blocking solution containing chicken anti-GFP (1:500, Abcam, ab13970) and either rabbit anti-tyrosine hydroxylase (TH; 1:500, Millipore, AB152) or mouse anti-calbindin D-28K (1:2,000, Swant, McAB 300). Sections were washed before incubation in secondary antibody diluted in blocking solution (Alexa 488-conjugated goat anti-chicken; 1:500, Invitrogen, A-11039) and either Alexa 568-conjugated goat anti-rabbit (1:500, Invitrogen, A-11011) or Alexa 568-conjugated goat anti mouse (1:500, Invitrogen, A-11031). Sections were then washed, mounted, and coverslipped using Vectashield mounting medium containing DAPI (4',6-diamidino-2-phenylindole) counterstain (Vector Laboratories, Burlingame, CA, USA).

Brightfield microscopic imaging

Brightfield microscopy images from Camk2a-tTA²¹ and Prnp-tTA⁴ mice were acquired using an automated Olympus Bx52 microscope, equipped with a motorized stage (LEP MAC5000, LUDL Electronic Products Ltd., Hawthorne, NY, USA), an Optronics MicroFire digital camera (Optronics Goleta, CA USA), and NeuroLucida v6.0 Virtual Slice software (MicroBrightField Inc., Williston, VT, USA) with a 20x objective yielding images with a resolution of 1.4 pixels/ μ m. All other images were acquired using a Zeiss Axioscan Z1 slide scanner running Zeiss Zen Software (Carl Zeiss MicroImaging, Jena, Germany) with a 20x objective yielding images with a 0.22 μ m/pixel resolution. Images were exported in Tagged Information File Format (TIFF).

Fluorescence microscopic imaging

Fluorescence microscopy images of selected immunostained sections from one Pitx3-tTA and one Pcp2-tTA animal (see above) were imaged with a Zeiss Pascal laser scanning microscope (Zeiss, Germany) using a Plan Neofluar, 40x immersion objective (n.a. 1.3, oil). Images were acquired sequentially, with a pinhole size of about 1 airy unit, and a scan speed of 12–13 μ s/pixel. Laser wavelengths for the green and red channels were 488 and 543 nm, respectively. The Z-stacks were obtained according to the Nyquist theorem with an optical slice of 0.9 μ m, using a slice thickness of 0.45 μ m. Excited with the appropriate laser, the fluorophores were captured sequentially, i.e. in green (goat anti-chicken 488) and red (goat anti-rabbit 568).

Registration with anatomical reference atlas

All images were registered to the Allen Mouse CCF v.2²⁴ using the QuickNII software tool³². This semiautomatic tool provides custom atlas maps cut at angles of orientation matching the experimental images, which can compensate for deviations in data collected from standard cutting planes. The atlas maps are superimposed and registered to the experimental section images (Fig. 2) by use of affine transformations (scaling, panning, and rotation) to achieve a global match of multiple anatomical landmarks (Fig. 3). For the semi-quantitative analysis (see below), the number of atlas structure delineations was reduced by grouping regions that were smaller than \sim 200 μ m in diameter.

Web-based interactive display of images

For evaluation of β -galactosidase labeling, images were organized in the Navigator3 web-based image management system developed and hosted by the University of Oslo, Norway. This system provides access to an interactive web-microscopy viewer tool that allows users to display microscopic images with atlas overlay atlas maps, annotate points of interest in reference atlas space, and view annotated points of interest together with three-dimensional (3-D) surface models of the Allen Mouse Brain Atlas.

Semi-quantitative scoring of labeled cells

To provide comparable measures of the X-gal-labeled cells across different brain regions in all animals (Data Citation 1), the density of labeling was assessed by two independent researchers using a semi-quantitative grading system from 0–4, introduced in Yetman *et al.*²² (Fig. 2e). Here grade 0 represents

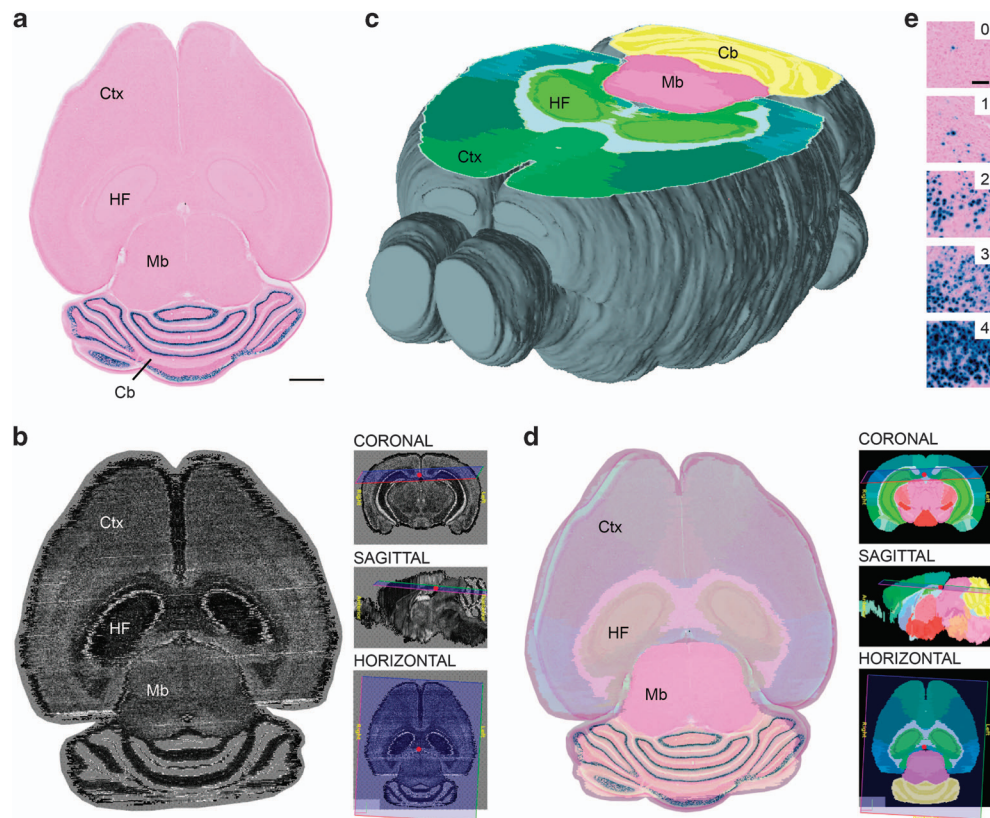


Figure 2. Registration of images to the Allen Mouse CCF v.2 reference atlas. Illustration of the principle used for spatial registration of microscopic mouse brain images to a three-dimensional reference atlas (a–d) and semi-quantitative scoring system used for analysis of labeling (e). (a) Image of a X-gal labeled horizontal section from the brain of a Pcp2-tTA mouse. (b) Slice from the Allen Mouse CCF v.2 reference atlas with position and angle of orientation matching the experimental section in (a). Insets indicate the virtual sectioning plane in coronal, sagittal, and horizontal views. (c) 3-D rendering of the Allen Mouse CCF v.2 atlas showing the virtual cutting plane used in (b) with delineations of major brain structures. This custom atlas diagram is superimposed and spatially aligned with the original section image (d). (e) A semi-quantitative grading scale from 0 to 4 is used to score the density of labeled elements in different brain regions (see methods section for details). Cb, cerebellum; Ctx, cerebral cortex; HF, hippocampal formation; Mb, midbrain. Scale bars, (a–e) 1 mm (e) 100 μm .

absence of labeled cells (less than 1 per 0.01 mm^2), grade 1 - low density (few cells, possible to count), grade 2 - medium density (several cells that can be individually discerned, but not readily counted), grade 3 - high density (many labeled cells with large degree of overlap), and grade 4 - very high density (where individual cells cannot be discerned). The comparison is based on semiquantitative scores of labeling in one representative case for each tTA line (Data Citation 1), with all results verified in the other cases (Fig. 4). Scores did not vary more than 1 grade between cases or researchers in any regions. The highest numbers were reported. If the density of labeling was found to vary substantially within a region, the highest observed score was recorded.

Code availability

The image data are shared in standard TIFF format that can be viewed and analyzed with a range of tools. The software used to register images to the reference atlas (QuickNII) is shared via NITRC (www.nitrc.org/projects/quicknii). The software tools (LocalZoom, MeshView) used here for visualization and analysis are embedded in the Navigator3 image management system, developed and hosted by the Neural Systems Laboratory at the University of Oslo, Norway. These tools are available from the Human Brain Project web page (www.humanbrainproject.eu) upon user registration.

Registration and curation of data in the Human Brain Project infrastructure

Image data and metadata were made publicly available through services for data storage, management, and professional data curation offered by the EU Human Brain Project (www.humanbrainproject.eu).

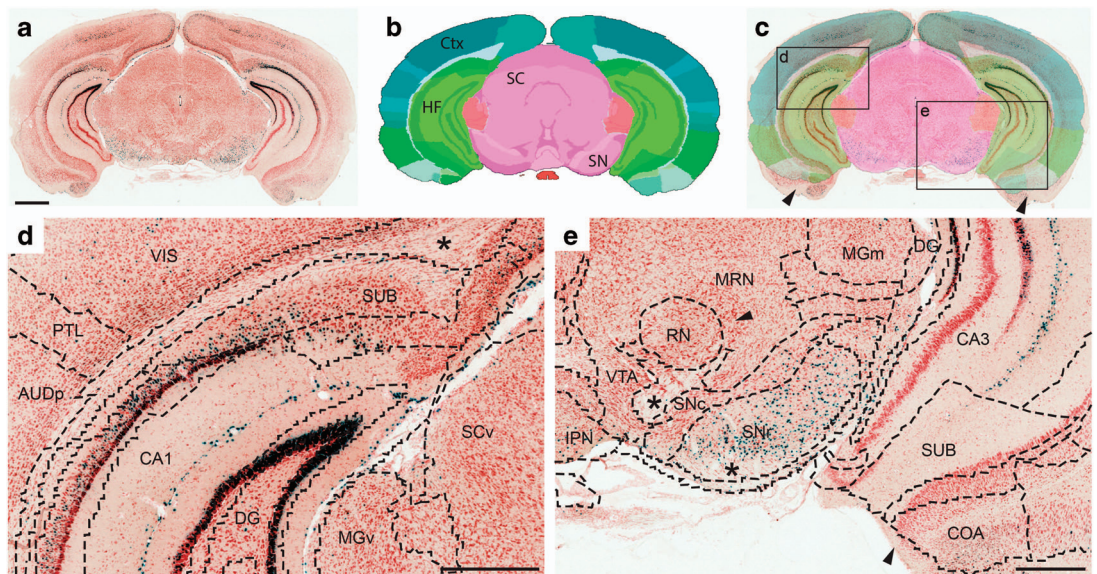


Figure 3. Precision of image registration to atlas. (a) X-gal stained coronal section from a Prnp-tTA/tetO-lacZ mouse (case #388.12). (b) A corresponding custom virtual atlas map from the Allen Mouse CCF v.2. (c) Semi-transparent atlas map superimposed on the section image. (d,e) Higher magnifications from framed areas indicated in (c), with dashed lines indicating anatomical boundaries derived from the atlas. Note the spatial correspondence between atlas delineations and the underlying cytoarchitecture in the hippocampal region (see, e.g. CA1, CA3, DG, SUB) and midbrain (e.g. SNc, SNr), and the partial mismatch of the atlas delineations with the ventral part of the brain (arrowheads in c,e). CA1, cornu ammonis area 1; CA3, cornu ammonis area 3; cc, corpus callosum; Ctx, cerebral cortex; COA, cortical amygdalar area; DG, dentate gyrus; GEnD, medial geniculate complex; HF, hippocampal formation; MB, midbrain; MRN, midbrain reticular nucleus; PA, posterior amygdalar nucleus; PAG, periaqueductal gray; RN, red nucleus; PP, peripeduncular nucleus; RSP, retrosplenial area; SC, superior colliculus; SNc, substantia nigra compact part; SNr, substantia nigra reticular part; SPF, subparafascicular nucleus; SUB, subiculum; VIS, visual cortex; VTA, ventral tegmental area. Scale bar, 1 mm.

The data are Findable, Accessible, Interoperable, and Reusable, in accordance with the FAIR guiding principles³³. The Human Brain Project curation service provides DataCite Digital Object Identifiers (DOIs) for each data set, structured metadata describing basic parameters on data provenance, compliance with regulations on ethical conduct, conditions for use, license for sharing, and validated location metadata defining the location of data in a common anatomical reference atlas.

Data Records

The image files and associated metadata are shared via the web page of the Human Brain Project (www.humanbrainproject.eu; Data Citation 2–13). The tTA image collection comprises series of microscopic images from five tTA-expressing transgenic mouse lines ($n = 1–4$ animals/line). Each data set consists of series of uncompressed high-resolution TIFF images and a data descriptor file (TXT format) and has been given a DataCite DOI. For each data set, a link is provided to a web-microscopy viewer tool featuring functions for exploring and analyzing data, including 1) interactive zooming and panning of images, 2) toggling of customized atlas delineations registered to each image, 3) hover-activated display of anatomical names, and 4) annotation and exact spatial coordinates for points of interest defined in the Allen Mouse CCF v.2 reference atlas. The comparative overview of labeling density for each of the tTA lines is provided as a derived data set with a separate DOI (Data Citation 1). Table 1 provides an overview of the materials included. The ‘usage notes’ below provide suggestions about how the interactive web-microscopy viewer can be engaged.

The images are also shared in the Navigator3 image management system accessible from the Rodent Brain Workbench (www.rbwb.org; select “Brain atlas of tTA driver lines”). This web resource gives 1) overview of the data sets included in the present collection, 2) links to the Human Brain Project web-microscopy viewer system, and 3) options for downloading collections of original TIFF images with spatially matching low resolution Portable Network Graphics (PNG) atlas maps.

All image series include coronal brain sections, with horizontal sections available for the Nop, Pitx3, and Pcp2 driver lines (Table 1; Data Citation 2–13). Each series contains between 15 and 57 images,

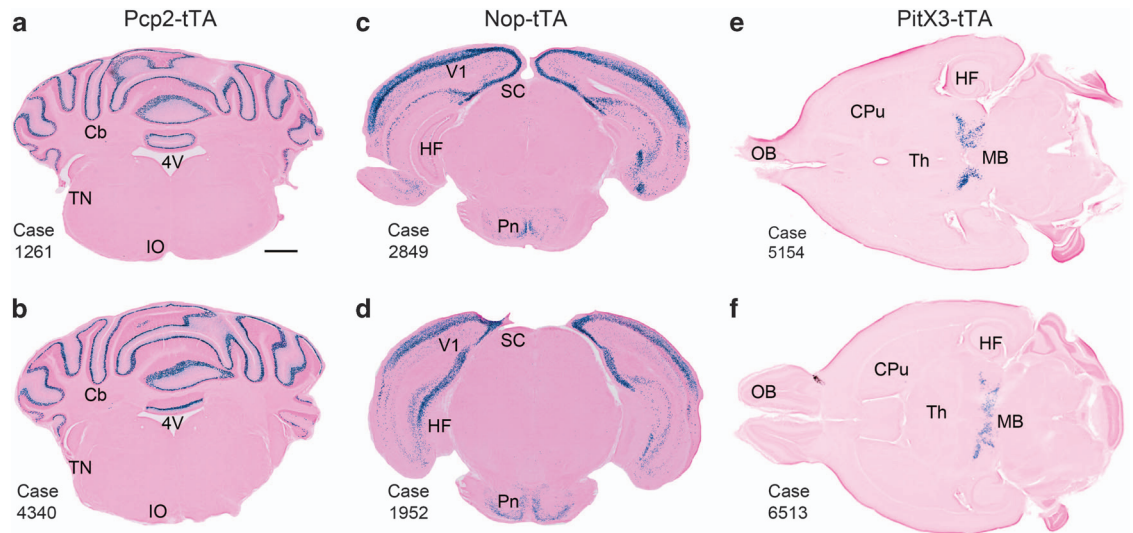


Figure 4. Consistency of labeling across animals. Images of spatially corresponding sections from Pcp2-tTA/tetO-lacZ-nls-GFP (a,b), Nop-tTA/tetO-lacZ-nls-GFP (c,d) and Pitx3-tTA/tetO-lacZ-nls-GFP (e,f) animals showing highly consistent patterns of X-gal labeling in animals of the same strain. 4 V, fourth ventricle; Cb, cerebellum; CPu, caudate putamen; HF, hippocampal formation; IO, inferior olive; MB, midbrain; OB, olfactory bulb; Pn, pontine nuclei; SC, superior collicle; Th, Thalamus; TN, trigeminal nerve; V1, primary visual area. Scale bars, 1 mm.

sampled to cover all major brain regions. The file names encode the animal number (first four digits), genotype, staining (X-gal), serial number (_s followed by three digits), and pixel dimensions (extension _1.4 or _0.22, indicating $\mu\text{m}/\text{pixel}$). For each microscopic image, an atlas map is provided as a 1024 pixel-wide PNG image that represents the same physical space as the higher resolution microscopic images. Each atlas map is named to match its corresponding TIFF image with an additional extension (_segmentation). The total folder size for each series ranges between 4 and 11 gigabytes.

The microscopic images of coronal sections range in size from 25,000 \times 30,000 pixels to 35,000–55,000 pixels (file size 42–230 megabytes, LZW compressed TIFF), while horizontal images range in size from 35,000 \times 35,000 to 50,000 \times 70,000 pixels (file size 100–350 megabytes, LZW compressed TIFF). It should be noted that several of the original TIFF files exceed the maximum limit that can be opened in some common image processing software. These images can, however, be viewed using open-access software tools like e.g. GIMP (<https://www.gimp.org/>).

Technical Validation

Data quality was ensured for each step of data collection and processing. The histological material was prepared to preserve morphological integrity and to cover all major brain regions. Counterstaining was used to highlight anatomical boundaries. Care was taken to define the orientation of section planes, and to ensure proper serial order of the sections. All section images were registered to a common mouse brain reference atlas. This facilitates comparison across specimens, even when the plane of sectioning differs. The accuracy of registration was validated by two independent researchers. The density of cellular labeling was scored by two independent researchers. Consistency of labeling was validated by analysis of X-gal labeling in multiple animals from each line.

Sensitivity and specificity of X-gal staining

X-gal staining is based on the enzymatic cleavage of a colorimetric substrate that continues until the reactants are fully depleted. This stain thus provides a sensitive readout of β -galactosidase localization, but does not offer a quantitative measure of tTA expression levels. Since lysosomal β -galactosidase is present in all tissues, and some tissues have endogenous enzyme activity³⁴, background labeling should be evaluated and excluded. For three of the five tTA lines examined (Nop, Pitx3, and Pcp2), this could be done by directly comparing the overlap between X-gal labeling and GFP fluorescence co-expressed in the reporter construct. The GFP signal was overall less intense compared to X-gal, but the expression pattern largely overlapped. Additionally, no X-gal labeling could be detected in single transgenic control animals (tetO-lacZ-nls-GFP) stained alongside the bigenic samples²².

Since the same protocol was used to visualize X-gal staining in all of the models, the semi-quantitative assessment of labeling density should be comparable across lines. It should be noted, however, that tissue sections differ in thickness and were processed in different laboratories.

Variability in ages and sexes

The present repository provides the first comprehensive comparison of brain-wide expression patterns in tTA driver-reporter lines. It furthermore demonstrates that it is possible to build repositories of comparable image data originating from different laboratories. Both male and female mice are included in the present data collection and animals span a range of ages from 5–42 weeks at harvest. (Table 1). While expression patterns in these lines are not known to vary with age or sex in adulthood, this possibility cannot be excluded and should be taken into consideration when interpreting the data. Since the data repository is hosted in an infrastructure allowing addition of data sets, the present collection can be expanded with future data sets that may clarify whether expression varies in any of the lines as a function of age or sex.

Accuracy of image registration

The registration of custom atlas maps to each section image is achieved by considering multiple anatomical landmarks for each section image, as well as for its adjacent images. The approach used here was to match the atlas map globally to the image, i.e. most landmarks will have a correct position. The anatomical accuracy of image registration to the common reference atlas was validated by two independent researchers. Overall, most brain regions aligned well with the atlas (Fig. 3), but registration was less precise in some brain regions that were displaced or distorted during histological processing, or different in shape relative to the atlas used (Fig. 3c,e). Such registration errors are difficult to quantify, but may vary from tens to hundreds of micrometers. Comparison of 3-D distributions of labelled cells between four cases sectioned in different planes of orientation (see below), confirms that the registration of images to the reference atlas was sufficiently accurate to yield consistent results across cases. Nevertheless, in regions where differences in shape could not be compensated by affine transformations, the position of the atlas overlays were temporarily adjusted during the semi-quantitative evaluation of expression density, to achieve a better match between local anatomical landmarks and ensure appropriate structural assignment.

Validation of the morphological phenotype of Pitx3 and Pcp2 lines

Pitx3 is a transcriptional regulator important for differentiation and maintenance of meso-diencephalic dopaminergic neurons during development, and the Pitx3-tTA line was created to investigate degeneration of these cells in Parkinson's disease¹⁹. Purkinje cell protein 2 (Pcp2) is expressed in cerebellar Purkinje cells and retinal bipolar cells, and the Pcp2-tTA line was created to investigate neural degeneration in a mouse model of spinocerebellar ataxia type 1³⁵. In these lines, the cellular identity of X-gal-positive cells was confirmed by immunostaining against tyrosine hydroxylase for dopaminergic cells or calbindin for Purkinje cells.

In sections from Pitx3-tTA brains, dense populations of X-gal labeled cells were found in the substantia nigra pars compacta (SNc) and the ventral tegmental area (VTA), corresponding well with earlier publications (Fig. 4e,f and Fig. 5a,b)^{19,36}. Confocal microscopic examination of sections immunostained for tyrosine hydroxylase confirmed earlier reports that the expression of Pitx3-tTA was restricted to a subset of dopaminergic neurons in the SNc and VTA (Fig. 5c–e). Some X-gal labeling was also observed in the midbrain raphe nuclei, inferior colliculus, midbrain reticular nucleus, and periaqueductal grey, indicating some Pitx3-tTA promoter activity also occurs outside the SNc and VTA. This is illustrated in Fig. 6, showing a 3-D co-visualization of the location of labeled cells. In two of the four animals investigated, a few scattered X-gal labeled cells were also found in the main and accessory olfactory bulb.

In sections from Pcp2-tTA brains, X-gal labeling was exclusively observed in cerebellar Purkinje cells (Fig. 4a,b and Fig. 7a–c), consistent with previous reports^{35,37}. Confocal microscopy of sections immunostained for calbindin confirmed that tTA dependent expression was restricted to Purkinje cells (Fig. 7d,e). The labeled cells were distributed across the entire cerebellum, including most, but not all Purkinje cells.

Usage Notes

Accessing and viewing images from tTA driver lines

Each data set can be directly accessed via DOIs (Data Citation 2–13), or query tools provided via the Human Brain Project web page. For each data set, a landing page provides access to downloadable high-resolution image files, basic metadata with data provenance and license information, and a link to an interactive viewer tool. The viewer provides a “filmstrip” overview of serial images from one animal, and features panning and zooming of individual high-resolution images, with a semi-transparent graphical overlay images showing the custom atlas mapped to fit the images. The atlas diagrams provide a reasonable starting point for anatomical analyses, but additional methods may be necessary to make more precise statements about anatomical locations.

Examples of use

Below, we outline three example scenarios in which the present collection of images from tTA driver lines may provide a useful resource.

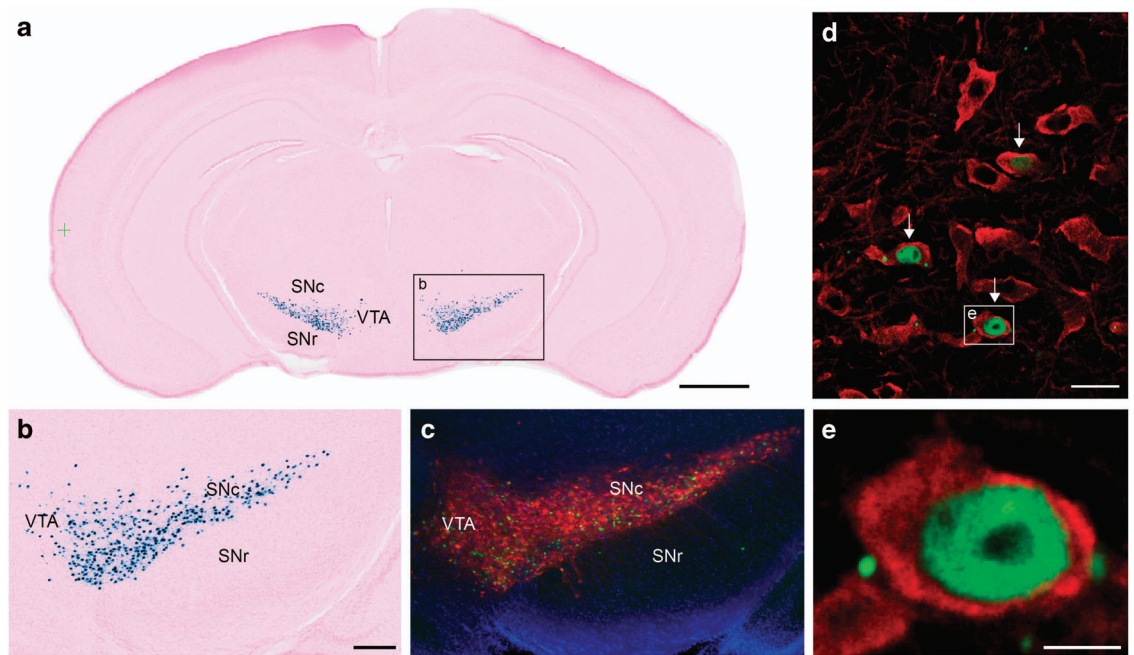


Figure 5. Validation of the cell-type specificity in the Pitx3-tTA line. (a) X-gal stained coronal section from a Pitx3-tTA/tetO-lacZ-nls-GFP mouse brain, with atlas derived annotations shown in the left hemisphere. (b) Enlarged detail from (a) showing part of the midbrain containing the substantia nigra. (c–e) Confocal microscopic images with increasing magnification of a green fluorescent protein (GFP), tyrosine hydroxylase (TH) and DAPI stained section adjacent to the section in (a,b). TH immunohistochemistry is used to identify dopaminergic cells in the brain, and TH positive cells appear red in (c–e). Cells co-labeled with GFP and TH (arrows) in the SNc are shown in (d) and a single co-labeled cell in (e). Note that GFP, and thus also lacZ, is expressed only in a subset of TH positive cells. SNc, substantia nigra compact part; SNr, substantia nigra reticular part; VTA, ventral tegmental area. Scale bars, (a) 1 mm (b,c) 100 μ m (d) 20 μ m (e), and 2 μ m.

Example 1: Comparing tTA expression patterns to find a driver line suitable for conditional transgene expression in a specific region of interest. A researcher investigating Parkinson's disease wants to create a conditional mouse model in which she can specifically regulate the expression of a gene of interest in the substantia nigra. She chooses to use the tet-transactivator system, and therefore needs a tTA-expressing line active in her region of interest. She queries the Human Brain Project database for tTA driver lines, and finds several collections of image data and a derived data set providing an overview of promoter expression (Data Citation 1). The tabular overview shows that two tTA driver lines are active in the substantia nigra. The Prnp-tTA line features widespread X-gal labeling in numerous brain regions, including the substantia nigra, while the Pitx3-tTA line has more spatially restricted labeling in the substantia nigra, ventral tegmental area, and a few other regions. She clicks on the link to launch the online virtual microscope viewer, in which she can inspect and compare serial images and corresponding atlas maps from these two lines (Fig. 8), or download original images for use with other tools. Since sections from both lines are registered to the same reference atlas, she can easily find and compare corresponding sections. Using the online image viewer she can also identify the coordinates of a point of interest in one section and compare this to coordinates extracted from other image series (Fig. 6). In this way she can quickly examine the spatial pattern and specificity of reporter expression in the two relevant driver lines, and consider whether this is compatible with her desired experimental paradigm. Inspecting corresponding sections from the two lines, she discovers that within the substantia nigra, the Prnp promoter line mainly drives transgene expression in the reticular part, while Pitx3 promoter activity is restricted to the compact part (Fig. 8a–d). For the Pitx3-tTA line she can look up additional documentation confirming that the labeled cells are positive for tyrosine hydroxylase and therefore dopaminergic neurons. The Prnp-tTA line drives transgene expression in the reticular part of the substantia nigra (Fig. 8a,c), but also in many other brain regions (Fig. 3a), while the Pitx3-tTA line drives transgene expression selectively in dopaminergic neurons of substantia nigra pars compacta and ventral tegmental area (Fig. 8b,d). With this information, she can choose the tTA line best suited for her purposes. Finally, to compare the spatial distribution of labeling among cases from one tTA line, she can also use the manual annotation function in the online image viewer tool to record the positions of labeled

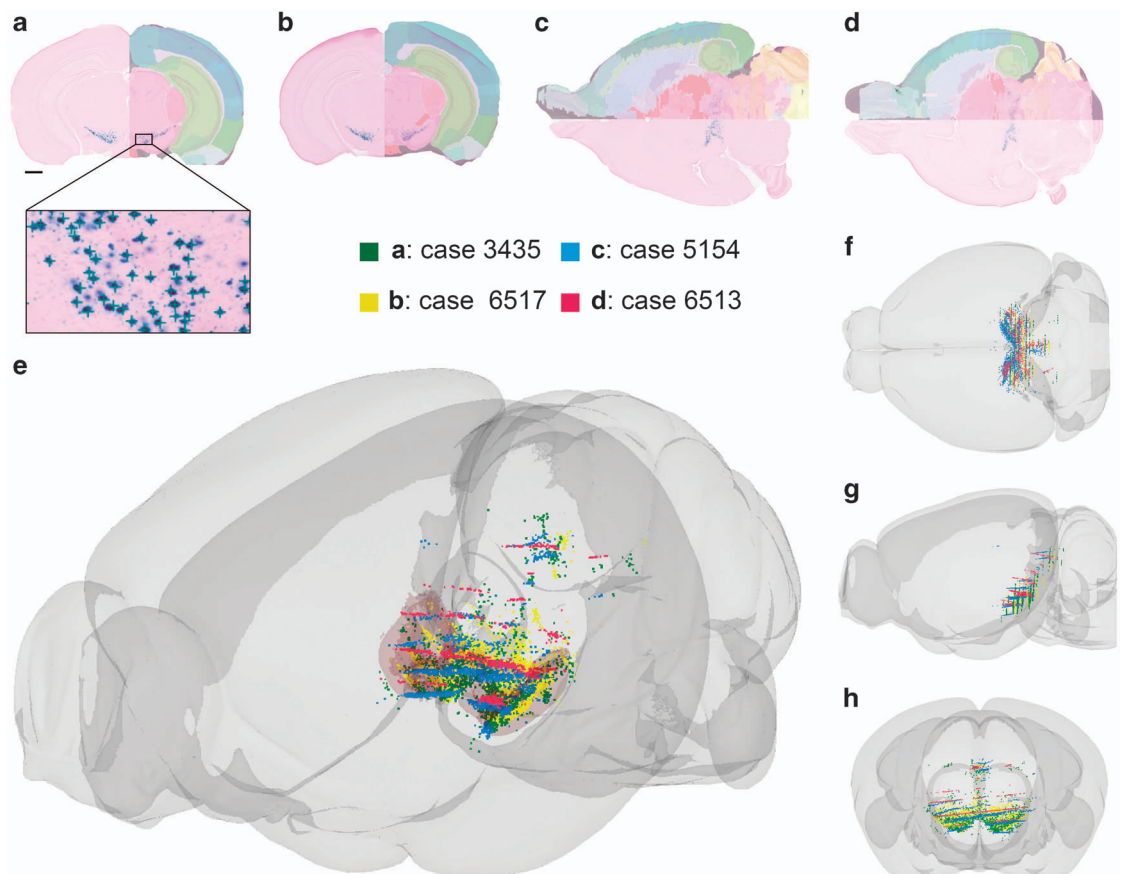


Figure 6. 3-D representation of data from different Pitx3-tTA cases. (a–d) Section images showing X-gal labeling in four Pitx3-tTA cases, two sectioned coronally (a,b) and two sectioned horizontally (c,d), with atlas overlay shown on one side. The positions of labeled cells were manually recorded from all section images by placing point coordinates on each labeled cell using the annotation tool in the LocaliZoom viewer (exemplified in the enlarged inset in a). (e–h) The point coordinates were color-coded and co-visualized together with atlas structures in a 3-D viewer. Views from anterolateral (e), dorsal (f), lateral (g), and anterior (h) are provided. In (e), the outer boundaries of the substantia nigra and ventral tegmental area are shown as transparent pink surfaces. The 3-D visualization allows comparison of data derived from coronal and horizontal section images, and demonstrates that labeled cells are similarly distributed in the four Pitx3-tTA cases, with high densities in the substantia nigra and ventral tegmental area, but also with labeling in more dorsal parts of the mesencephalon. Scale bar, 1 mm.

cells in the reference atlas space for all sections from the Pitx3-tTA cases, and co-display these in a 3-D viewer tool (Fig. 6).

Example 2: Interpreting findings from a disease model using a tTA driver line. The Nop-tTA driver line has been described as primarily restricted to the medial entorhinal cortex and pre- and parasubiculum²⁹, but brain-wide examination of reporter expression has revealed activity in many additional brain regions²². A researcher investigating possible axonal spread of pathological protein aggregates in a conditional mouse model of Alzheimer’s disease based on the Nop-tTA line would like to know which cells initially express the transgenic protein of interest. The researcher expects pathological aggregates will appear in regions where the responder gene is transcribed and possibly also in regions to which these cells project axonal connections. The interpretation of findings thus requires specific knowledge of where the Nop-tTA driver is active and the axonal connections of those regions. The researcher can use the tabular overview of the online tTA atlas to identify where X-gal labeling occurs in Nop-tTA mice (Data Citation 1). Subsequently he can inspect the detailed labeling patterns in coronal (Fig. 4c,d) and horizontal sections. He can then enlist other resources such as the Allen Mouse Brain Connectivity Atlas to examine neural connections made by the identified regions²⁴. The interactive Connectivity Atlas provides access to a large number of volumetric images showing anterograde axonal

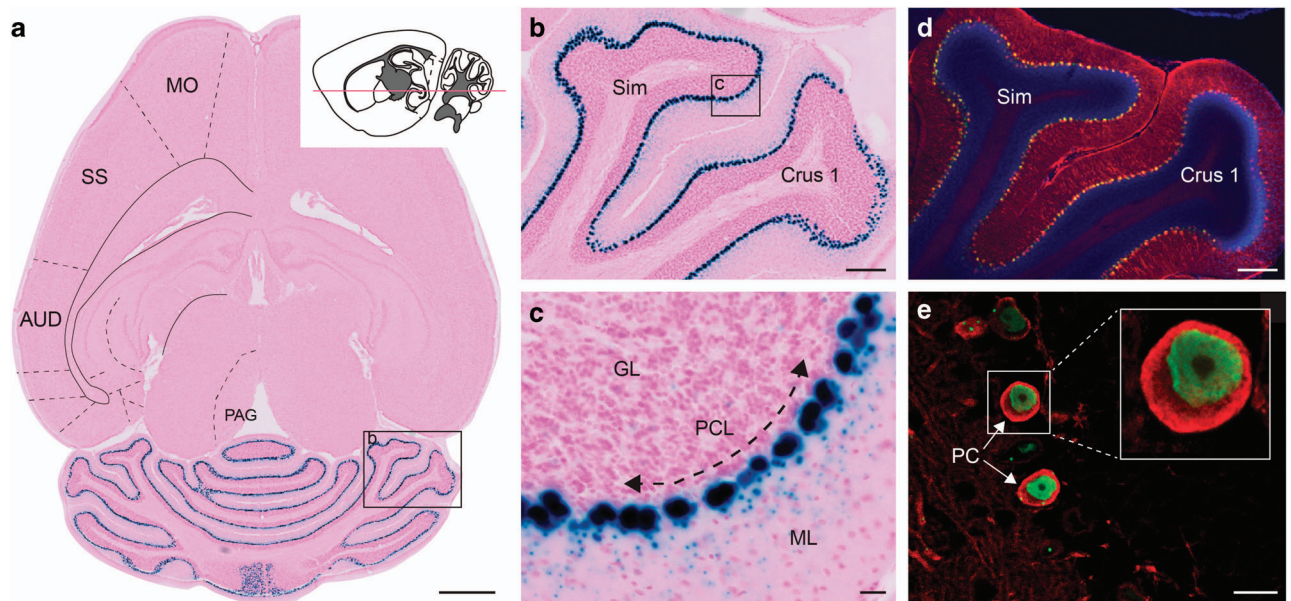


Figure 7. Validation of cell-type specificity in the Pcp2-tTA line. (a) X-gal stained horizontal section from a Pcp2-tTA/tetO-lacZ-nls-GFP mouse brain. The left hemisphere has annotations corresponding to a virtual atlas map from the Allen Mouse CCF v.2. The cartoon drawing of a sagittal section shows the approximate cutting plane as a red line. (b) Enlarged detail from the section in (a) showing part of the cerebellum. (c) Further magnified detail from the section in (a,b) showing labeling between the cerebellar granular layer and the molecular layer. (d) Confocal microscopic image of a green fluorescent protein (GFP), calbindin, and DAPI stained section adjacent to the section in (a-c). Calbindin is a marker for Purkinje cells, and with high magnification one can clearly identify cells co-labeled for GFP and calbindin (e). Since expression of GFP and lacZ are both driven by the Pcp2 promoter, this verifies that the X-gal labeled cells in (a-c) are also Purkinje cells. AUD, primary auditory area; Crus 1, cerebellar crus 1, GL, granular cell layer; ML, molecular cell layer; MO, primary motor area; PAG, periaqueductal gray; PC, Purkinje cell; PCL, Purkinje cell layer; SS, primary somatosensory area; Sim, simple lobule. Scale bars, (a) 1 mm (b,d), and 200 μm (c,e) 20 μm .

labeling across entire mouse brains. Using the tabular overview of brain regions with X-gal labeling in Nop-tTA mice as a starting point, the researcher can systematically cross-check the outcome of tracer injections to corresponding locations in the Allen Mouse Brain Connectivity atlas (<http://connectivity.brain-map.org>). Such comparisons are readily done since all images in the Brain atlas of tTA driver lines are spatially defined using the common reference atlas.

Example 3: Comparing transgene expression in tTA driver lines with gene distribution patterns from other repositories. A researcher studying gene expression in the mouse brain wants to compare the spatial distribution of promoter activity in a tTA transgenic line with that of a particular transcript in the normal mouse brain. The Allen Institute hosts data from *in situ* hybridization experiments showing gene expression in the adult mouse brain for > 20,000 independent transcripts (<http://mouse.brain-map.org>). The Allen Institute repository can be queried for genes of interest, and expression patterns can be viewed in serial section images. The researcher can then perform side-by-side comparisons of corresponding sections from the Brain atlas of tTA driver lines and the Allen Institute repository (Fig. 8e,f), or download images for more detailed analysis using other tools.

Future use and expansion of the image repository

All images shared in the present data collection have been spatially integrated by registration to a common reference atlas and made publicly available. This facilitates integration of data not only within the collection, but also makes it possible to relate our tTA data with the growing collection of heterogeneous data accumulated by the Human Brain Project. The Human Brain Project database is open for new data, and provides data curation services and tools for registering image data to the Allen Mouse Common Coordinate Framework²⁴. The present collection of tTA image data is now available for new data to be added: should other investigators conduct similar intercrosses on new driver-reporter lines,

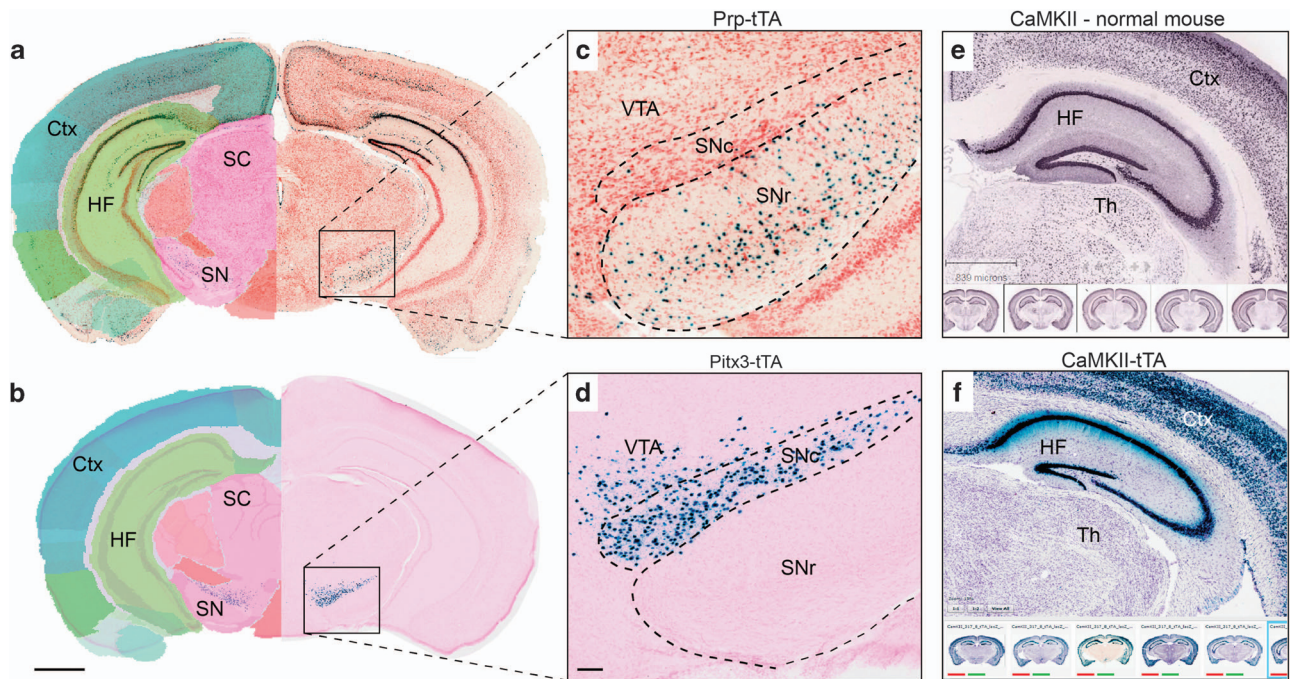


Figure 8. Examples of use. (a–d) X-gal labeled coronal sections through the midbrain from Prnp-tTA/tetO-lacZ (a,c) and Pitx3-tTA/tetO-lacZ-nls-GFP (b,d) mice. The left hemispheres are presented with semi-transparent overlays of custom atlas maps as available in the online viewer. (c,d) Higher-magnification details from the substantia nigra showing notably different labeling patterns between the two lines. In this region the Prnp-tTA line mainly has labeled cells within the reticular part (c), while the Pitx3-tTA line displays labeling highly restricted to the compact part and the ventral tegmental area. (d). Note that for the Prnp-tTA line, labeling also occurs in several other regions such as the hippocampal formation and the cerebral cortex. (e) Shows a screenshot of *in situ* hybridization data representing gene distribution of the Camk2a gene in the hippocampal area of a normal mouse from the Allen Institute repository (www-brain-map.org). (f) Shows a screenshot of a corresponding X-gal labeled section from a Camk2a-tTA/tetO-lacZ mouse, available from the rodent brain workbench. Similar viewers facilitate comparison of native gene distribution patterns and tTA dependent transgene expression patterns. Ctx, cerebral cortex; HF, hippocampal formation; SC, superior colliculus; SN, substantia nigra; SNc, substantia nigra, compact part; SNr, substantia nigra, reticular part; Th, thalamus; VTA, ventral tegmental area. Scale bars, 1 mm (a,b), 100 μm (c,d).

their microscopic image data can leverage the workflow developed here to integrate new data sets with the existing collections. Inclusion of data from additional tTA lines or from other ages/sexes of the tTA lines presented here will substantially increase the scientific value of the repository. Researchers working with tTA animals are therefore encouraged to share their data and expand this public collection of tTA promoter expression data.

References

- Safar, J. G. *et al.* Prion clearance in bigenic mice. *J. Gen. Virol.* **86**, 2913–2923 (2005).
- Nuber, S. *et al.* Neurodegeneration and motor dysfunction in a conditional model of Parkinson's disease. *J. Neurosci.* **28**, 2471–2484 (2008).
- Choi, D. S., Wang, D., Dadgar, J., Chang, W. S. & Messing, R. O. Conditional rescue of protein kinase C epsilon regulates ethanol preference and hypnotic sensitivity in adult mice. *J. Neurosci.* **22**, 9905–9911 (2002).
- Boy, J. *et al.* Expression mapping of tetracycline-responsive prion protein promoter: digital atlasing for generating cell-specific disease models. *NeuroImage* **33**, 449–462 (2006).
- Yamamoto, A., Lucas, J. J. & Hen, R. Reversal of neuropathology and motor dysfunction in a conditional model of Huntington's disease. *Cell* **101**, 57–66 (2000).
- Jankowsky, J. L. *et al.* Persistent amyloidosis following suppression of Abeta production in a transgenic model of Alzheimer disease. *PLoS Med.* **2**, e355 (2005).
- Rowland, D. C. *et al.* Transgenically targeted rabies virus demonstrates a major monosynaptic projection from hippocampal area CA2 to medial entorhinal layer II neurons. *J. Neurosci.* **33**, 14889–14898 (2013).
- Lein, E. S. *et al.* Genome-wide atlas of gene expression in the adult mouse brain. *Nature* **445**, 168–176 (2007).
- de Calignon, A. *et al.* Propagation of tau pathology in a model of early Alzheimer's disease. *Neuron* **73**, 685–697 (2012).
- Liu, L. *et al.* Trans-synaptic spread of tau pathology *in vivo*. *PLoS One* **7**, e31302 (2012).

11. Gossen, M. & Bujard, H. Tight control of gene expression in mammalian cells by tetracycline-responsive promoters. *Proc. Natl. Acad. Sci. U.S.A.* **89**, 5547–5551 (1992).
12. Lewandoski, M. Conditional control of gene expression in the mouse. *Nat. Rev. Genet.* **2**, 743–755 (2001).
13. Sun, Y., Chen, X. & Xiao, D. Tetracycline-inducible expression systems: new strategies and practices in the transgenic mouse modeling. *Acta Biochim. Biophys. Sin. (Shanghai)* **39**, 235–246 (2007).
14. Schonig, K., Freundlieb, S. & Gossen, M. Tet-Transgenic Rodents: a comprehensive, up-to date database. *Transgenic Res.* **22**, 251–254 (2013).
15. Canzoniere, D. *et al.* Dual control of neurogenesis by PC3 through cell cycle inhibition and induction of Math1. *J. Neurosci.* **24**, 3355–3369 (2004).
16. Katsantoni, E. Z. *et al.* Ubiquitous expression of the rtTA2S-M2 inducible system in transgenic mice driven by the human hnRNPA2B1/CBX3 CpG island. *BMC Dev. Biol.* **7**, 108 (2007).
17. Audero, E. *et al.* Sporadic autonomic dysregulation and death associated with excessive serotonin autoinhibition. *Science* **321**, 130–133 (2008).
18. Maxwell, S. L., Ho, H. Y., Kuehner, E., Zhao, S. & Li, M. Pitx3 regulates tyrosine hydroxylase expression in the substantia nigra and identifies a subgroup of mesencephalic dopaminergic progenitor neurons during mouse development. *Dev. Biol.* **282**, 467–479 (2005).
19. Lin, X. *et al.* Conditional expression of Parkinson's disease-related mutant alpha-synuclein in the midbrain dopaminergic neurons causes progressive neurodegeneration and degradation of transcription factor nuclear receptor related 1. *J. Neurosci.* **32**, 9248–9264 (2012).
20. Oberto, A., Acquadro, E., Bus, T., Sprengel, R. & Eva, C. Expression patterns of promoters for NPY Y(1) and Y(5) receptors in Y (5)RitTA and Y(1)RVenus BAC-transgenic mice. *Eur. J. Neurosci.* **26**, 155–170 (2007).
21. Odeh, F. *et al.* Atlas of transgenic Tet-Off Ca2+/calmodulin-dependent protein kinase II and prion protein promoter activity in the mouse brain. *NeuroImage* **54**, 2603–2611 (2011).
22. Yetman, M. J., Lillehaug, S., Bjaalie, J. G., Leergaard, T. B. & Jankowsky, J. L. Transgene expression in the Nop-tTA driver line is not inherently restricted to the entorhinal cortex. *Brain Struct. Funct.* **221**, 2231–2249 (2016).
23. Amunts, K. *et al.* The Human Brain Project: Creating a European Research Infrastructure to Decode the Human Brain. *Neuron* **92**, 574–581 (2016).
24. Oh, S. W. *et al.* A mesoscale connectome of the mouse brain. *Nature* **508**, 207–214 (2014).
25. Tremblay, P. *et al.* Doxycycline control of prion protein transgene expression modulates prion disease in mice. *Proc. Natl. Acad. Sci. U.S.A.* **95**, 12580–12585 (1998).
26. Mayford, M., Baranes, D., Podsypanina, K. & Kandel, E. R. The 3'-untranslated region of Camk2a alpha is a cis-acting signal for the localization and translation of mRNA in dendrites. *Proc. Natl. Acad. Sci. U.S.A.* **93**, 13250–13255 (1996).
27. Baron, U., Freundlieb, S., Gossen, M. & Bujard, H. Co-regulation of two gene activities by tetracycline via a bidirectional promoter. *Nucleic Acids Res* **23**, 3605–3606 (1995).
28. Schonig, K. & Bujard, H. Generating conditional mouse mutants via tetracycline-controlled gene expression. *Methods Mol. Biol.* **209**, 69–104 (2003).
29. Yasuda, M. & Mayford, M. R. Camk2a activation in the entorhinal cortex disrupts previously encoded spatial memory. *Neuron* **50**, 309–318 (2006).
30. Holt, S. & O'Sullivan, D. Studies in enzyme cytochemistry I. Principles of cytochemical staining methods. *Proc. R. Soc. Lond. B. Biol. Sci.* **148**, 465–480 (1958).
31. Cepko, C., Ryder, E., Fekete, D. M. & Bruhn, S. In *Cells: A Laboratory Manual, Volume 3: Subcellular Location of Genes and Their Products* (eds D. L. Spector, R. D. Goldman, & L. A. Leinwand) (Cold Spring Harbor Laboratory Press, 1998).
32. Puchades, M. A. *et al.* QuickNII: Neuroinformatics Tool and Workflow for Anchoring of Serial Histological Images in Rodent Brain 3D Space. Abstract no. 532.12 in *Neuroscience Meeting Planner*. (Washington, DC: Society for Neuroscience, 2017).
33. Wilkinson, M. D. *et al.* The FAIR Guiding Principles for scientific data management and stewardship. *Sci. Data* **3**, 160018 (2016).
34. Rosenberg, W. S., Breakefield, X. O., DeAntonio, C. & Isacson, O. Authentic and artifactual detection of the E. coli lacZ gene product in the rat brain by histochemical methods. *Brain Res. Mol. Brain Res.* **16**, 311–315 (1992).
35. Zu, T. *et al.* Recovery from polyglutamine-induced neurodegeneration in conditional SCA1 transgenic mice. *J. Neurosci.* **24**, 8853–8861 (2004).
36. Sgobio, C. *et al.* Optogenetic measurement of presynaptic calcium transients using conditional genetically encoded calcium indicator expression in dopaminergic neurons. *PLoS One* **9**, e111749 (2014).
37. Echigo, R., Nakao, K., Fukaya, M., Watanabe, M. & Aiba, A. Generation of L7-tTA knock-in mice. *Kobe J. Med. Sci.* **54**, E272–E278 (2009).

Data Citations

1. Lillehaug, S. *et al.* Human Brain Project Neuroinformatics Platform <https://doi.org/10.25493/ARKS-R7H> (2018).
2. Lillehaug, S. *et al.* Human Brain Project Neuroinformatics Platform <https://doi.org/10.25493/A2EG-VPR> (2018).
3. Lillehaug, S. *et al.* Human Brain Project Neuroinformatics Platform <https://doi.org/10.25493/D1PR-55A> (2018).
4. Lillehaug, S. *et al.* Human Brain Project Neuroinformatics Platform <https://doi.org/10.25493/YCGE-ADC> (2018).
5. Lillehaug, S. *et al.* Human Brain Project Neuroinformatics Platform <https://doi.org/10.25493/FMGJ-4N3> (2018).
6. Lillehaug, S. *et al.* Human Brain Project Neuroinformatics Platform <https://doi.org/10.25493/2382-AYM> (2018).
7. Lillehaug, S. *et al.* Human Brain Project Neuroinformatics Platform <https://doi.org/10.25493/1AH7-T1A> (2018).
8. Lillehaug, S. *et al.* Human Brain Project Neuroinformatics Platform <https://doi.org/10.25493/DTB3-OKP> (2018).
9. Yetman, M., Lillehaug, S., Bjaalie, J., Leergaard, T. & Jankowsky, J. Human Brain Project Neuroinformatics Platform <https://doi.org/10.25493/5H13-1Q0> (2018).
10. Yetman, M., Lillehaug, S., Bjaalie, J., Leergaard, T. & Jankowsky, J. Human Brain Project Neuroinformatics Platform <https://doi.org/10.25493/WB6K-V72> (2018).
11. Yetman, M., Lillehaug, S., Bjaalie, J., Leergaard, T. & Jankowsky, J. Human Brain Project Neuroinformatics Platform <https://doi.org/10.25493/AYBB-BXV> (2018).
12. Odeh, F. *et al.* Human Brain Project Neuroinformatics Platform <https://doi.org/10.25493/W97C-01R> (2018).
13. Boy, J. *et al.* Human Brain Project Neuroinformatics Platform <https://doi.org/10.25493/T9P1-WH4> (2018).

Acknowledgements

We thank Bryan Song and Rebecca Corrigan for outstanding animal care, Nirao Shah for methodological advice on X-gal staining, Mark Mayford for sharing the Nop-tTA, tetO-lacZ, and tetO-H2B-GFP lines, Milica Markovic and Krister A. Anderson for expert data management and curation, Oliver Schmid and Jeff C. Muller for integrating and disseminating data from the Neuroinformatics Platform of the Human

Brain Project, Dmitri Darine and Gergely Csucs for expert technical assistance with the online atlas application and related neuroinformatics tools. The histological material from Prnp-tTA and Camk2 α -tTA lines was prepared in collaboration with Jana Schmidt (née Boy), Thorsten Schmidt, and Olaf Riess (Univ. Tübingen, Germany). Histological section images were acquired at the NORBRAIN Slidescanning Facility at the Institute of Basic Medical Sciences, University of Oslo. This project was supported by the National Institutes of Health (NIH) Office of the Director (DP2 OD001734 to JLJ), National Institute of Neurological Disease and Stroke (R01 NS092615 to JLJ), National Institute of Aging (T32 AG000183 to MJY), The Research Council of Norway (214842 and the Norwegian Large Scale Infrastructure for Brain Research; NORBRAIN), and the European Union's Horizon 2020 Framework Programme for Research and Innovation under Specific Grant Agreements No. 720270 (Human Brain Project SGA1) and No. 785907 (Human Brain Project SGA2).

Author Contributions

S.L. acquired images and organized the image repository, registered images to atlas, performed anatomical analyses, made figures and contributed to writing the paper. M.J.Y. bred and genotyped animals, performed the histological processing, captured images, and contributed to writing the paper. M.A.P. validated image registration to atlas, made figures, curated metadata, and contributed to writing the paper. M.M.C. registered images to atlas, validated metadata, performed anatomical analyses, and contributed to writing the paper. HK organized and curated all data, metadata, and tables for public sharing, linked data elements in the public sharing platform, and contributed to writing the paper. J.L.J. designed the study, provided materials and funding, and contributed to writing the paper. J.G.B. designed the study, provided materials and funding, supervised tools development, and contributed to writing the paper. T.B.L. designed and supervised the study, provided materials and funding, and contributed to writing the paper.

Additional Information

Competing interests: The authors declare no competing interests.

How to cite this article: Lillehaug, S. *et al.* Brain-wide distribution of reporter expression in five transgenic tetracycline-transactivator mouse lines. *Sci. Data*. 6:190028 <https://doi.org/10.1038/sdata.2019.28> (2019).

Publisher's note: Springer Nature remains neutral with regard to jurisdictional claims in published maps and institutional affiliations.



Open Access This article is licensed under a Creative Commons Attribution 4.0 International License, which permits use, sharing, adaptation, distribution and reproduction in any medium or format, as long as you give appropriate credit to the original author(s) and the source, provide a link to the Creative Commons license, and indicate if changes were made. The images or other third party material in this article are included in the article's Creative Commons license, unless indicated otherwise in a credit line to the material. If material is not included in the article's Creative Commons license and your intended use is not permitted by statutory regulation or exceeds the permitted use, you will need to obtain permission directly from the copyright holder. To view a copy of this license, visit <http://creativecommons.org/licenses/by/4.0/>

The Creative Commons Public Domain Dedication waiver <http://creativecommons.org/publicdomain/zero/1.0/> applies to the metadata files made available in this article.

© The Author(s) 2019